August 2018

Integrative Signaling of Mitochondria, TRPA1 and TRPV1 in Vagal Neurons

Katherine Stanford
University of South Florida, kstanford@health.usf.edu

Integrative Signaling of Mitochondria, TRPA1 and TRPV1 in Vagal Neurons

by

Katherine Stanford

A dissertation submitted in partial fulfillment
of the requirements for the degree of
Doctor of Philosophy
Molecular Pharmacology and Physiology
College of Medicine
University of South Florida

Major Professor: Dr. Thomas Taylor-Clark, Ph.D.
Craig Doupnik, Ph.D.
Sami Noujaim, Ph.D.
Javier Cuevas, Ph.D.
Srinivas Tipparaju, Ph.D.

Date of Approval:
August 2, 2018

Keywords: ion channel, sensory nerves, pulmonary disease, reactive oxygen species

TABLE OF CONTENTS

LIST OF FIGURES

LIST OF TABLES

ABSTRACT

Sensory nerves detect conditions in the external and internal environment and permit behavioral and physiological responses to maintain homeostasis and ensure survival. As such, sensory nerves detect a wide variety of stimuli including heat, touch, pH, and vibration. The precise nature of these responses is dependent upon the initiating stimulus and site of activation. Potentially threatening stimuli (noxious heat, cellular damage, chemical irritants) activate nociceptive sensory nerves through the gating of ion channels expressed at sensory nerve terminals, thereby evoking defensive reflexes such as cough, watering eyes and limb withdrawal as well as sensations of pain or discomfort. While these responses are typically protective, inflammation alters peripheral neuronal activity resulting in unpleasant sensations, and aberrant reflexes which are the hallmark symptoms of pulmonary disease(Costello et al., 1999).

Unfortunately, current treatments which focus on specific symptoms such as bronchospasm and inflammation are not effective for all individuals and fail to address underlying sensory nerve activity(Barnes, 2012). Therefore, understanding mechanisms underlying the increased activity of ion channels expressed at sensory nerve terminals such as the nonselective cation channels transient receptor potential channels ankyrin 1 (TRPA1) and vanilloid 1 (TRPV1) may lead to the development of novel therapeutics for the treatment of inflammatory pulmonary diseases. As inflammation induces mitochondrial dysfunction through inhibition of the electron transport chain (mETC), we investigated the impact of mitochondrial dysfunction on the activation of TRPA1 and TRPV1 using dissociated vagal neurons. Using live cell Ca^{2+} imaging to measure channel activation, we found that mitochondrial dysfunction induced with antimycin A (complex III inhibitor), carbonyl cyanide m-chlorophenyl hydrazone (CCCP, mitochondrial uncoupling agent),

and rotenone (complex I inhibitor) activates a portion of vagal neurons expressing TRPA1 and/or TRPV1.

Using antimycin A, we discovered that across all neurons were Ca^{2+} responses were diminished (averaged across all neurons) with knockout/inhibition of either TRPA1 or TRPV1 and largely abolished with dual knockout/inhibition of both channels. Interestingly, the diminished response with TRPA1 knockout or inhibition can be attributed to a decrease in the magnitude of the Ca^{2+} flux in neurons responding while decreased responses with TRPV1 knockout or inhibition were associated with the decrease in percentage of neurons which responded, not Ca^{2+} flux magnitude. Mitochondrial dysfunction results in the increased reproduction of ROS and mitochondrial depolarization. Therefore, we evaluated the relationship between mitochondrial depolarization (using JC-1) and ROS production (using mitoSOX Red) and channel activation (Ca^{2+} imaging with FURA-2AM). Although only a portion of TRPA1/TRPV1 expressing neurons responded to mitochondrial inhibition with CCCP, rotenone or antimycin A that there was no difference in ROS production or mitochondrial depolarization between responding and non-responding neurons.

We also investigated the impact of these ROS on the activation of TRPA1 and TRPV1. We found that the activation of TRPA1, but not TRPV1, is likely downstream of mitochondrial ROS production as 1) antimycin A induced Ca^{2+} fluxes were diminished by co-treatment with ROS scavengers in transfected HEK293 cells and dissociated vagal neurons, 2) ROS production (measured with mitoSOX Red simultaneously with Ca^{2+} imaging) was correlated with Ca^{2+} fluxes in TRPA1, but not TRPV1, expressing neurons, and 3) the ROS-unresponsive TRPA1 K620A mutant did not respond to antimycin A. As studies regarding ROS production are hindered by the lack of suitable methods to measure ROS production associated with caveats involved in the use of ROS sensitive dyes and the lack of sensitivity offered by redox sensitive proteins, we sought to increase the sensitivity of roGFP1, a redox sensitive variant of GFP by replacing one of the

reactive cysteines with selenocysteine, a more reactive nucleophile. We successfully produced a redox sensing protein with increased sensitivity. However, this protein exhibited low expression levels and a greatly diminished dynamic range.

CHAPTER 1

Introduction

AIRWAY SENSORY NERVES

The respiratory tract is innervated by sensory nerves which aid in maintaining homeostasis, coordinating respiration, and protecting the airways from threats to gas exchange. These nerves are classified by the ganglionic location of the cell body. Bronchopulmonary sensory nerves (and other visceral sensory nerves) are vagal nerves as their cell bodies are contained in the vagal ganglia which is comprised of both the nodose and jugular ganglia. Although the jugular and nodose ganglia are fused in the mouse and closely juxtaposed in humans, they have differing embryonic origins as nodose neurons originate placode and jugular neurons are of neural crest origin(Nassenstein et al., 2010). Furthermore, gene expression profiles in the jugular and nodose ganglia are distinct(Nassenstein et al., 2010), indicating that they perform differing physiologic functions. Despite these phenotypic and embryonic differences, both nodose and jugular portions of the vagal ganglia project nerve fibers along branches of the vagus nerve (cranial nerve X) to innervate visceral organs including the lungs. Activation of these vagal sensory nerves stimulates of the nucleus tractus solitarius (NTS) in the brainstem which processes sensory information to coordinate responses a wide variety of responses and reflexes dependent upon the nature of the initiating stimulus(Canning, 2007). Thus, activation of pulmonary sensory nerves can evoke reflexes including the Hering–Breuer reflex which terminates inspiration and initiates expiration as well as defensive reflexes such as cough which serve to protect the lungs(Canning et al., 2006; Chou et al., 2008). To coordinate these responses

NTS neurons are part of large neuronal networks, receiving both sensory inputs and inputs from higher brain centers(Kubin et al., 2006). In the NTS, these inputs are integrated and processed by secondary neurons. Output form these secondary neurons projects to the parasympathetic preganglionic nerves, motor neurons which control the respiratory muscles (larynx, diaphragm, glottis, etc.), and to higher brain centers(Bonham et al., 2006).

Indeed, vagus nerves contain both afferent sensory and efferent parasympathetic nerve fibers. The efferent parasympathetic fibers aid in regulating many bodily functions including heart rate, peristalsis, and mucus secretion(Agostoni et al., 1957; Paintal, 1973). Activation of pulmonary efferent parasympathetic nerves triggers mucus production and bronchospasm(Canning and Fischer, 2001; Rogers, 2001). As the airway smooth muscle lacks sympathetic innervation, these vagal parasympathetic nerves are the primary regulators of bronchial tone(Kesler and Canning, 1999; Lewis et al., 2006). Thus, output can cause bronchoconstriction and impair respiration. While efferent nerves are important to enacting responses to stimuli, over 80% of vagal neurons are afferent sensory nerves which detect conditions in the local environment(Agostoni et al., 1957; Berthound and Neuhuber, 2000).

Afferent vagal sensory nerves are classified using several criteria including axon conduction speed and type of activating stimuli (ex: mechanical versus noxious thermal stimuli). While these classifications are useful in understanding the properties and functions of sensory nerves, they are somewhat ambiguous as some neurons fall into intermediate categories. However, vagal sensory nerves fall into two main subtypes: the myelinated, rapidly conducting Aβ and Aδ fibers and the unmyelinated, slowly conducting C-fibers. The Aβ and Aδ fibers are low-threshold mechanosensitive nerves and are largely activated by pulmonary stretch generated during respiration(Yu, 2005). Thus, CNS input from these fibers is utilized to aid in respiratory control and homeostatic maintenance. Mechanosensitive nerves are further subdivided into the slowly adapting stretch receptors (SAR) and rapidly adapting pulmonary stretch receptors (RAR).

SAR are insensitive to chemical stimuli and respond to pulmonary stretch: exhibiting an increased firing rate during pulmonary inflation and a decreased firing rate during pulmonary deflation(Adrian, 1933). Activation of SAR initiates the Hering–Breuer reflex which halts inspiration and initiates expiration(Widdicombe, 1954). In the lower airways, the RAR are also activated by pulmonary stretch, as they are activated by changes in pulmonary volume such as those observed during inspiration. However, in the upper airways, the RAR are activated by mechanical and chemical stimuli associated with aspiration of food, drink or stomach acid such as low osmolality and H^+(Widdicombe, 2003; Chou et al., 2008). Therefore, in the upper airways (trachea and larynx) RAR activation can evoke defensive reflexes whereas in the lower airways they are largely involved in homeostatic and respiratory regulation(Chou et al., 2008).

While the RAR detect some threatening stimuli, this is primarily performed by nociceptive nerves, which are unmyelinated, slowly conducting C-fibers. Approximately 75% of vagal sensory nerves are nociceptive and detect potentially harmful stimuli(Carr and Undem, 2003; Taylor-Clark et al., 2015). Indeed, the lungs are faced with threats from pollution, viral infections, and chemical irritants. These stimuli activate nociceptive nerves and elicit centrally mediated defensive reflexes such as cough, bronchospasm and mucus secretion to protect the lungs(Lee and Yu, 2014; Mazzone and Undem, 2016). Nociceptor activation can also evoke an axonal reflex involving the release of neuropeptides. A small portion of jugular nociceptors express neuropeptides such as tachykinins, and calcitonin gene related peptide (CGRP) which are stored in vesicles(Lundberg et al., 1984b; Dinh et al., 2003; Yu et al., 2005). In this subset of sensory nerves, activation triggers release of these neuropeptides into surrounding tissues producing local bronchoconstriction, mucus secretion and triggering a neurogenic inflammatory reaction(Lundberg et al., 1984a; Lou, 1993; D'Agostino et al., 2002; Quarcoo et al., 2004). Thus, inhalation of irritants such as cigarette smoke can evoke both defensive reflexes and inflammation(Andre et al., 2008). However, the importance of the axonal reflex in humans is likely

minimal as few neurons express these neuropeptides as compared to model organisms such as the guinea pig and rat (Ellis et al., 1997).

Protecting the lungs requires the detection of many, diverse potentially threatening stimuli. The key to this broad sensitivity is the expression of ion channels at the sensory nerve terminals. Each of these ion channels is activated by a specific set of stimuli. Thus, the sensitivity of sensory nerves to a specific stimulus is a direct result of the expression of specific ion channels. For instance, nociceptors express ion channels which are activated by potentially threatening stimuli as they express ion channels which are activated by potential harms such as noxious heat and cellular damage. Activation of these channels at sensory nerve terminals produces an influx of cations and a graded depolarization. If sufficient in magnitude, this results in sensory nerve activation and can evoke defensive reflexes and unpleasant sensations. Examples of these channels include acid sensing ion channels which detect low pH(Kollarik and Undem, 2002) and $P2X_{2/3}$ channels which are activated by extracellular ATP released from damaged cells(Weigand et al., 2012). However, two of the most studied ion channels expressed on nociceptive nerves are the nonselective cation channels transient receptor potential channels ankyrin 1 (TRPA1) and vanilloid 1 (TRPV1).

TRPA1 AND TRPV1

TRPA1 and TRPV1 are homotetrameric channels belonging to the TRP ion channel superfamily. Each subunit contains six transmembrane domains, a TRP box, and a cytosolic ankyrin repeat domain which mediates protein-protein interactions(Wu et al., 2010a). Members of the TRP ion channel superfamily are expressed on a wide variety of cell types and are activated by both chemical and physical stimuli including temperature, stretch, vibration, and osmotic pressure(Wu et al., 2010a). However, TRPA1 and TRPV1 are expressed almost exclusively on unmyelinated nociceptive neurons and are activated by threatening stimuli(Caterina et al., 1997;

Bessac and Jordt, 2008). TRPV1 expression is often used to identify nociceptive neurons as it is expressed on virtually all nociceptors(Szolcsanyi et al., 1988). TRPA1 is expressed in 39% of vagal neurons and is present 66% of vagal neurons which express TRPV1(Michael and Priestley, 1999; Kobayashi et al., 2005; Nassenstein et al., 2008). A wide array of potentially threatening stimuli activate TRPA1 and TRPV1 resulting in an influx of monovalent and divalent cations including Na^+ and Ca^{2+}(Tominaga et al., 1998; Bobkov et al., 2011). If large enough, this depolarization results in sensory nerve activation and initiates defensive reflexes and unpleasant sensations(Canning et al., 2004; Birrell et al., 2009). Additionally, the influx of Ca^{2+} can alter cellular signaling and trigger the release of neuropeptides. Thus, activation of TRPA1 and TRPV1 can trigger both defensive reflexes and neurogenic inflammation(Andre et al., 2008; Boillat et al., 2014). Although there are many TRPA1 and TRPV1 are expressed on many of the same nerves and both respond to a wide array of threatening stimuli, their regulation and specific sets of activating stimuli differ.

TRPV1 is best known as the “capsaicin receptor” as it is activated by capsaicin, a compound in hot peppers(Caterina et al., 1997). However, TRPV1 is polymodal and activated by a wide array of noxious compounds including low pH, N-arachidonoyl dopamine and lipoxygenase products(Caterina et al., 1997; Hwang et al., 2000; Bessac and Jordt, 2008; Morales-Lázaro et al., 2013). In addition to its function as a ligand gated channel, TRPV1 is thermosensitive as it is activated by noxious heat (>43^{o}C)(Caterina et al., 1997). Interestingly, extracellular H^+ increases the thermosensitivity of TRPV1, making it active at physiologic temperatures (37^{o}C)(Tominaga et al., 1998). It is believed that the hyperthermia observed during treatment with TRPV1 antagonists is due to blocking of this acid sensing function(Garami et al., 2010). Unfortunately, this has hindered the development of TRPV1 antagonists to treat pain disorders and other conditions involving the increased activity of TRPV1. The regulation of TRPV1 is complex and involves many competing factors including cytosolic Ca^{2+}, phosphatidylinositol 4,5-bisphosphate (PIP_2)(Prescott

and Julius, 2003), and signaling pathways including the phospholipase C/protein kinase C (PLC/PKC) and protein kinase A (PKA) pathways(Mohapatra and Nau, 2005; Lee et al., 2012). Interestingly, the PLC/PKC pathway sensitizes TRPV1 through several mechanisms(Rohacs et al., 2008). PIP_2, found in the inner leaflet of the cytosolic membrane constitutively inhibits TRPV1(Cao et al., 2013). PLC activation results in translocation to the cell membrane where it cleaves PIP_2, generating diacylglycerol (DAG) and inositol 1,4,5-trisphosphate (IP_3). Not only does this release PIP_2 inhibition, but DAG directly activates TRPV1(Woo et al., 2008). The IP_3 generated during cleavage of PIP_2 results in Ca^{2+} release form the endoplasmic reticulum. Together, the increased cytosolic Ca^{2+} and DAG activate PKC, which phosphorylates and sensitizes TRPV1(Vellani et al., 2001; Mandadi et al., 2006b; Wang et al., 2015).

As with TRPV1, TRPA1 is activated by a wide array of threatening stimuli. Activators of TRPA1 include noxious low temperatures (<17^{o}C), phytochemicals (ex: allyl isothiocyanate, AITC, in wasabi and allicin in garlic), chemical irritants found in pollution (ex: toluene and O_3^-)(Story et al., 2003; Bautista et al., 2005; Bautista et al., 2006; Bessac and Jordt, 2008; Taylor-Clark et al., 2009b; Taylor-Clark and Undem, 2010). In addition to being activated by exogenous compounds, TRPA1 is also activated by endogenous electrophilic compounds including reactive oxygen species (ROS), reactive nitrogen species (NOS) and 4-hydroxy-nonenal(Taylor-Clark et al., 2007; Trevisani et al., 2007; Andersson et al., 2008; Takahashi et al., 2008; Taylor-Clark et al., 2009a). This broad sensitivity of TRPA1 is a result of its generalized activation by electrophilic compounds which permits the detection of many threats to gas exchange such as smoke, inflammatory mediators, pollution and chemical irritants(Macpherson et al., 2007). The key to this sensitivity are highly reactive residues in the cytosolic domain, most notably the cysteine at amino acid 621(Bahia et al., 2016). This cysteine forms reversible covalent bonds with electrophiles, producing TRPA1 activation (Hinman et al., 2006; Macpherson et al., 2007; Bahia et al., 2016). This generalized electrophilic sensitivity results in activation of TRPA1 by most (if not all)

electrophiles, even with exposure to minute concentrations. Regulation of TRPA1 is performed by several factors including cytosolic Ca^{2+} and G coupled protein receptors such as the bradykinin receptor(Bautista et al., 2006). Interestingly, TRPA1 is both potentiated and inactivated by cytosolic Ca^{2+}: small increases in cytosolic Ca^{2+} potentiate TRPA1 while large increases in cytosolic Ca^{2+} inactivate TRPA1(Wang et al., 2008).

While TRPA1 and TRPV1 are activated by distinct stimuli and regulated through different mechanisms, their activity is linked through functional and physical interactions. Thus, the presence and activation of one channel affects the activity of the other channel. Simultaneous application of TRPA1 and TRPV1 agonists results in synergistic activation of sensory neurons(Hsu and Lee, 2015; Lin et al., 2015). Furthermore, activation of one channel (TRPA1 or TRPV1) produces Ca^{2+}-dependent desensitization of the other. TRPA1 desensitization resulting from TRPV1 activation occurs as a direct result of the elevation of intracellular Ca^{2+}(Ruparel et al., 2008). However, TRPA1 activation-induced TRPV1 desensitization occurs through dephosphorylation by the Ca^{2+}-dependent phosphatase calcineurin(Ruparel et al., 2008). In addition to these functional interactions, there is a physical interaction between the TRPA1 and TRPV1. It has been suggested that TRPA1 and TRPV1 can form heteromeric channels(Salas et al., 2009; Staruschenko et al., 2010) and functional TRPV1::TRPA1 concactomers which are sensitive to TRPV1 but not TRPA1 agonists have been generated(Fischer et al., 2014). More recently, it has been proposed that the physical association of TRPA1 and TRPV1 occurs through the transmembrane protein tMEM100(Weng et al., 2015). In the presence of tMEM100, the modulation of channel activity is dependent on the presence of one (TRPA1 or TRPV1) vs. both (TRPA1 and TRPV1) ion channels(Weng et al., 2015). As such, tMEM100 acts to increase TRPA1 activity in the presence of TRPV1 and decrease the TRPV1 activity when TRPA1 is not present(Weng et al., 2015). At this time, little is known of the precise nature of these interactions and the role they play, if any, in the development of disease states.

SENSORY NERVE ACTIVITY IN DISEASE STATES

In inflammatory pulmonary diseases, sensory nerves exhibit increased and aberrant activity, possibly due to increased TRPA1 and TRPV1 activation(Hathaway et al., 1993; Caceres et al., 2009). In murine models of asthma, a lower concentration of bronchoconstrictive compounds such as methacholine and histamine are required to elicit bronchoconstriction(Lewis and Broadley, 1995; Costello et al., 1999). Individuals suffering from inflammatory pulmonary diseases including asthma and COPD exhibit increased sensitivity to inhaled TRPV1 agonists, requiring a decreased concentration to elicit cough(Hathaway et al., 1993; Doherty et al., 2000). Taken together, indicates a state of sensory nerve hyperexcitability wherein sensory nerves exhibit increased activity and are activated by a lower stimulus threshold. This aberrant activity provides increased stimulation of the NTS and evokes excessive defensive reflexes (cough, bronchospasm, mucus secretion) and unpleasant sensations (dyspnea). While typically protective, these reflexes become debilitating and form the hallmark symptoms of pulmonary diseases. Interestingly, sensory nerve hyperexcitability and excessive defensive reflexes also contribute to the development of other disease states including diabetic neuropathy, and irritable bowel syndrome, gastroesophageal reflux disease and bladder dysfunction(Marchand et al., 2005; Hughes et al., 2013; McMahon et al., 2015). However, the mechanisms underlying the development of hyperexcitability, particularly under the influence of inflammation are poorly understood.

INFLAMMATION

Inflammation from events such as viral infection increases sensory nerve activity and produces symptomatic exacerbations of pulmonary diseases(Undem et al., 1999; Lee and Widdicombe, 2001; Zaccone and Undem, 2016). In murine models, inhalation of inflammatory agents (allergens) induce inflammation and sensory nerve hyperexcitability(Morris et al., 2003).

Further evidence supporting a role for sensory nerve hyperexcitability in disease is that vagotomy reverses allergen-induced airway hyperreactivity in response to methacholine(McAlexander et al., 2015). Additionally, ablation of TRPV1 expressing neurons prevents ovalbumin induced airway hyperreactivity(Trankner et al., 2014), indicating that sensory nerves play a large role in the development of pulmonary disease. However, how inflammation acts to alter their activity is not well understood. Inflammatory states are associated with many changes in the lungs including increased ROS, presence of inflammatory mediators, white blood cell infiltration and mitochondrial dysfunction(McBride et al., 1994; Braunstahl et al., 2003; Brozmanova et al., 2007). Furthermore, eosinophil and ROS levels are correlated with airway hyperresponsiveness(Jatakanon et al., 1998). Individuals with inflammatory pulmonary diseases have increased levels of pulmonary endogenous inflammatory mediators including H^+, lipoxygenase products, ROS, prostaglandin E_2 (PGE_2) and bradykinin(Kharitonov and Barnes, 2001; Rahman et al., 2002; Braunstahl et al., 2003). It has been shown that these inflammatory mediators, including PGE_2 and ROS (H_2O_2), can increase sensory nerve excitability(Ho et al., 2000; Lee and Widdicombe, 2001; Ruan et al., 2005). Not only is this association between inflammation and sensory nerve hyperexcitability present in disease states, but it is also present in inflammatory reactions arising from injury or infection. Peripheral injection of proinflammatory agents such as Complete Freund's Adjuvant (CFA) or carrageenan induces mechanical and thermal hyperalgesia. This hyperalgesia is greatly diminished by inhibition/knockout of either TRPA1 or TRPV1(Davis et al., 2000; Eid et al., 2008; Fernandes et al., 2010). While TRPA1 and TRPV1 are activated and sensitized by many individual inflammatory mediators and singling pathways(Carr et al., 2003; Kim et al., 2004; Grace et al., 2012), the role of individual mediators and signaling pathways in the development of hyperexcitability during inflammatory states is largely unknown. This opens the possibility that other, overlooked, factors may influence the development of sensory nerve hyperexcitability.

MITOCHONDRIA

One of these under-studied factors which may play a role in the development of sensory nerve hyperexcitability is mitochondrial dysfunction. Mitochondria are double membrane bound organelles best known for their role in ATP production. The outer membrane is highly porous and permeable to many ions and molecules under 5000 daltons. The inner membrane encloses the matrix and is folded and compartmentalized into cristae. These folds serve to increase surface area which is beneficial as the components of the mETC which is used for the generation of ATP are contained in the inner membrane. The initial substrates for the mETC are NADH and $FADH_2$ which are reduced at complexes I and II (respectively), releasing an electron. This released electron is transferred along a series of electron donors and acceptors to the terminal electron acceptor, O_2, generating water. At complexes I, III and IV, the energy generated from electron transfer pumps H^+ into the intermembrane space between the inner and outer mitochondrial membranes. This generates a negative electrochemical gradient (-150 to -180mV) relative to the cytoplasm which is used to drive production of ATP at complex V (ATP synthase). At complex V, the entry of H^+ into the matrix drives the reaction between ADP and a phosphate to generate ATP. While the mETC is highly efficient, electrons prematurely slip and partially reduce O_2 forming ROS such as O_2^- and H_2O_2. Although ROS are involved in cellular signaling(D'Autréaux and Toledano, 2007), they cause cellular damage through the oxidation of proteins and lipids(Radak et al., 2011). Therefore, cells express many proteins and molecules such as SOD, Catalase and GSH to convert ROS to H_2O to prevent cellular damage(Stowe and Camara, 2009).

While the production of ATP is essential to cellular function, the mitochondria play many other roles including regulating Ca^{2+} homeostasis and coordinating cellular stress responses(Wang and Wei, 2017). Thus, they serve as signaling hubs for pathways involving cellular growth, proliferation and stress responses(Chandel, 2014). Mitochondria are also the major source of cellular ROS which not only damages cells via the oxidation of lipids and proteins,

but it also serves to regulate cellular signaling(D'Autréaux and Toledano, 2007; Radak et al., 2011; Forrester et al., 2018). Inflammatory signaling pathways (TNFα and IL-1β) directly inhibit the mitochondrial electron transport chain (mETC) resulting in depolarization, increased ROS production, Ca^{2+} release, and initiating signaling events associated with cellular stress responses(Zell et al., 1997; Moe et al., 2004; Mariappan et al., 2009). This indicates a state of mitochondrial dysfunction which can lead to apoptosis; however, this is not always the case(Veatch et al., 2009; Guerra et al., 2017). Although mitochondrial dysfunction is present during inflammatory states and correlated with sensory nerve hyperexcitability, the influence of mitochondrial function on sensory nerve activity is unknown. Mitochondria are densely packed at sensory nerve terminals whereas axons contain relatively few mitochondria and handle much larger electrical currents(Hung et al., 1973; von During and Andres, 1988). This large number is likely not required for ATP production as inhibition of ATP synthase does not alter nerve behavior(Gover et al., 2007). However, this large number may serve to amplify the impact of the mitochondria on signaling events at the nerve terminal.

Evidence from clinical studies and animal models also suggest a role for mitochondria in the development of sensory nerve hyperexcitability in inflammatory pulmonary diseases. In murine models, mitochondrial dysfunction is correlated with the development of sensory nerve hyperexcitability(Mabalirajan et al., 2008). Asthmatics have an increased rate of specific mitochondrial DNA mutations(Zifa et al., 2012). Lung samples from individuals with inflammatory pulmonary diseases and experimental allergic asthma animal models contain mitochondria exhibiting morphological characteristics associated with dysfunction, increased levels of ROS and altered ROS scavenger activity(Emelyanov et al., 2001; Mabalirajan et al., 2008; Fitzpatrick et al., 2009; Reddy, 2011; Celik et al., 2012). In murine models, exposure to allergens such as pollen dust triggers ROS production and oxidative damage to mETC chain proteins(Aguilera-Aguirre et al., 2009). Several studies demonstrate that ROS such as H_2O_2 and O_2^- can sensitize and activate

bronchopulmonary C-fibers(Ho and Lee, 1998; Ruan et al., 2003; Lin et al., 2010). Several clinical studies demonstrate that antioxidant therapy decreases the severity of asthma(Gvozdjáková et al., 2005; Mabalirajan et al., 2009). However, despite this large body of evidence suggesting a role for mitochondrial dysfunction in the development of pulmonary disease, little is known of its direct impact on sensory nerve activity.

Inflammatory signaling results in many changes in cellular function which may alter TRPA1 and TRPV1 activity, to independently evaluate the impact of mitochondrial function on these channels specific mitochondrial modulators such as antimycin A (complex III inhibitor), carbonyl cyanide m-chlorophenyl hydrazone (CCCP, mitochondrial uncoupling agent), and rotenone (mETC complex I inhibitor) can be used (Fig. 1.1). Our lab has previously demonstrated that inhibition of the mETC complex III with antimycin A activates bronchopulmonary C-fibers likely through gating of TRPA1 and TRPV1. Antimycin A and the inhibition of mETC complex III induces mitochondrial depolarization, mitochondrial Ca^{2+} release, and ROS production(Potter and Reif, 1952; Slater, 1973; Reddy, 2011). Thus, mETC inhibition results in large-scale changes in cellular homeostasis and signaling many of which may serve to activate TRPA1 and TRPV1. TRPA1 is likely activated by increased mitochondrial ROS production as it is highly sensitive to activation by electrophiles, including ROS such as O_2^- and H_2O_2(Andersson et al., 2008; Takahashi et al., 2008). Furthermore, as TRPA1 reacts with electrophiles at a rate far greater than that for cellular antioxidant enzymes, this may allow for activation even in the presence of cellular antioxidant enzymes(Bahia et al., 2016). However, few studies demonstrate the activation of TRPV1 by oxidizing agents(Taylor-Clark and Undem, 2011). In studies which indicate the involvement of TRPV1 activation by oxidizing agents

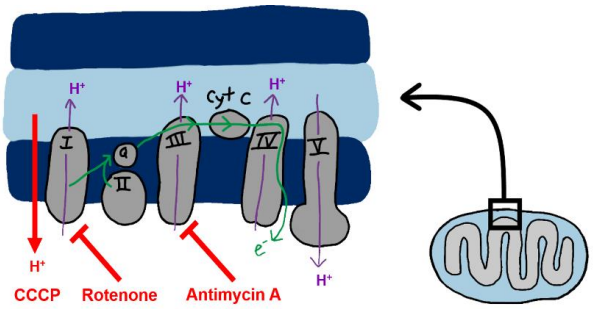

Figure 1.1: Action sites of specific mitochondrial modulators on the mETC and inner mitochondrial membrane.

used high concentrations (> 1mM) of H_2O_2(Susankova et al., 2006; Chuang and Lin, 2009). Although H_2O_2 induces sensory nerve hyperexcitability which is partially mediated by TRPV1(Ruan et al., 2005, 2006), H_2O_2 alters cellular signaling pathways including the PLC/PKC and NF-κB pathways(Cosentino-Gomes et al., 2012; Forrester et al., 2018) many of which sensitize and activate TRPV1. Therefore, TRPV1 activation during mitochondrial dysfunction likely occurs via another mechanism, possibly downstream of mitochondrial Ca^{2+} release. TRPV1 mediated sensitization in inflammatory states involves phosphorylation PKC(Ferreira et al., 2005). Furthermore, antimycin A can cause the activation and translocation of PKC(Wu et al., 2010b; Hadley et al., 2014) as well as mitochondrial Ca^{2+} release can also activate PLC(Cuchillo-Ibáñez et al., 2004). Taken together, this may induce TRPV1 activation though the production of DAG, depletion of PIP_2 and phosphorylation by PKC(Wu et al., 2010b; Hadley et al., 2014).

MEASURING TRPA1 AND TRPV1 ACTIVATION

Much evidence suggests that mitochondrial dysfunction and the increased activity of TRPA1 and TRPV1 contribute to sensory nerve hyperexcitability. However, little is known of the direct impact of mitochondria on sensory nerve function. One reason for this may be the requirement to study both mitochondrial function and ion channel activation. Another difficulty is the heterogenous nature of vagal neurons and the presence of many cell types in the vagal ganglia. Vagal neurons exhibit differential protein expression thus are functionally distinct. As a consequence, stimulus response differs between individual neurons, making it impossible to assay whole ganglia for mitochondrial function or ion channel activation. Thus, to study responses, measurements of individual neurons must be obtained. This can be achieved through using ex-vivo measurements of individual nerve fibers or measurements from dissociated neurons on coverslips. Nerve fiber recordings involve identifying nerve fibers of interest (ex: C-fibers) and measuring action potentials generated following ion channel activation. In dissociated neurons

there are two primary methods to measure ion channel activation: live cell cation imaging and electrophysiology. Electrophysiological methods involve both voltage and current patch clamp (whole cell, perforated patch, etc.). Voltage clamp measures channel activation though measuring current (largely Na^+) flowing through open ion channels whereas current clamp measures voltage changes generated during action potentials. While electrophysiological methods (patch clamp and nerve fiber recordings) are useful in studying activation of TRPA1 and TRPV1, obtaining data from a large number of cells is time consuming and labor intensive. Additionally, studying the impact of the mitochondria on TRPA1 and TRPV1 activation requires additional measurements of mitochondrial function such as mitochondrial depolarization and ROS production which are not easily combined with electrophysiological methods.

On the other hand, live cell imaging allows for simultaneous measurement of mitochondrial function (ROS production and mitochondrial polarization) and channel activation as well as the collection of data from many cells. As TRPA1 and TRPV1 are non-selective cation channels, their activation results in increased in cytosolic Na^+ and Ca^{2+}(Tominaga et al., 1998; Bobkov et al., 2011). Thus, channel activation can be measured using cytosolic Na^+ or Ca^{2+} indicator dyes which exhibit altered fluorescence when bound to these ions. Many such dyes are available, each differing in terms of their fluorescent properties (excitation/emission wavelengths), ionic specificity (ex: Na^+ vs Ca^{2+}), photostability, cellular loading efficiency, etc. This diversity of indicators allows for the selection of a dye which is best suited for the requirements of each individual experiment. As cytosolic Ca^{2+} is tightly regulated and resting concentrations are low(~100nM), TRPA1 and TRPV1 activation evokes a large fold change in cytosolic Ca^{2+}. However, Na^+ concentrations are less tightly controlled and there is a lower fold change with TRPA1 and TRPV1 activation. This lower fold change in cation concentration makes visualizing fluxes more difficult. Thus, Ca^{2+} imaging is the preferred method to measure TRPA1 and TRPV1 activation.

While there are many fluorescent cytosolic Ca^{2+} indicators, one of the most commonly used is FURA-2AM as it is highly specific for Ca^{2+}, is ratiometric, has a high fluorescence intensity, and its fluorescence is not significantly altered by cellular conditions such as pH. The key to its efficient loading and high cellular retention is that it is bound to two acetoxymethyl (AM) groups through an ester bond. These AM groups make the dye uncharged and membrane permeable. Upon diffusing into the cytosol, these groups are cleaved by cytosolic esterases, giving it a negative charge, rendering it membrane impermeable which decreases dye leak. Another key benefit of FURA-2AM is that it is ratiometric allowing for reliable measurements even with unequal cell loading and experimental irregularities. While not bound to calcium, FURA exhibits low fluorescence with 340nm excitation (510nm emission) and higher fluorescence with 380nm excitation (510nm emission). However, Ca^{2+}-bound FURA exhibits increased emissions with 340nm excitation and decreased emissions with 380nm excitation. As such, cytosolic calcium is measured using 340/380nm excitation ratio. While Ca^{2+} imaging using FURA-2AM is well suited to measure TRPA1 and TRPV1 activation, it can also be used to determine whether increases in cytosolic Ca^{2+} arises from an intracellular or extracellular source. To identify the source of the calcium flux, cells are exposed to a buffer lacking Ca^{2+} or a buffer with Ca^{2+} buffered to match the concentration of cytosolic Ca^{2+}(~100nM). Thus, in these buffers, ion channel activation fails to evoke increased cytosolic Ca^{2+}. However, if the source is from intracellular, an increase in cytosolic Ca^{2+} will be observed. Another way to perform these experiments is to block calcium entry with a pore blocker such as ruthenium red or gadolinium.

MEASURING MITOCHONDRIAL FUNCTION

Just as fluorescent indicator dyes can provide insights into channel activation, other dyes are available to investigate aspects of mitochondrial function including ROS production and mitochondrial membrane potential. The key to detecting mitochondrial membrane potential is the

cationic nature of membrane potential indicators and the highly negative mitochondrial membrane potential (-150 to -180 mV) relative to the cytoplasm. Thus, these positively charged dyes accumulate in the mitochondria via the electrochemical gradient. When the mitochondria depolarize, the negative membrane potential is lost, and the electrochemical gradient is no longer sufficient to retain the dye and it diffuses into the cytoplasm. One such dye, JC-1, forms J-aggregates at high concentrations in polarized mitochondria which exhibit red fluorescence (590nm emission)(Reers et al., 1991). Mitochondrial depolarization results in the dye diffusing into the cytoplasm. Under these conditions (lower concentrations), it is in monomeric form and exhibits green fluorescence (525nm emission). Although this allows for ratiometric measurements (red/green) of mitochondrial membrane potential, the J-aggregates require long incubation times to reach equilibrium(Perry et al., 2011). Therefore, measurements of only the monomeric form (equilibrium in ~15 minutes) are often used.

Although measurements of mitochondrial membrane potential provide important insights into mitochondrial function, ROS measurements are also essential to assessing the impact of mitochondria on TRPA1 and TRPV1 activation. While many ROS sensitive dyes are available, the principle underling ROS detection is similar: unreacted dyes exhibit low fluorescence and upon oxidation by ROS florescence increases(Zhang and Gao, 2015). One useful property of these dyes is that they possess varying specificities for different ROS such as H_2O_2 versus O_2^-. Furthermore, cationic ROS indicators, such as MitoSOX Red, accumulate in the mitochondria permitting measurements of mitochondrial ROS while eliminating the influence of ROS from other cellular sources(Dickinson et al., 2010). Unfortunately, most of dyes are neither ratiometric nor reversible and there are often caveats to their use. One such caveat for dihydroethidium the requirement for it to bind DNA after oxidation to produce a fluorescent signal(Ortega-Villasante et al., 2016). Another redox indicator, dihydrorhodamine 123, requires the presence a cofactor (Fe^{2+} or cytochrome c) for oxidation to occur(Ortega-Villasante et al., 2016). One method to measure

ROS that avoids many of these caveats is use of genetically encoded redox sensing proteins. However, these proteins lack the sensitivity offered by dyes.

INCREASING THE SENSITIVITY OF roGFP1

Genetically engineered redox sensitive proteins are ratiometric, reversible and can be targeted to subcellular compartments such as the mitochondrial intermembrane space and endoplasmic reticulum(Hanson et al., 2004; Delic et al., 2010). Currently available genetically encoded redox sensors include redox sensitive green, red, and yellow fluorescent proteins(Sugiura et al., 2015). Their function relies on the reversible reduction and oxidation of two reactive cysteines which serve as a biological switch. Oxidation by ROS results in disulfide bond formation which alters protein conformation and fluorescence(Dooley et al., 2004; Hanson et al., 2004). Reduction breaks this bond, restoring the protein to its original state(Hanson et al., 2004). In the case of roGFP1, a variant of redox sensitive green fluorescent protein, oxidation/reduction shifts fluorescence between two excitation maxima (405nm and 470nm; 510nm emission)(Dooley et al., 2004; Hanson et al., 2004). Thus, cellular ROS production is measured using the 405nm/470nm excitation ratio. While these reversible and ratiometric properties make roGFP1 well suited for measuring ROS, it lacks the sensitivity required to detect small scale changes in ROS which are involved in cellular signaling events. One factor contributing to the relative insensitivity of roGFP1 is the protonation of its redox-sensitive cysteines under physiologic cellular conditions: only deprotonated cysteines are able to react with ROS(Roberts et al., 1986). Several attempts have been made to improve the sensitivity of roGFP1 by mutating amino acids surrounding the reactive cysteines decrease their pKa (from ~8.2)(Cannon and Remington, 2006). While these changes have improved sensitivity, these proteins still lack the sensitivity of redox-sensitive dyes and are unable to measure many physiologically relevant changes in ROS production.

One potential method to improve the sensitivity of roGFP1 is the use of a more reactive amino acid such as selenocysteine in place of one, or both cysteines(Dooley, 2006). Selenocysteine is structurally identical to cysteine however, in the place of sulphur it contains selenium. This substitution makes it a more reactive nucleophile (pKa of 5.5 vs 8.2)(Byun and Kang, 2011). As selenocysteine forms bridges with both itself and cysteine, replacing one or both of the reactive cysteines in roGFP1 with selenocysteines should generate a functional redox sensor(Müller et al., 1994). However, selenocysteine incorporation is more complex and inefficient compared to insertion of canonical amino acids as its incorporation occurs at UGA codons which typically serve to stop protein translation(Chambers et al., 1986). Thus, incorporation requires additional elements including a selenocysteine insertion sequence (SECIS) in the 3' untranslated region of the mRNA and a selenocysteine specific elongation factor. However, even in the presence of all required elements, insertion remains inefficient with translation stalling at the UGA codon, producing in protein truncation. To increase incorporation, selenoproteins can be co-expressed with selenocysteine binding protein 2 (SBP2), which helps coordinate the proximity of the required insertional elements(Zinoni et al., 1990; Tujebajeva et al., 2000). Thus, SBP2 decreases stalling at the UGA codon, increasing insertional efficiency and decreasing truncation. Therefore, co-expression of SBP1 with a roGFP selenoprotein should permit sufficient expression to measure ROS production in live cell imaging experiments.

LIVE CELL CO-IMAGING

The many methods available for live cell imaging allows for the selection of an indicator dye with specific properties ideally suited for each experiment. In the case of understanding the impact of mitochondrial function on the activation of TRPA1 and TRPV1, this requires the simultaneous use of two indicators: one to measure cytosolic cation fluxes and another to measure mitochondrial function. While traditional live cell imaging employs one dye and

measures one aspect of cellular function, the differing spectral properties of these indictors allows for the simultaneous use of two indicators(Miyazaki and Ross, 2015). However, indicators whose spectral excitation and emission wavelengths differ are required. For example: to measure ion channel activation and mitochondrial membrane potential, a combination of FURA-2AM and JC-1 can be used and to measure ROS production and ion channel activation a combination of MitoSOX Red and FURA-2AM can be used. Measurements of the fluorescence of both dyes simultaneously can be achieved using sequential excitation of all required excitation and emission wavelengths. Thus, using live cell co-imaging, correlations can be made between ion channel activation and mitochondrial function.

CHAPTER 2

Relative contributions of TRPA1 and TRPV1 in the response to mitochondrial inhibition

INTRODUCTION

Activation of TRPA1 and TRPV1 results in nociceptive sensory nerve activation and evokes sensations of dyspnea and defensive reflexes such as cough, bronchospasm and mucus secretion(Tatar et al., 1988; Nassenstein et al., 2008; Birrell et al., 2009; Brozmanova et al., 2012). Inflammation alters peripheral nerve activity and results in aberrant sensory nerve activity which evokes excessive, defensive reflexes which serve no protective function and are detrimental(Lee and Widdicombe, 2001). Much evidence suggests a role for TRPA1 and TRPV1 in the development of aberrant sensory nerve activity under the influence of inflammation. Individuals with inflammatory pulmonary diseases have in increased sensitivity to TRPV1 agonists, requiring a lower concentration to evoke cough(Nakajima et al., 2006). Inhibition of TRPA1 decreases cough following exposure to inflammatory mediators including PGE_2 and bradykinin(Grace et al., 2012). Furthermore, TRPA1 and TRPV1 are involved in the development of mechanical and thermal hyperalgesia in many mouse models of inflammatory pain(Davis et al., 2000; Petrus et al., 2007; Fernandes et al., 2010). Inflammatory states have a profound impact in the lungs including a decreased pH, white blood cell infiltration, increased ROS, mitochondrial dysfunction, activation of signaling pathways involved in cellular stress responses. Due to this wide array of effects and the polymodal nature of TRPA1 and TRPV1, it is likely that overlooked factors such as mitochondrial dysfunction may play a role in the increased activity of these ion channels in inflammatory states.

Our lab has previously studied the effects of mitochondrial dysfunction on sensory nerve activation by using antimycin A(Nesuashvili et al., 2013), a mETC complex III inhibitor which inhibits the Q_i site on complex III, blocking electron transfer(Potter and Reif, 1952; Turrens et al., 1985a). Not only does this inhibit ATP production, but this inhibition also causes mitochondrial depolarization, mitochondrial Ca^{2+} release and increases electron slippage from the mETC. As these released electrons incompletely reduce O_2, complex III inhibition results in increased H_2O_2 and O_2^- production(Gyulkhandanyan and Pennefather, 2004; Muller et al., 2004; Stowe and Camara, 2009). As these same events are observed in mitochondrial dysfunction induced with inflammatory signaling(López-Armada et al., 2013; Strzelak et al., 2018), this method provides a valid approach to studying the effects of mitochondrial function on sensory nerve activity. We found that antimycin A selectively activates nociceptive C-fibers (ex-vivo lung-vagal ganglia preparation) and isolated vagal neurons (Ca^{2+} imaging) which express TRPA1 and/or TRPV1. In isolated vagal neurons, this activation was abolished in the absence of extracellular Ca^{2+}, indicating that a plasma membrane Ca^{2+} permeable ion channel, such as TRPA1 and/or TRPV1 was involved. Indeed, both KO and inhibition of TRPA1 and TRPV1 decreased the action potential discharge in the ex-vivo lung-vagal prep and decreased Ca^{2+} fluxes in isolated vagal neurons. These responses were largely abolished with dual inhibition of TRPA1 and TRPV1 in isolated vagal neurons. These findings were confirmed in HEK293 cells as TRPA1 and TRPV1 transfected but not non-transfected cells as antimycin A evoked a Ca^{2+} flux in Ca^{2+} imaging experiments and increased current in whole cell patch clamp experiments.

Here, we further investigated responses antimycin A evoked mitochondrial dysfunction in isolated vagal neurons to evaluate the relative contributions of TRPA1 and TRPV1 using live cell Ca^{2+} imaging of dissociated vagal neurons. These studies are complicated by the co-expression TRPA1 and TRPV1 on most nociceptive neurons as well as the functional and physical interactions between these two channels. Not only can activation of one channel affect the activity

of the other, but the expression of one versus both channels affects channel activity(Salas et al., 2009; Weng et al., 2015). Therefore, it is important to study the contributions of each channel using both inhibition and knockout (KO) models. Given that antimycin A induced responses appear dependent on TRPA1 and TRPV1 which are heterogeneously expressed in vagal neurons, we have chosen to use VR1 CreRosa which expresses td Tomato in TRPV1 lineage neurons to aid in the identification of nociceptive neurons. However, TRPA1 responses in vagal VR1 CreRosa neurons have not yet be characterized. Therefore, we first characterized TRPA1 responses to establish the feasibility of this approach. We found that 78% of neurons expressed td Tomato with 76% of these td Tomato+ neurons exhibiting a Ca^{2+} flux during AITC and/or capsaicin treatment. Of the 22% of neurons did not express td Tomato and 18% of these td Tomato- neurons responded to ATIC or capsaicin. Therefore, using VR1 CreRosa neurons, nociceptors were defined as being either TRPV1 lineage neurons (express td Tomato) or non-TRPV1 lineage neurons which responded to AITC (see methods). However, in KO models this method of nociceptor classification is not possible. Therefore, in experiments using KO mice, nociceptors were identified based on the functional responses to AITC (TRPV1 KO) or capsaicin (TRPA1 KO).

Using this method for nociceptor identification, we found that antimycin A activated only a portion of nociceptive neurons with non-responding nociceptors exhibiting a response similar to that of non-nociceptive neurons. The Ca^{2+} influx across all neurons was diminished with TRPA1 KO, TRPA1 inhibition, TRPV1 KO, and TRPV1 inhibition and further reduced with dual knockout/inhibition for both channels. Interestingly, neither inhibition nor KO of TRPA1 diminished the percentage of neurons which responded to Antimycin A. However, inhibition and KO of TRPA1 diminished the Ca^{2+} flux in responding neurons. Conversely, inhibition and knockout of TRPV1 decreased in the percentage of responding neurons while having no effect on the Ca^{2+} flux in responding neurons. While large-scare Ca^{2+} fluxes were isolated to a portion of

nociceptive neurons, both non-nociceptive neurons and non-responding neurons also exhibited an increase in cytosolic Ca^{2+}, albeit much lower than that for responding neurons. This influx was prevented using the Ca^{2+} channel blockers GD^{3+} + Ruthenium red and with extracellular Ca^{2+} buffered to match cytosolic Ca^{2+} (100mM), indicating the involvement of another plasma membrane Ca^{2+} permeable ion channel. However, our attempts to block this with inhibition of TRPM7, a ROS-sensitive, Ca^{2+} permeable channel that is expressed on all neurons, were unsuccessful. Therefore, the identity of the channel involved in the small-scale Ca^{2+} fluxes remains unknown.

RESULTS

Characterization of VR1 CreRosa

Due to the difficulties posed in the classification of nociceptive versus non-nociceptive neurons, we used a VR1 CreRosa mouse model to classify TRPV1 lineage neurons. This mouse model expresses td Tomato in all cells which have ever expressed TRPV1. Thus, TRPV1 lineage neurons can be identified using td Tomato fluorescence. We found that there was a large Ca^{2+} flux in response to AITC and capsaicin which was largely isolated to neurons expressing td Tomato (Fig. 2.1 A and B). It is important to note that the classification of capsaicin responses was complicated by the lack of washout following AITC treatment. However, 61% of neurons (n = 68) expressed td Tomato and responded to AITC and/or capsaicin (Fig. 1.1 C) and therefore likely currently express TRPA1 and/or TRPV1. td Tomato was present in an additional 17% of neurons (n = 21) which did not exhibit a Ca^{2+} flux in response to ATIC or capsaicin. The remaining 22% of neurons (n = 28) did not express td Tomato. Of these td Tomato- neurons, only 5 (4% of all neurons) responded to AITC or capsaicin. Taken together, this indicates that classifying nociceptors as the population of neurons which is either of TRPV1 lineage (expresses td Tomato) or responds to AITC is likely to identify all neurons which express TRPA1 and/or TRPV1.

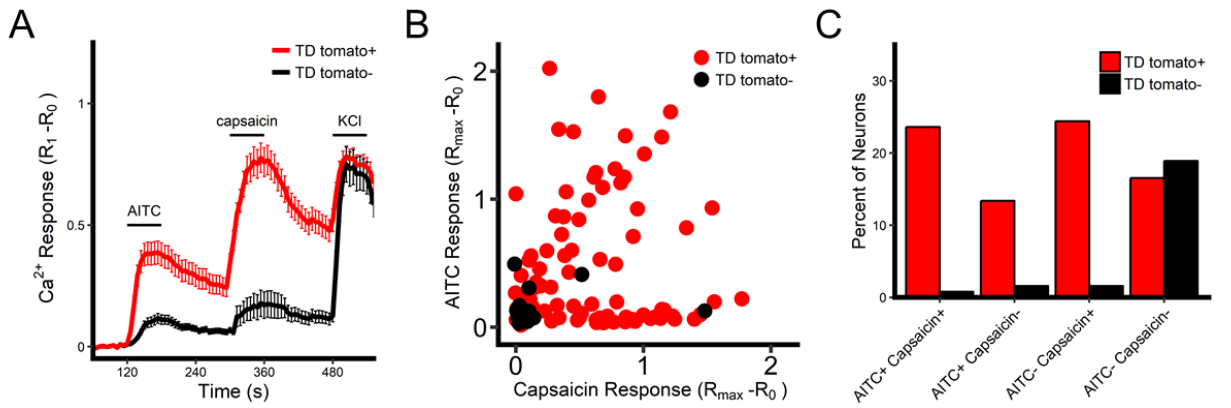

Figure 2.1: AITC and Capsaicin responses are largely isolated to td Tomato expressing neurons. Time course of cytosolic Ca^{2+} fluxes in td Tomato expressing and non-expressing neurons (A) with the magnitude of Ca^{2+} fluxes in response to ATIC and capsaicin (b) and barograph depicting the percentage of neurons which express td Tomato and respond to AITC or capsaicin.

Antimycin A activates a portion of vagal neurons

To evaluate the relative contributions of TRPA1 and TRPV1 in the response to mitochondrial modulation, we first evaluated antimycin A-evoked cytosolic Ca^{2+} fluxes in VR1 CreRosa neurons. As TRPA1 and TRPV1 are non-selective cation channels, their activation results in increased in cytosolic Ca^{2+}. Indeed, antimycin A evoked a large increase in cytosolic Ca^{2+} (averaged across all neurons) (Fig. 2.1 A and B). Consistent with our hypothesis, these responses were isolated to nociceptive neurons, many of which express TRPA1 and/or TRPV1. However, only a portion of these neurons responded with nonresponding nociceptors exhibiting a response similar to that of non-nociceptive neurons. Indeed, these experiments demonstrate a great heterogeneity of responses between responding nociceptors, non-responding nociceptors and non-nociceptors (Fig. 2.2 C). In Fig. 2.2 C, it is important to note that the AITC and capsaicin responses were affected by prior exposures which did not return to baseline due to the long time periods involved in reversing Ca^{2+} fluxes. Therefore, we used the baseline prior to antimycin A treatment to calculate responses.

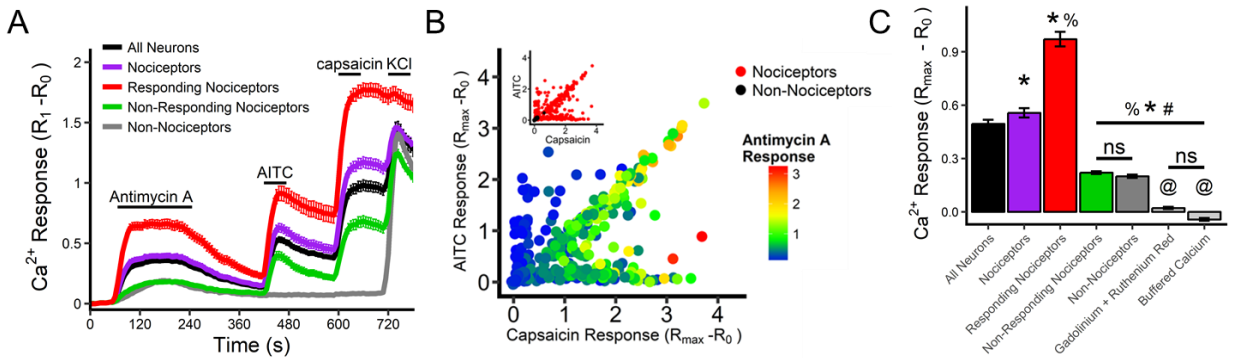

Figure 2.2: Antimycin A evokes Ca^{2+} responses in a portion of nociceptors. Cytosolic Ca^{2+} fluxes averaged across all neurons, and in neuronal subpopulations as defined by nociceptive status and antimycin A responses as time course (A) and bar graph (B) which also contains buffered calcium and calcium blocking responses (all neurons). * denotes $p < .05$ versus all neurons. % denotes $p < .05$ versus nociceptive neurons. # denotes $p < .05$ versus all responding nociceptors. @ denotes difference vs non-responding nociceptors and non-nociceptors.

Blocking and buffering external Ca^{2+}

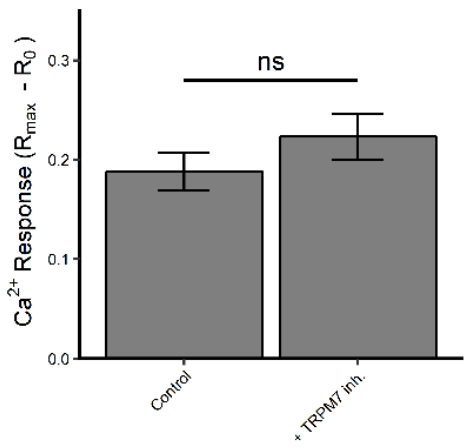

Figure 2.3: TRPM7 inhibition with NS8593 has no effect on Ca^{2+} fluxes in non-nociceptive neurons.

While large responses were isolated to nociceptive vagal neurons, we observed a cytosolic Ca^{2+} flux of a much lower magnitude in both non-nociceptive neurons and non-responding nociceptors. As antimycin A evokes mitochondrial depolarization and calcium release, there is the possibility that this flux is a result of the release of internal Ca^{2+} stores or the activation of a Ca^{2+} permeable ion channel on the plasma membrane. We investigated the source of this Ca^{2+} flux using two methods: 1) buffering external Ca^{2+} to match the cytosolic Ca^{2+} concentration (100nM) and 2) blocking external Ca^{2+} with the Ca^{2+} channel blockers Gd^{3+} + Ruthenium Red. As both these methods prevented the Ca^{2+} flux ($p < .05$ vs non-nociceptive) (Fig. 2.2 C), this indicated that the activation of an ion channel on the

plasma membrane was responsible these Ca^{2+} fluxes. We further investigated this hypothesis by inhibiting TRPM7(Wu et al., 2010a), a Ca^{2+} permeable ion channel which is expressed in all sensory neurons, activated by H_2O_2(Yoshida et al., 2006), and blocked by Ruthenium Red and Gd^{3+}(Numata et al., 2007). However, inhibition of TRPM7 using NS8593(Chubanov et al., 2012) failed to diminish Ca^{2+} fluxes ($p > .05$) (Fig. 2.3).

Relative contributions of TRPA1 and TRPV1

Due to the heterogeneity of responses and difficulties posed by nociceptor classifications, we evaluated the relative contributions of TRPA1 and TRPV1 using 1) the Ca^{2+} flux magnitude across all neurons 2) the portion of neurons which responded and 3) the Ca^{2+} flux magnitude in responding neurons. We isolated the contributions of TRPA1 and TRPV1 using both KO and inhibition to remove the influence of the other channel. As such, to study the impact of TRPV1 we used we used KO ($TRPA1^{-/-}$) and inhibition ($TRPA1_{inh}$: A967079) of TRPA1 and to study the impact of TRPA1 we used KO ($TRPV1^{-/-}$) and inhibition of TRPV1 ($TRPV1_{inh}$: iodoresiniferatoxin, I-RTX). To eliminate the influence of both channels, we used dual KO/inhibition of both TRPA1 and TRPV1 using three conditions: 1) $TRPV1_{inh}$ + $TRPA1_{inh}$, 2) $TRPV1_{inh}$ + $TRPA1^{-/-}$ and 3) $TRPV1^{-/-}$ + $TRPA1_{inh}$. Using these experimental conditions, we were able to evaluate the relative contributions of TRPA1 and TRPV1 while controlling for the interactions between TRPA1 and TRPV1. In both TRPV1 only ($TRPA1^{-/-}$ $p<.05$, $TRPA1_{inh}$ $p<.05$), and TRPA1 only ($TRPV1^{-/-}$ $p<.05$, $TRPV1_{inh}$ $p<.05$)(Fig. 2.4 A, B, D) conditions diminished Ca^{2+} flux (averaged across all neurons) which was further decreased in dual inhibition/KO conditions ($p< .05$ vs. VR1 CreRosa, TRPV1 only, and TRPA1 only) (Fig. 2.4 C, D). Interestingly, the percentage of responding neurons was diminished in TRPA1 only ($TRPV1_{inh}$ 17% $p<.05$, $TRPV1^{-/-}$ 13% $p<.05$) but not TRPV1 only ($TRPA1^{-/-}$ 38%, $TRPA1_{inh}$ 36%) conditions (Fig. 2.4 E) as compared to VR1 CreRosa (36%). With eliminating of the influence of both TRPA1 and TRPV1 using dual KO/inhibition, fewer than 5%

of neurons responded (p<.05 vs VR1 CreRosa, TRPA1 only and TRPV1 only) (Fig. 2.4 E). As so few neurons responded, these conditions were eliminated from further analyses of the Ca^{2+} flux in responding nociceptors. In the responding neurons, there was a diminished Ca^{2+} flux in TRPV1 only (p <.05, $TRPA1^{-/-}$ and $TRPA1_{inh}$) but not TRPA1 only (p>.05, $TRPV1^{-/-}$ and $TRPV1_{inh}$) conditions (Fig. 2.4 F).

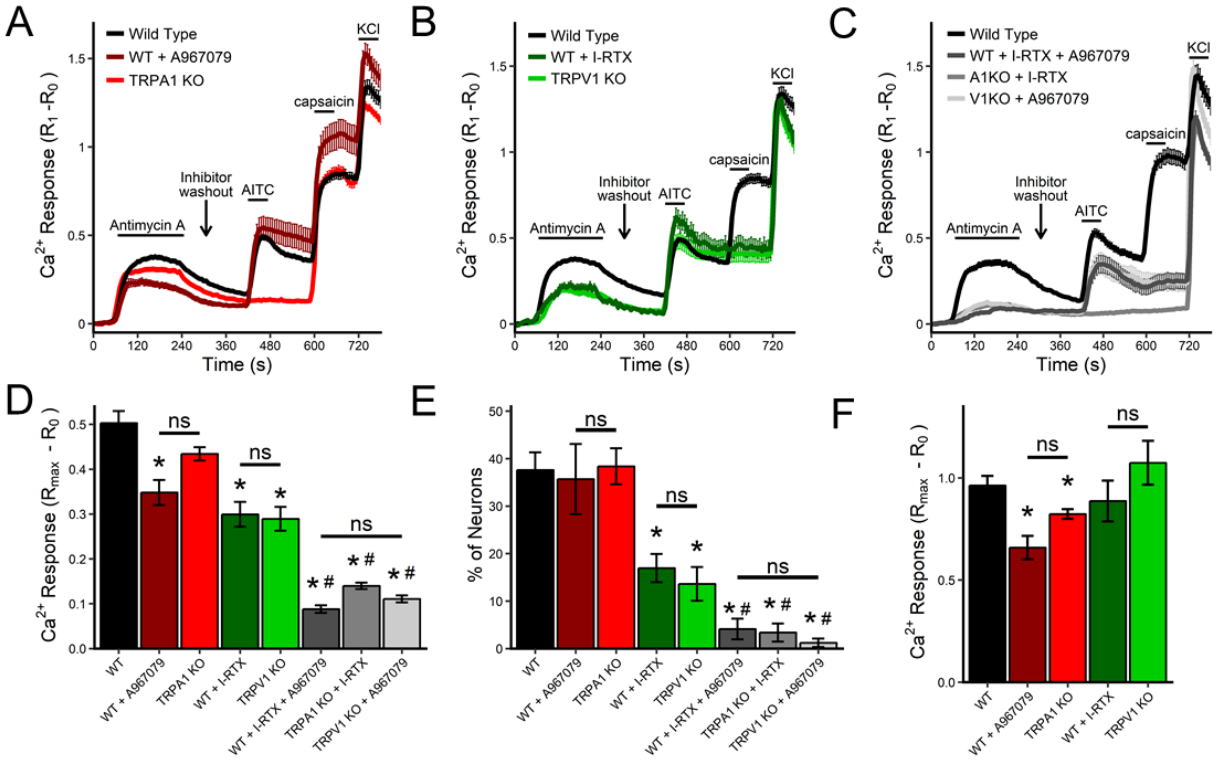

Figure 2.4: Antimycin A evoked Ca^{2+} fluxes (all neurons) are decreased KO and inhibition of TRPA1 or TRPV1 and further decreased with dual KO/inhibition. Ca^{2+} fluxes are diminished with (A)TRPA1-/-, TRPA1inh (B)TRPV1, TRPV1 and further decreased with (C)$TRPA1_{inh}$ + $TRPV1_{inh}$, $TRPA1^{-/-}$ + $TRPV1_{inh}$ and $TRPA1_{inh}$ + $TRPV1^{-/-}$. Bar graphs depicting mean +/- SEM (D)Ca^{2+} flux, (E)percentage of responding neurons, and (F)Ca^{2+} flux in responding neurons. * denotes difference from wild type (p < .05), # denotes difference from single KO/inhibition of TRPA1 or TRPV1 (p < .05).

Due to the impact of TRPA1 and TRPV1 on both the percentage on neurons responding and the Ca^{2+} flux magnitude, we depicted this relationship using density histograms. (Fig. 2.5). It must be noted that although we used the VR1 CreRosa mouse model for all wild type conditions, we used wild type mice for the WT + IRTX condition. Therefore, classifications in WT + I-RTX

neurons relied on functional responses to AITC and capsaicin. Overall, in wild type neurons a large portion of nociceptors exhibit a large Ca^{2+} flux while the non-responding nociceptors exhibit a response similar to that of non-nociceptive neurons (Fig. 2.5 A). However, in dual inhibition/KO conditions with neither TRPA1 nor TRPV1 is available, responses are largely abolished (Fig. 2.5 B-D). In studies of the contribution of TRPV1 ($TRPA1^{-/-}$ and $TRPA1_{inh}$), there is a decreased overall Ca^{2+} flux attributed to the decreased response in responding nociceptors as there was no change in the percent of responding neurons. (Fig. 2.5 E-F, Fig 2.4 E-F). The opposite was true in studies of the contribution of TRPA1 ($TRPV1^{-/-}$ and $TRPV1_{inh}$), as the Ca^{2+} flux in responding neurons was unchanged while there was a decrease in the percent of responding neurons (Fig 2.2 E-F, Fig 2.4 G-H).

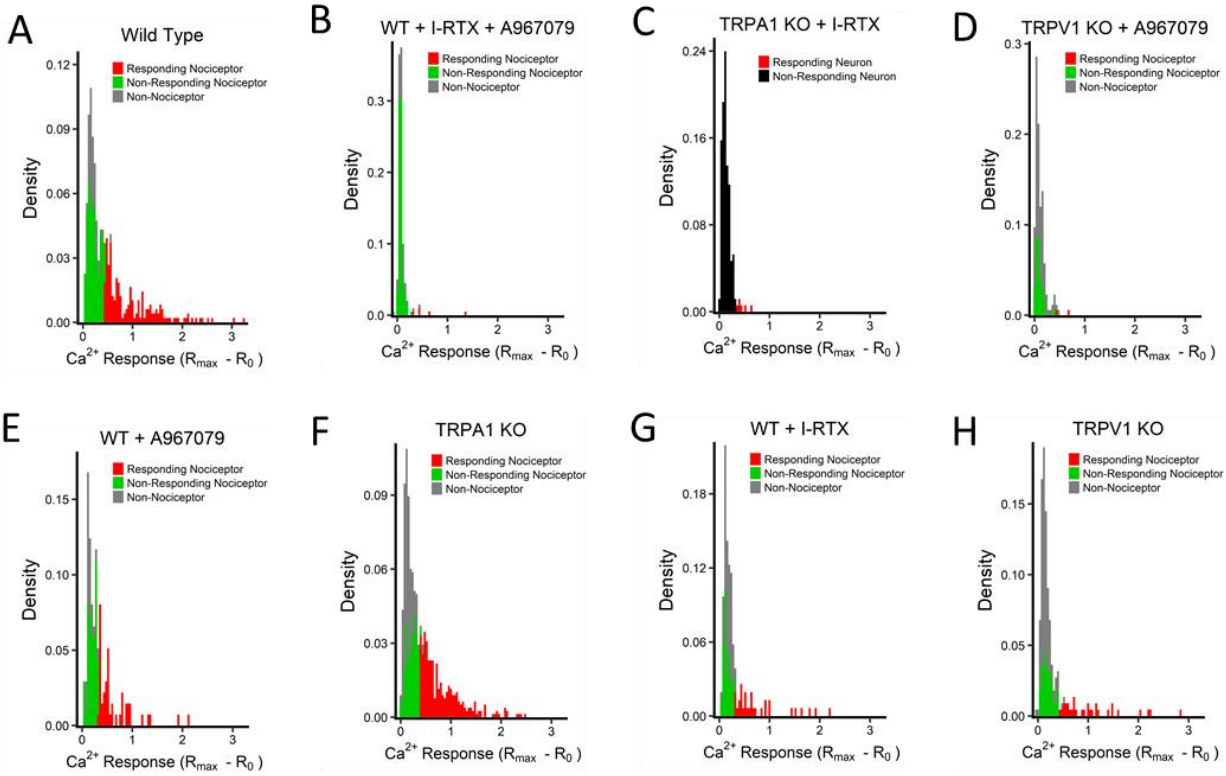

Figure 2.5: Density histograms for antimycin A evoked cytosolic Ca^{2+} fluxes in (A) wild type, (B)$TRPA1_{inh}$ + $TRPV1_{inh}$, (C)$TRPA1^{-/-}$ + $TRPV1_{inh}$, (D) $TRPA1_{inh}$ + $TRPV1^{-/-}$, (E)$TRPA1_{inh}$, (F)$TRPA1^{-/-}$, (G)$TRPV1_{inh}$, and (H)$TRPV1^{-/-}$ in non-nociceptive, responding nociceptive and non-responding nociceptive neurons.

DISCUSSION

Here, we characterized the VR1 CreRosa mouse model which expresses td Tomato in all cells which have ever expressed TRPV1 (including those that no longer express TRPV1). We found that with this model, 82% of vagal neurons were classified as nociceptive which is in line with current knowledge indicating that 77% of vagal neurons respond to TRPA1 and/or TRPV1 agonists(Taylor-Clark et al., 2007). Using our classification system (see common methods), only 4% of nociceptors did not express td Tomato yet responded to AITC or capsaicin. This is largely due to TRPA1 expression in non-TRPV1 lineage neurons as not all TRPA1 expressing neurons express TRPV1. It has been previously demonstrated that TRPA1 is expressed in approximately 9% of neurons which do not express TRPV1(Taylor-Clark et al., 2008a). However, we did observe a Ca^{2+} flux during treatment with capsaicin in two of these neurons. This could be due to either the recent expression of TRPV1 in the mouse prior to euthanasia or expressional changes which occur during cell culture as TRPV1 and TRPA1 expression is increased by growth factors(Diogenes et al., 2007; Xue et al., 2007) present in the fetal bovine serum (FBS) used to supplement the media. Although FBS must be used for neuronal survival, its effects on protein expression are minimized by using neurons within 24 hours of isolation. Additionally, due to the low number of neurons which responded to capsaicin, this is unlikely to affect nociceptor classification or experimental results.

Confirming our lab's prior work, antimycin A evoked a large Ca^{2+} flux which was isolated to nociceptive neurons most of which express TRPA1 and/or TRPV1. However, while large-scale Ca^{2+} fluxes were isolated to nociceptive neurons, there was a much smaller Ca^{2+} flux observed in but non-nociceptive neurons and non-responding nociceptors. This could be due to either extracellular or intracellular calcium sources. As antimycin A evokes mitochondrial depolarization and Ca^{2+} release, the release of mitochondrial Ca^{2+} stores could explain this flux. However, this could be due to activation of a Ca^{2+} permeable plasma membrane ion channel. We investigated

these possibilities by preventing cellular Ca^{2+} entry using channel blockers (Gd^{3+} + Ruthenium red) and buffering the extracellular Ca^{2+} concentration to match the intercellular Ca^{2+} concentration. As these methods blocked these Ca^{2+} fluxes, this suggests the activation of a Ca^{2+} permeable plasma membrane ion channel. We identified TRPM7 as a possible contributor to this response. However, inhibiting TRPM7 failed to diminish this Ca^{2+} flux. Although it is possible that buffering extracellular Ca^{2+} and blocking cellular Ca^{2+} entry alters Ca^{2+} homeostasis in such a way that Antimycin A is incapable of triggering calcium release, it is more likely that this Ca^{2+} flux is due to the activation of an unknown plasma membrane ion channel.

Despite these small-scale Ca^{2+} fluxes in all neurons, it is evident that either TRPA1 or TRPV1 are required for the larger-scale Ca^{2+} fluxes observed in a portion (60% of nociceptors, 36% of all neurons) of nociceptive neurons. This is demonstrated by the decreased Ca^{2+} fluxes observed with inhibition and KO of TRPA1 or TRPV1 and the abolishment Ca^{2+} flux observe with in dual KO/inhibition of TRPA1 and TRPV1. Interestingly, TRPA1 and TRPV1 affected Ca^{2+} fluxes in different ways. While TRPV1 KO and inhibition largely affected the percentage of responding neurons (no effect on Ca^{2+} flux magnitude in responding neurons), TRPA1 KO and inhibition largely affected the magnitude of Ca^{2+} fluxes in responding neurons (no effect on percentage of neurons responding). These relationships between the percentage of responding neurons and magnitude of Ca^{2+} fluxes are most easily visualized in the density histograms. Although TRPA1 is expressed in a much lower percentage of vagal neurons (37% of neurons) in comparison to TRPV1 (66% of neurons)(Nassenstein et al., 2008; Nassenstein et al., 2010), the impact of this on the percentage of neurons which responded with TRPV1 inhibition and KO conditions is unclear. Unfortunately, studying the influence of expressional differences in antimycin A evoked Ca^{2+} fluxes is complicated by the long times required for calcium responses to return to baseline, possible desensitization of TRPA1 following antimycin A treatment which hiders identification of TRPA1 expressing neurons. Furthermore, there is no mouse model

equivalent to VR1 CreRosa for TRPA1 that can facilitate identification of TRPA1 expressing neurons.

One of the most interesting findings is that only a portion of nociceptors responded during antimycin A treatment. Using our dual KO/inhibition conditions we confirmed that the large-scale Ca^{2+} fluxes were indeed a result of TRPA1 and TRPV1 activation. Interestingly, many neurons expressing TRPA1 and/or TRPV1, many did not respond to antimycin A treatment. The reason underlying these differential responses (response vs non-response) is unknown. However, these differential responses could be due to the heterogeneous nature of vagal neurons, baseline cellular redox state, mitochondrial metabolic status or other cellular signaling status. In the next chapter we investigate aspects of mitochondrial function including mitochondrial polarization and ROS production on channel activation to provide insight into the relationship between mitochondrial function and the activation of TRPA1 and TRPV1.

UNIQUE METHODS

No unique methods used.

CHAPTER 3

Mitochondrial modulation-induced activation of vagal sensory neuronal subsets by antimycin A, but not CCCP or rotenone, correlates with mitochondrial superoxide production[1]

INTRODUCTION

Inflammation, infection, physical damage and exogenous irritants are capable of significant nociceptor activation. As such, excessive activation of this sensory subpopulation contributes to a wide-range of disease states including chronic pain, irritable bowel disease, colitis, arthritis and asthma(Marchand et al., 2005; McMahon et al., 2015). It has been shown that nociceptive neurons, many of which express TRPA1 and/or TRPV1 are important to the development of sensory nerve hyperexcitability in allergic asthma(Buckley and Nijkamp, 1994; Trankner et al., 2014). Currently, the effects of inflammatory states on sensory nerve activity are not fully understood. One potential way in which inflammation may cause nociceptor activation is by inducing the dysfunction of mitochondria, which are densely packed within sensory nerve terminals(Hung et al., 1973; von During and Andres, 1988). Mitochondrial dysfunction encompasses events including morphology changes, ROS production, mitochondrial depolarization and calcium release. While catastrophic mitochondrial dysfunction induces apoptosis, mitochondrial dysfunction also initiates signaling events involved in cellular stress responses. Chronic inflammation induces changes in mitochondrial morphology associated with

[1] This study has been previously published in PLoS One Stanford, K.R., and T.E. Taylor-Clark. 2018. Mitochondrial modulation-induced activation of vagal sensory neuronal subsets by antimycin A, but not CCCP or rotenone, correlates with mitochondrial superoxide production. *PLoS One*. 13:e0197106. and is included with permission under the Creative Commons Attribution (CC BY) license.

dysfunction(Mabalirajan et al., 2008), and there are reports of an increased rate of mitochondrial DNA mutations and altered activity of ROS scavengers such as glutathione and superoxide dismutase in inflammatory states(Raby et al., 2007; López-Armada et al., 2013; Van Tilburg et al., 2014). Inflammatory signaling has been shown to directly inhibit complexes I, II, and IV of the mitochondrial electron transport chain (mETC), resulting in ROS production and mitochondrial depolarization(Stadler et al., 1992; Colell et al., 1997; Zell et al., 1997; Lopez-Armada et al., 2006). However, the direct impact of this on sensory nerve activity is largely unknown.

We have previously demonstrated that mitochondrial dysfunction induced by antimycin A, an mETC complex III inhibitor, activates vagal sensory neurons and bronchopulmonary C-fibers via the gating of TRPA1 and TRPV1(Nesuashvili et al., 2013). Inhibition of complex III by antimycin A induces ROS production and mitochondrial depolarization(Chinopoulos et al., 1999; Starkov and Fiskum, 2001), but the role of these events in mitochondrial dysfunction-induced neuronal activation has not been established. Here we investigated the influence of mitochondrial dysfunction on the activation of vagal sensory neurons using three mitochondrial agents: antimycin A, carbonyl cyanide m-chlorophenyl hydrazone (CCCP, mitochondrial uncoupling agent), and rotenone (mETC complex I inhibitor). Using live cell co-imaging, we simultaneously monitored cytosolic calcium (as a surrogate for neuronal activation) and either mitochondrial superoxide production or changes in mitochondrial polarization. We found that the three agents activated (i.e. caused significant calcium fluxes) only a subset of TRPA1 and/or TRPV1 expressing (A1/V1+) neurons, yet there was no difference in mitochondrial superoxide production or mitochondrial depolarization between ‘responding’ and ‘non-responding’ A1/V1+ neurons. Nevertheless, we observed a significant correlation between antimycin A-induced calcium responses and mitochondrial superoxide production in wild-type ‘responding’ A1/V1+ neurons, which was eliminated in TRPA1$^{-/-}$ neurons, but not TRPV1$^{-/-}$ neurons. CCCP-induced calcium responses did not correlate with either superoxide production or mitochondrial depolarization.

Rotenone-induced calcium responses correlated with mitochondrial depolarization but not superoxide production. Our data are consistent with the hypothesis that mitochondrial dysfunction causes the activation of a subset of A1/V1+ neurons via ROS-dependent and ROS-independent mechanisms.

RESULTS

Correlation between mitochondrial O_2^- production and Ca^{2+} responses

Endogenous mediators modulate mitochondria at several different sites, thus we investigated neuronal responses to three mitochondrial agents: antimycin A (Complex III inhibitor), CCCP (uncoupling agent) and rotenone (Complex I inhibitor). We evaluated the contribution of mitochondrial superoxide production to neuronal activation by simultaneously measuring mitochondrial superoxide (MitoSOX Red) and cytosolic calcium (Fura-2AM) in dissociated vagal neurons using live cell co-imaging in response to antimycin A (10μM, n = 282 from 8 experiments), CCCP (10μM, n = 266 from 10 experiments), rotenone (5μM, n = 177 from 6 experiments) or DMSO vehicle (0.1%, n = 122 from 7 experiments). Approximately 60% of vagal sensory neurons were defined as A1/V1+, i.e. they subsequently responded to a combined treatment of 1μM capsaicin and 100μM AITC. All three agents produced a substantially larger increase in $[Ca^{2+}]_i$ in the A1/V1+ neuronal population compared to the A1-V1- population ($p<0.05$)(Fig. 3.1 A, B, C, I). Indeed the vehicle also produced a minor, yet significant, increase in $[Ca^{2+}]_i$ in A1/V1+ neurons versus A1-V1- neurons ($p<0.05$)(Fig. 3.1D, I). Nevertheless the increase in $[Ca^{2+}]_i$ in A1/V1+ neurons in response to antimycin A, CCCP and rotenone was significantly greater than that evoked by vehicle ($p<0.05$)(Fig. 3.1 I). This data is consistent with our previous studies demonstrating antimycin A evoked calcium transients that were dependent on extracellular calcium and TRPA1 and TRPV1(Nesuashvili et al., 2013). Only CCCP evoked an increase in $[Ca^{2+}]_i$ in A1-V1- neurons that was greater than vehicle ($p<0.05$)(Fig. 3.1 B, D I).

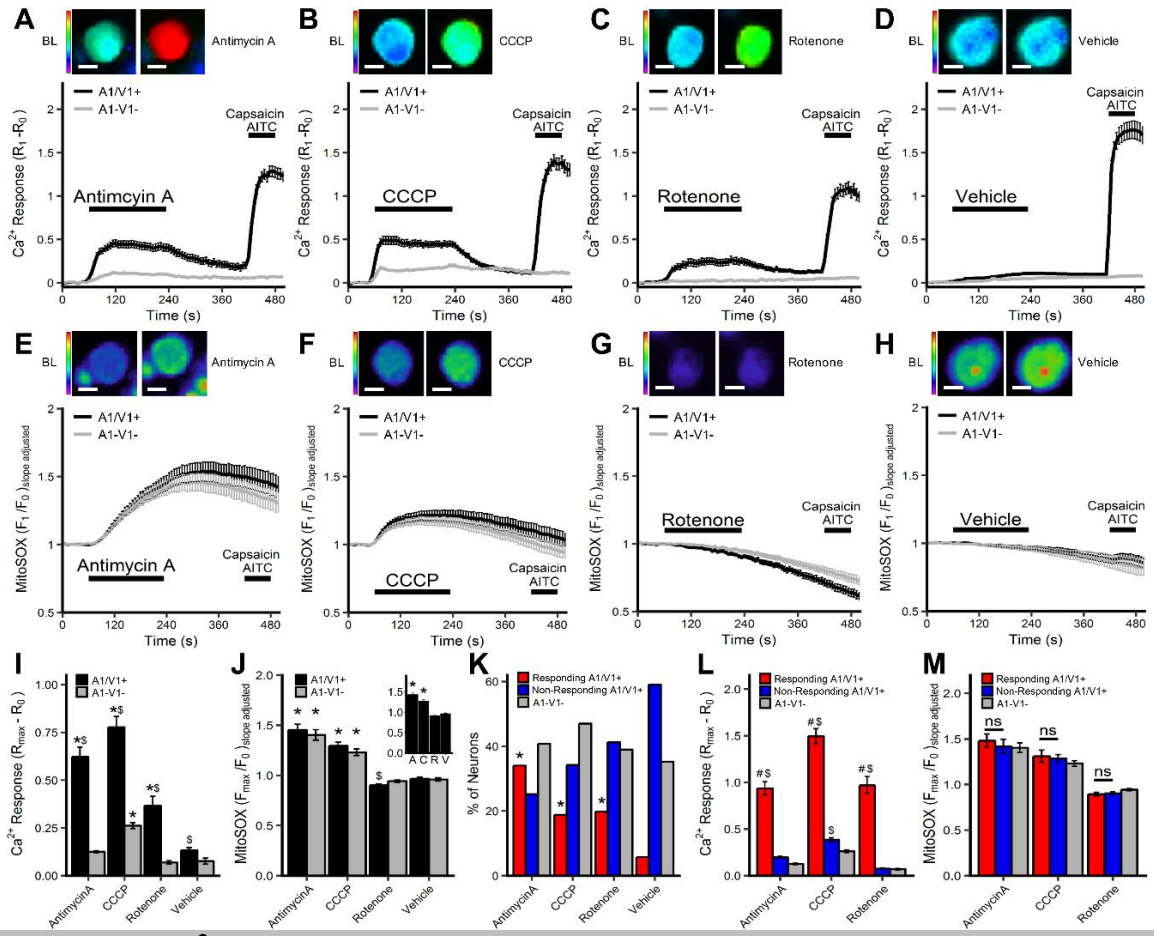

Figure 3.1: $[Ca^{2+}]_i$ and mitochondrial superoxide responses of vagal neurons to antimycin A, CCCP, rotenone and vehicle. Mean +/- SEM $[Ca^{2+}]_i$ responses (A–D) and mitochondrial superoxide (MitoSOX) responses (E–H) in A1/V1+ (black line) and A1-V1- (grey line) neurons treated with 10μM antimycin A (A, E), 10μMCCCP (B, F), 5μM rotenone (C, G) and 0.1% DMSO (D, H). Each panel includes representative Fura-2AM/MitoSOX image of an A1/V1+ neuron before and after treatment with the mitochondrial agent. A1/V1+ neurons are defined by increase in $[Ca^{2+}]_i$ following AITC/Caps treatment. (I) Mean +/- SEM maximal $[Ca^{2+}]_i$ response ofA1/V1+ and A1-V1- neurons. (J) Mean +/- SEM maximal mitochondrial superoxide response ofA1/V1+ and A1-V1- neurons (insert, mean +/- SEM maximal mitochondrial superoxide response of all neurons). (K) Percentage of neurons defined as 'responding' A1/V1+ neurons, 'non-responding' A1/V1+ neurons and A1-V1- neurons. (L) Mean +/- SEM maximal $[Ca^{2+}]_i$ response of responding' A1/V1+ neurons, 'non-responding' A1/V1+ neurons and A1-V1- neurons. (M) Mean +/- SEM maximal mitochondrial superoxide response of 'responding' A1/V1+ neurons, 'non-responding' A1/V1+ neurons and A1-V1- neurons. * denotes significant difference compared to vehicle ($p<0.05$), $ denotes significant difference between A1/V1+ and A1-V1- groups ($p<0.05$), # denotes significant difference between 'responding' and 'non-responding' A1/V1+ groups ($p<0.05$), ns denotes non-significance ($p>0.05$).

MitoSOX measurements in the dual imaging studies showed that antimycin A and CCCP evoked significant mitochondrial superoxide production compared to vehicle in A1/V1+ neurons,

A1-V1- neurons and the total neuronal population ($p<0.05$)(Fig. 3.1 E, F, H, J) ($p<0.05$). Despite the differences in calcium responses between A1/V1+ and A1-V1- populations, there was no differences in the magnitude of mitochondrial superoxide production in A1/V1+ and A1-V1- neurons evoked by either antimycin A or CCCP ($p>0.05$)(Fig. 3.1 E, F J). Rotenone failed to evoke significant mitochondrial superoxide production in either A1/V1+, A1-V1- or total populations compared to vehicle (Fig. 3.1 G, H, J). In general, rotenone had a minor inhibitory effect on the accumulation of MitoSOX fluorescence, which was more pronounced in the A1/V1+ population compared to the A1-V1- population ($p<0.05$)(Fig. 3.1 G, J).

When we evaluated the calcium responses on a cell-by-cell basis we found that the mitochondrial agents only increased $[Ca^{2+}]_i$ beyond that evoked in A1-V1- neurons in a proportion of A1/V1+ neurons (see methods for definition of the threshold): antimycin A: 96/167, CCCP: 50/141, rotenone: 35/108 (Fig. 3.1 K). This 'responding' A1/V1+ population represents the A1/V1+ neurons 'activated' by the mitochondrial modulators and, consistent with this, the increase in $[Ca^{2+}]_i$ evoked by antimycin A, CCCP and rotenone was significantly greater in the 'responding' A1/V1+ population than either the 'non-responding' A1/V1+ or A1-V1- populations ($p<0.05$)(Fig. 3.1 L). CCCP-evoked increases in $[Ca^{2+}]_i$ were marginally yet significantly greater in 'non-responding' A1/V1+ compared to A1-V1- neurons ($p<0.05$), but this was not the case for either antimycin A or rotenone ($p>0.05$)(Fig. 3.1 L). Importantly, there was no difference in mitochondrial superoxide production between 'responding' and 'non-responding' A1/V1+ neurons or A1-V1- neurons for any of the mitochondrial modulators ($p>0.05$)(Fig. 3.1 M).

Scatterplot analysis of the calcium and MitoSOX responses (Fig. 3.2) showed that mitochondrial superoxide production in response to antimycin A and CCCP was highly variable in all neuronal populations (i.e. 'responding' A1/V1+, 'non-responding' A1/V1+, and A1-V1- groups). Overall, only 40% and 23% of neurons exhibited an increase in mitochondrial superoxide production following treatment with antimycin A and CCCP, respectively (compared to 1.6% for

vehicle, see methods for calculation). Antimycin A-evoked calcium responses correlated with mitochondrial superoxide production in the responding A1/V1+ population and in the total A1/V1+ population ($p<0.05$)(Fig. 3.2 A, Table 3.1). However, there was no correlation between calcium and MitoSOX responses for CCCP in any neuronal population ($p>0.05$)(Fig. 3.2 B, Table 3.1). Rotenone failed to evoke mitochondrial superoxide production in any neuronal population (0%) and as such there was no correlation between calcium and MitoSOX responses ($p>0.05$)(Fig. 3.2 C, Table 3.1).

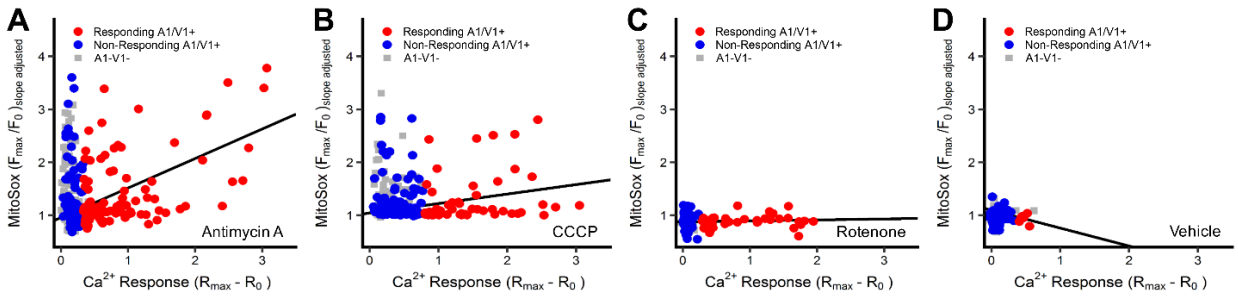

Figure 3.2: Mitochondrial superoxide responses correlates with $[Ca^{2+}]_i$ responses for antimycin A, but not CCCP or rotenone. Co-imaging of $[Ca^{2+}]_i$ and superoxide in neurons treated with 10μM antimycin A (A), 10μM CCCP (B), 5μM rotenone (C) and 0.1% DMSO (D). Trendlines depict the correlation across all A1/V1+ neurons. Slope and significance of each trendline is presented in Table 3.1.

Table 3.1: Trendlines for the correlation of $[Ca^{2+}]_i$ and mitochondrial superoxide in subsets of vagal A1/V1+ neurons after treatment with antimycin, CCCP and rotenone.
* denotes $p < 0.05$

	Responding A1/V1+			Non-responding A1/V1+			A1/V1+		
	Slope	**p**	**Sig**	**Slope**	**p**	**Sig**	**Slope**	**p**	**Sig**
Wild Type									
Antimycin A	0.48	3.03e-8	*	-0.04	0.99		0.31	2.68e-6	*
CCCP	0.27	0.06		-0.03	0.72		0.13	0.15	
Rotenone	0.41	0.31		-0.02	0.71		-0.06	0.51	
Vehicle	-0.15	0.69		0.10	0.13		0.00	0.51	
TRPA1 -/-									
Antimycin A	0.04	0.23		-0.01	0.84		0.05	0.10	
TRPV1 -/-									
Antimycin A	0.42	0.03	*	-0.01	0.95		-0.04	0.74	

We have shown previously that antimycin A-induced calcium responses in nociceptive neurons were largely dependent on calcium influx through the cation channels TRPA1 and TRPV1(Nesuashvili et al., 2013). Here, we found in a separate series of Fura-2AM studies in vagal neurons (n = 381) that increases in $[Ca^{2+}]_i$ in A1/V1+ neurons in response mitochondrial modulation were largely dependent on extracellular calcium (Fig. 3.3). There were no differences in calcium responses in A1/V1+ and A1-V1- neurons in response to antimycin A (10μM), CCCP (10μM), rotenone (5μM) or DMSO vehicle (0.1%) when extracellular calcium was buffered to 75nM with EGTA ($p>0.05$). Only CCCP evoked significantly greater responses in vagal neurons compared to vehicle ($p<0.05$), suggesting that some of the CCCP-evoked calcium transient (in both A1/V1+ and A1-V1- neurons) was dependent on intracellular stores.

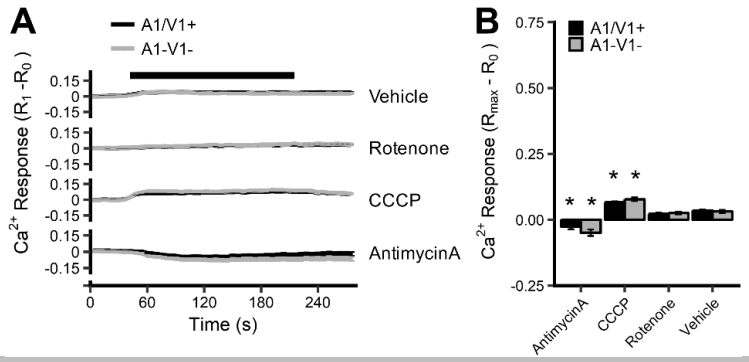

Figure 3.3: $[Ca^{2+}]_i$ responses of vagal neurons to antimycin A, CCCP, rotenone and vehicle in the nominal absence of extracellular calcium. (A) Mean +/- SEM $[Ca^{2+}]_i$ responses in A1/V1+ (black line) and A1-V1- (grey line) neurons treated with 10μM antimycin A, 10μM CCCP, 5μM rotenone and 0.1% DMSO. Blocked line denotes stimulus application. A1/V1+ neurons are defined by increase in $[Ca^{2+}]_i$ following AITC/Caps treatment in the presence of 2.5mM $CaCl_2$ (data not shown). (B) Mean +/- SEM maximal $[Ca^{2+}]_i$ response of A1/V1+ and A1-V1- neurons. * denotes significant difference compared to vehicle ($p<0.05$), $ denotes significant difference between A1/V1+ and A1-V1- groups ($p<0.05$).

TRPA1 is directly activated by ROS(Andersson et al., 2008; Sawada et al., 2008; Takahashi et al., 2008), whereas there is little evidence that TRPV1 is activated by ROS(Andersson et al., 2008; Sawada et al., 2008; Ogawa et al., 2016). We therefore investigated antimycin A-evoked Fura-2AM calcium and MitoSOX responses in vagal neurons from $TRPA1^{-/-}$ and $TRPV1^{-/-}$ mice (n = 258 from 9 experiments and n = 201 from 10 experiments, respectively).

$[Ca^{2+}]_i$ and mitochondrial superoxide production correlated in 'responding' trpv1$^{-/-}$ A1+ neurons ($p<0.05$)(Fig. 3.4 A, Table 3.1) but not in 'responding' trpa1$^{-/-}$ V1+ neurons ($p>0.05$)(Fig. 3.4 B, Table 3.1). Similar to the wild-type A1/V1+ neurons, mitochondrial modulation with antimycin A failed to evoke calcium responses in all trpv1$^{-/-}$ A1+ neurons, suggesting the possibility that some neurons expressing the TRPA1 channel were insensitive to ROS. Sequential exposure of vagal neurons from TRPV1$^{-/-}$ mice (n = 202 from 7 experiments) to antimycin A (10μM), H_2O_2 (300μM) and then AITC (100μM), showed that a significant proportion of antimycin-insensitive, A1+ neurons did indeed respond to the H_2O_2 with an increase in calcium (Fig. 3.4 C, D). This data confirms the sensitivity of TRPA1 channels in these neurons to exogenously applied ROS H_2O_2.

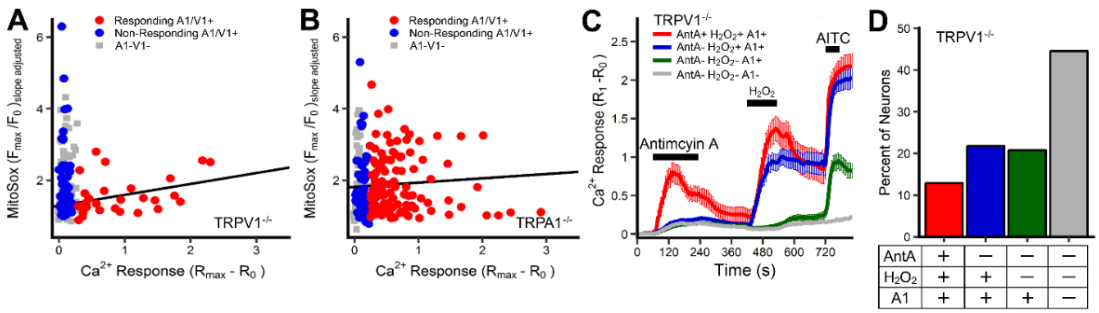

Figure 3.4: Antimycin A-induced $[Ca^{2+}]_i$ responses correlates with mitochondrial superoxide responses in trpv1-/- A1+ neurons but not trpa1-/- V1+ neurons. Co-imaging of $[Ca^{2+}]_i$ and superoxide in neurons treated with 10μM antimycin A in neurons from TRPV1-/- (A) and TRPA1-/- (B) mice. Trendlines depict the correlation across all A1/V1+ neurons. Slope and significance of each trendline is presented in Table 1. (C) Mean +/- SEM $[Ca^{2+}]_i$ responses in neurons from TRPV1-/- mice treated with 10μM antimycin A, 300μM H_2O_2 and 100μM AITC. Neurons allocated to groups based upon sensitivity to the stimuli. A1+ defined by response to AITC. (D) Percentage of neurons from TRPV1-/- mice allocated to groups shown in C.

Correlation between mitochondrial depolarization and Ca^{2+} responses

Given that our data suggests that mitochondrial superoxide is not the only determinant of mitochondrial modulation-induced A1/V1+ neuronal activation, we next investigated mitochondrial depolarization–another hallmark of mitochondrial dysfunction. We performed live cell co-imaging of cytosolic Ca^{2+} (Fura-2AM) and mitochondrial polarization (JC-1) during treatment with antimycin A (10μM, n = 90 from 6 experiments), CCCP (10μM, n = 210 from 10 experiments),

rotenone (5μM, n = 112 from 7 experiments) and DMSO vehicle (0.1%, n = 129 from 8 experiments) (Fig. 3.5).

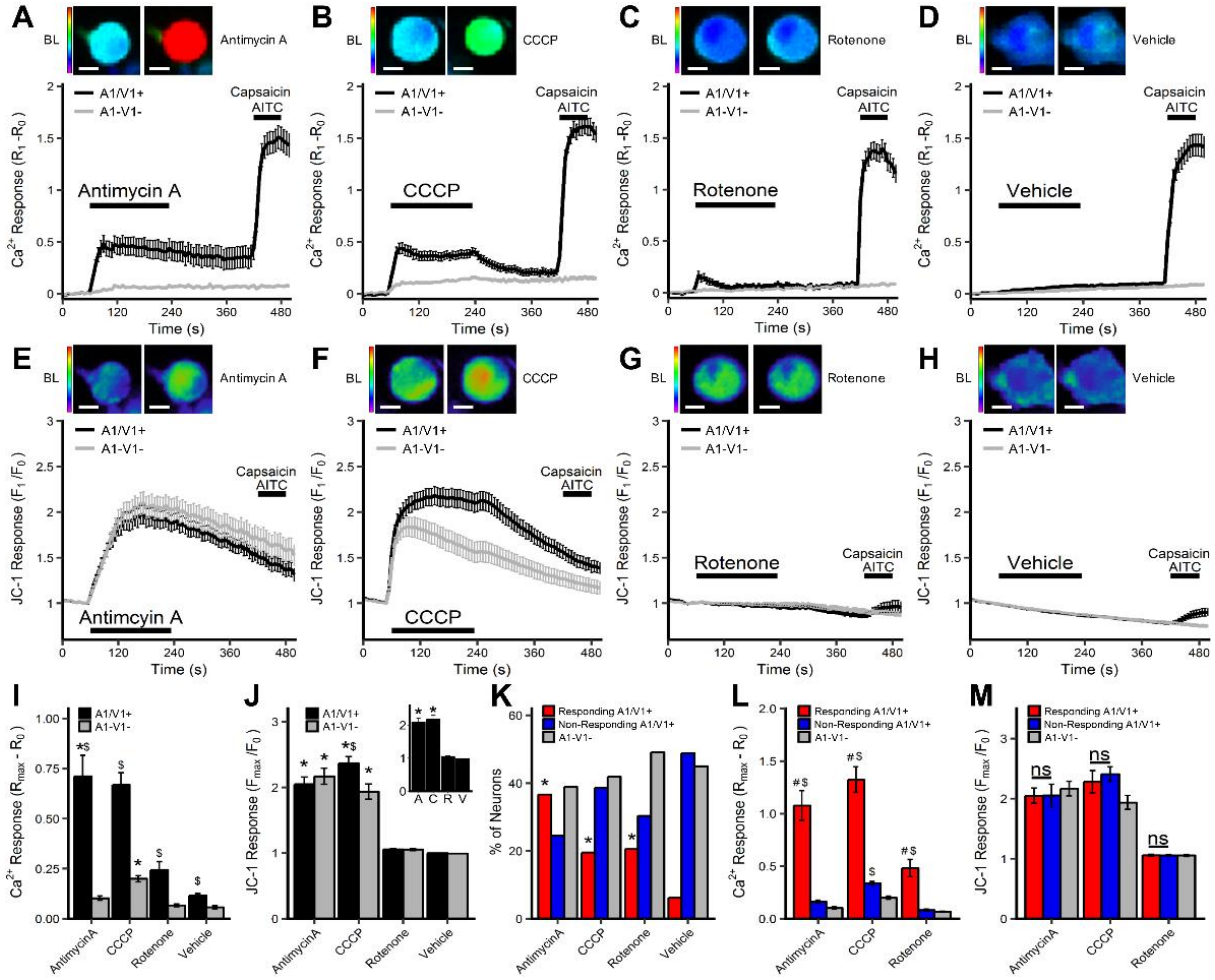

Figure 3.5: $[Ca^{2+}]_i$ and mitochondrial polarization responses of vagal neurons to antimycin A, CCCP, rotenone and vehicle. Mean +/- SEM $[Ca^{2+}]_i$ responses (A–D) and mitochondrial polarization (JC-1) responses (E–H) in A1/V1+ (black line) and A1-V1- (grey line) neurons treated with 10μM antimycin A (A, E), 10μM CCCP (B, F), 5μM rotenone (C, G) and 0.1% DMSO (D, H). Each panel includes representative Fura-2AM/JC-1 image of an A1/V1+ neuron before and after treatment with the mitochondrial agent. A1/V1+ neurons are defined by increase in $[Ca^{2+}]_i$ following AITC/Caps treatment. (I) Mean +/- SEM maximal $[Ca^{2+}]_i$ response of A1/V1+ and A1-V1- neurons. (J) Mean +/- SEM maximal mitochondrial depolarization of A1/V1+ and A1-V1- neurons (insert, mean +/- SEM maximal mitochondrial depolarization of all neurons). (K) Percentage of neurons defined as 'responding' A1/V1+, 'non-responding' A1/V1+ and A1-V1-. (L) Mean +/- SEM maximal $[Ca^{2+}]_i$ response of 'responding' A1/V1+, 'non-responding' A1/V1+ and A1-V1-. (M) Mean +/- SEM maximal mitochondrial depolarization of 'responding' A1/V1+, 'nonresponding' A1/V1+ and A1-V1-. * denotes significant difference compared to vehicle ($p<0.05$), $ denotes significant difference between A1/V1+ and A1-V1- groups ($p<0.05$), # denotes significant difference between 'responding' and 'non-responding' A1/V1+ groups ($p<0.05$), ns denotes non-significance ($p>0.05$).

Again, approximately 60% of vagal sensory neurons were defined as A1/V1+, and all three mitochondrial agents evoked substantially larger increases in $[Ca^{2+}]_i$ in the A1/V1+ neuronal population compared to the A1-V1- population ($p<0.05$)(Fig. 3.5 A, B, C, I), and these responses were significantly greater than those evoked by vehicle ($p<0.05$)(Fig. 3.5 D, I). Again, CCCP alone evoked an increase in $[Ca^{2+}]_i$ in A1-V1- neurons that was greater than vehicle ($p<0.05$)(Fig. 3.5 B, D, I). Antimycin A and CCCP both caused significant mitochondrial depolarization compared to vehicle ($p<0.05$) but there were no differences between A1/V1+ and A1-V1- populations ($p>0.05$)(Fig. 3.5 E, F, H, J). Mitochondrial depolarization occurred in 97% and 80% of neurons in response to antimycin A and CCCP, respectively (compared to 0.8% for vehicle). Although rotenone failed to evoke significant mitochondrial depolarization compared to vehicle in the total, A1/V1+ and A1-V1- populations overall (Fig. 3.5 G, J), rotenone did evoke mitochondrial depolarization in 38% of neurons (compared to 0.8% for vehicle).

Analysis of individual neuronal responses showed again that the mitochondrial agents only increased $[Ca^{2+}]_i$ beyond that evoked in A1-V1- neurons in a proportion of A1/V1+ neurons: antimycin A: 33/55, CCCP: 41/122, rotenone: 23/57 (Fig. 3.5 K). Indeed, the increase in $[Ca^{2+}]_i$ evoked by antimycin A, CCCP and rotenone was significantly greater in the 'responding' A1/V1+ population than either the 'non-responding' A1/V1+ or A1-V1- populations ($p<0.05$)(Fig. 3.5 L). Notably, there were no differences in mitochondrial depolarization between 'responding' A1/V1+ and 'non-responding' A1/V1+ neurons for each of the agents ($p>0.05$)(Fig. 3.5 M). Using scatterplots of the cell-by-cell responses, we found there was no correlation of calcium responses evoked by either antimycin A or CCCP to mitochondrial depolarization in 'responding' A1/V1+ neurons ($p>0.05$)(Fig. 3.6 A, B, Table 3.2). Nevertheless, there was a minor, yet significant correlation of rotenone-induced calcium responses to mitochondrial depolarization in 'responding' A1/V1+ neurons ($p>0.05$)(Fig. 3.6 C, Table 3.2), consistent with the finding that some neurons exhibited mitochondrial depolarization with rotenone.

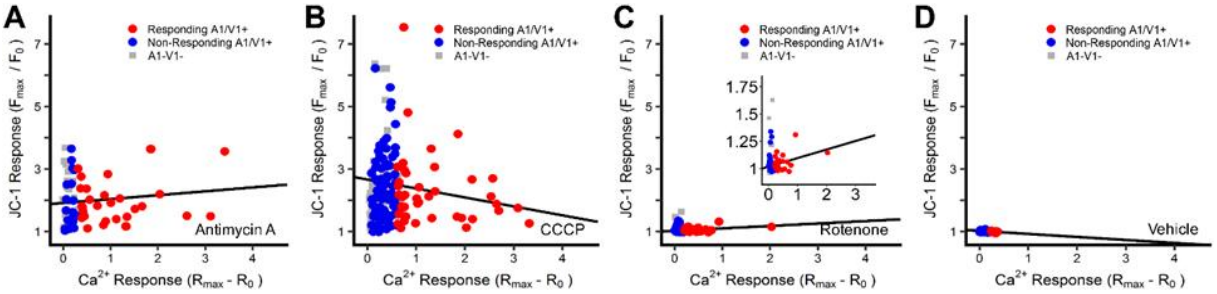

Figure 3.6: Mitochondrial depolarization responses correlates with $[Ca^{2+}]_i$ responses for rotenone, but not antimycin A or CCCP. Co-imaging of $[Ca^{2+}]_i$ and mitochondrial polarization in neurons treated with 10μM antimycin A (A), 10μM CCCP (B), 5μM rotenone (C) and 0.1% DMSO (D). Trendlines depict the correlation across all A1/V1+ neurons. Slope and significance of each trendline is presented in Table 3.2.

Table 3.2: Trendlines for the correlation of $[Ca^{2+}]_i$ and mitochondrial depolarization in subsets of vagal A1/V1+ neurons after treatment with antimycin, CCCP and rotenone.
* denotes p<0.05

	Responding A1/V1+			Non-responding A1/V1+			A1/V1+		
	Slope	**p**	**Sig**	**Slope**	**p**	**Sig**	**Slope**	**p**	**Sig**
Wild Type									
Antimycin A	0.15	0.22		0.02	0.13		0.09	0.26	
CCCP	-0.12	0.88		0.03	0.03	*	-0.05	0.82	
Rotenone	2.08	0.03	*	-0.12	0.87		0.71	0.09	
Vehicle	-0.45	0.69		0.13	0.37		-0.48	0.81	

DISCUSSION

Nociceptive activation is a hallmark of inflammation in multiple organs, resulting in debilitating symptoms (e.g. pain) and reflexes (e.g. vasodilation, edema, bronchospasm, etc.)(Tatar et al., 1988; Gold and Gebhart, 2010; Biringerova et al., 2013). While inflammatory signaling pathways involving TNFα, ceramides and neurotrophins inhibit complexes of the mETC and induce mitochondrial dysfunction (ROS production, depolarization, and Ca^{2+} release)(Stadler et al., 1992; Colell et al., 1997; Zell et al., 1997; Lopez-Armada et al., 2006), the mechanisms linking these factors to C-fiber activity are largely unknown. In a previous study, we demonstrated that inhibition of mETC complex III with antimycin A activated bronchopulmonary C-fibers via the

activation of TRPA1 and TRPV1(Nesuashvili et al., 2013)–Ca^{2+}-permeable cation channels selectively expressed on many nociceptive sensory neurons(Nassenstein et al., 2008; Taylor-Clark et al., 2008b; Nesuashvili et al., 2013). However, the influence of specific aspects of mitochondrial function on TRPA1 and TRPV1 activation remains unknown. Here, we investigated the correlation of mitochondrial depolarization and superoxide production on calcium fluxes in dissociated vagal neurons following mitochondrial modulation.

As inflammatory signaling inhibits the mETC at multiple sites, we performed these experiments using three mitochondrial agents: antimycin A (complex III inhibitor), rotenone (complex I inhibitor), and CCCP (mitochondrial uncoupling agent). Here, we found that all three agents caused robust increases in $[Ca^{2+}]_i$ in the vagal A1/V1+ neuronal population. These data are consistent with our previous study that antimycin A evoked a selective increase in $[Ca^{2+}]_i$ in A1/V1+ vagal neurons that was abolished by the removal of extracellular Ca^{2+} or by the genetic and pharmacological blockade of the nociceptive-specific ion channels TRPA1 and TRPV1(Nesuashvili et al., 2013). Given that TRPA1/TRPV1 were required for antimycin A-induced bronchopulmonary C-fiber activation(Nesuashvili et al., 2013), it is likely that the mitochondrial agent-evoked increases in $[Ca^{2+}]_i$ in A1/V1+ neurons observed in this study represents preferential activation of A1/V1+ neurons. However, not all A1/V1+ neurons 'responded' to mitochondrial modulation: approximately 60%, 35% and 35% of A1/V1+ neurons exhibited an increase in $[Ca^{2+}]_i$ to antimycin A, CCCP and rotenone, respectively. In general, antimycin A and CCCP evoked greater increases in $[Ca^{2+}]_i$ in 'responding' A1/V1+ neurons than rotenone. There was no correlation between responses in individual A1/V1+ neurons and their proximity to other neurons (data not shown), suggesting that calcium responses in each neuron was independent of the effects of mitochondrial modulation in other neurons.

Mitochondrial modulation can evoke ROS production, most notably at complexes I and III, when electrons leak and incompletely oxidize O_2 resulting in $O_2^{\bullet-}$ (superoxide) formation(Han et

al., 2001; Chen et al., 2003; Turrens, 2003; Lai et al., 2005). Superoxide is membrane impermeable and highly reactive, thus is capable of damaging DNA, proteins and lipids. In cells, superoxide dismutase rapidly converts superoxide to H_2O_2 which is membrane permeable but less reactive(Stowe and Camara, 2009). Here, we found that antimycin A increased mitochondrial superoxide production acutely in both A1/V1+ and A1-V1- neurons. Furthermore, there was no difference in the mitochondrial superoxide production evoked by antimycin A between the 'responding' A1/V1+ and 'non-responding' neurons. Nevertheless, there was a significant correlation between antimycin A-evoked mitochondrial superoxide production and the magnitude of calcium responses in 'responding' A1/V1+ neurons. Our interpretation of these data is that mitochondrial superoxide produced by antimycin A can lead to A1/V1+ neuronal activation, but this is dependent on another unknown factor that is not present in all A1/V1+ neurons. It should be noted that only 40% of all neurons exhibited increased superoxide production in response to antimycin A, raising the possibility that some neurons are insensitive to this mitochondrial modulating agent. However, this seems unlikely given the observation that 97% of neurons exhibited antimycin A-induced mitochondrial depolarization.

Both superoxide and H_2O_2 are potent activators of TRPA1(Sawada et al., 2008; Takahashi et al., 2008). Here, we found a significant correlation between antimycin A-evoked mitochondrial superoxide production and the magnitude of calcium responses in 'responding' trpv1$^{-/-}$ A1+ neurons, whose responses are presumed to be mediated by ROS-sensitive TRPA1 alone(Nesuashvili et al., 2013). Nevertheless, some trpv1$^{-/-}$ A1+ neurons failed to be activated despite substantial superoxide production, thus again suggesting that some other unknown factor is required for mitochondrial ROS-mediated TRPA1 activation. Separate studies confirmed that many non-responding trpv1$^{-/-}$ A1+ neurons were activated by exogenously-applied H_2O_2. Importantly, there was no correlation between antimycin A-evoked mitochondrial superoxide production and the magnitude of calcium responses in 'responding' trpa1$^{-/-}$ V1+ neurons, whose

responses are likely mediated by TRPV1(Nesuashvili et al., 2013). There is little evidence to suggest that TRPV1 is a major target of ROS and oxidative stress: TRPV1 is not activated by physiological concentrations of H_2O_2(Sawada et al., 2008; Ogawa et al., 2016) or most electrophilic products of lipid peroxidation(Gouin et al., 2017), although it is activated by high concentrations of 4-oxononenal(Taylor-Clark et al., 2008a). Instead, TRPV1 is activated by PIP_2 hydrolysis, GPCR signaling and arachidonic acid metabolites(Prescott and Julius, 2003; Watanabe et al., 2003; Wen et al., 2012; Gouin et al., 2017). Our data further suggests that TRPV1-mediated activation by antimycin A is not downstream of superoxide production.

Like antimycin A, CCCP evoked significant mitochondrial superoxide production in all neuronal populations, consistent with previous reports in isolated rat brain mitochondria(Votyakova and Reynolds, 2001), although other studies indicate that uncoupling agents such as CCCP do not increase ROS production(Sipos et al., 2003; Suski et al., 2012). However, there was no correlation between CCCP-induced mitochondrial superoxide production and the magnitude of calcium responses in 'responding' A1/V1+ neurons. Approximately 80% of neurons exhibited mitochondrial depolarization to CCCP, but there were no significant differences between the mitochondrial depolarization in 'responding' A1/V1+ and 'non-responding' neurons and there was no correlation between mitochondrial depolarization and the magnitude of calcium responses in 'responding' A1/V1+ neurons. We therefore conclude that factors other than mitochondrial superoxide production determine the CCCP-induced activation of A1/V1+ neurons and that mitochondrial depolarization alone is unable to account for these responses.

Rotenone failed to cause mitochondrial superoxide production in any neuronal population. Indeed, rotenone decreased baseline mitochondrial ROS production in A1/V1+ neurons. Previous studies have shown that rotenone can increase or decrease ROS production depending on metabolism of complex I versus complex II substrates(Chen et al., 2003; Hoffman and Brookes, 2009). Despite the lack of superoxide production, rotenone evoked an increase in $[Ca^{2+}]_i$ in

approximately 35% of A1/V1+ neurons in this study. Although rotenone caused mitochondrial depolarization in approximately 38% of all vagal neurons, there were no significant differences between the mitochondrial depolarization in 'responding' A1/V1+ and 'non-responding' neurons. Nevertheless, there was a significant correlation between rotenone-evoked mitochondrial depolarization and the magnitude of calcium responses in 'responding' A1/V1+ neurons. This suggests that mitochondrial depolarization alone can lead to A1/V1+ neuronal activation, but again this is dependent on another unknown factor that is not present in all A1/V1+ neurons.

Our data indicates that mitochondrial modulators (in particular antimycin A and CCCP) evoke mitochondrial superoxide production in a limited percentage of neurons despite the evident mitochondrial depolarization in the majority of neurons. The present study used quantitative measurements of mitochondrial superoxide using MitoSOX, which is neither ratiometric nor reversible, making it possibly susceptible, despite our efforts to normalize the data, to variations in loading and baseline redox state. MitoSOX is targeted to the mitochondrial matrix, thus it is possible that some of the superoxide produced from complex I and III may evade MitoSOX detection following its release into the intermembrane space(Han et al., 2001; St-Pierre et al., 2002; Muller et al., 2004). ROS produced within sensory neurons has 3 potential fates: reacting with signaling pathways, with endogenous antioxidant systems (e.g. glutathione) or with the ROS-sensitive dye. As such, the quantification of ROS production may be susceptible to significant error on a cell-by-cell basis. Nevertheless, even a qualitative analysis suggests that (A) mitochondrial modulation does not evoke significant calcium responses in all A1/V1+ neurons and (B) significant ROS production does not necessarily evoke calcium responses in A1/V1+ neurons. This suggests that factors in addition to superoxide determine the TRPA1- and TRPV1-mediated calcium responses in A1/V1+ neurons. The identity of these factors is presently unknown, but it is possible that these either involve the activity of antioxidant systems or the spatial/temporal arrangement of mitochondria, TRP channels and signaling molecules. Our rotenone studies

suggest that mitochondrial depolarization is able to contribute, but experiments with CCCP (and antimycin A) indicate that mitochondrial depolarization is not guaranteed to result in significant calcium responses in A1/V1+ neurons. How mitochondrial depolarization could contribute to A1/V1+ neuronal activation is not yet known. Mitochondrial depolarization causes calcium efflux from the matrix, and calcium is a regulator of multiple pathways such as phospholipases and protein kinases(Cuchillo-Ibáñez et al., 2004; Rizzuto et al., 2012) that can alter TRP channel activity(Bandell et al., 2004; Mandadi et al., 2006a; Cao et al., 2013; Gouin et al., 2017).

Unlike antimycin A and rotenone, CCCP evoked a significant increase in $[Ca^{2+}]_i$ in A1-V1- neurons, although these were much smaller than those in A1/V1+ neurons. As such, the threshold for determining the calcium 'responsiveness' of a particular neurons is greater for CCCP treatments. A1-V1- neurons do not express TRPA1 or TRPV1. Thus, the source of the CCCP-evoked calcium responses in A1-V1- is presently unknown. It is possible that calcium release from the mitochondrial matrix after robust mitochondrial depolarization contributes to these calcium transients(Shishkin et al., 2002), and this is consistent with (A) the significant calcium responses with CCCP in the nominal absence of extracellular calcium and (B) the significant correlation between CCCP-evoked mitochondrial depolarization and the magnitude of calcium responses in A1-V1- neurons (slope 0.035, $p<0.05$, data not shown).

The present study has investigated the correlation between mitochondrial ROS/depolarization and calcium transients evoked by mitochondrial modulators in vagal neurons. Our previous study identified the critical role of TRPA1 and TRPV1 in antimycin A-induced calcium responses and bronchopulmonary C-fiber activation(Nesuashvili et al., 2013). Although the specific role of TRPA1 and TRPV1 has not been extensively investigated in the present study, our data is consistent with TRPA1 and TRPV1 mediating the mitochondrial modulator-evoked calcium responses. It is important to note, however, that TRP channel sensitivity itself is not static and that multiple intracellular pathways, including oxidative stress, can promote either

sensitization or desensitization of TRPA1 and TRPV1 channels(Susankova et al., 2006; Wang et al., 2008; Rohacs, 2015; Meents et al., 2017). Furthermore, TRPA1 and TRPV1 have been reported to functionally modulate each other's sensitivity(Spahn et al., 2014; Weng et al., 2015). Although not addressed here, it is possible that mitochondrial modulation may impact TRP function beyond channel activation.

In summary, we have shown that mitochondrial modulation by antimycin A-induced TRPA1-mediated calcium responses in vagal A1/V1+ neurons correlates with mitochondrial superoxide production, but that other factors including mitochondrial depolarization may contribute to A1/V1+ neuronal calcium responses via TRPV1 and downstream of complex I inhibition and mitochondrial uncoupling. It should be emphasized that the conclusions here are based upon correlations, which do not necessarily imply causation. Thus, we note that these studies do not show a conclusive role of superoxide production in the A1/V1+ neuronal Ca^{2+} responses by mitochondrial modulators. Furthermore, we have focused our present study on the cell body of dissociated vagal neurons and it is possible that mechanisms linking mitochondrial superoxide production and depolarization with TRP channel activation may be different within sensory terminals in vivo. More studies are needed to fully understand the events linking mitochondrial dysfunction and nociceptor activation.

UNIQUE METHODS

Imaging analysis (MitoSOX and JC-1)

Images were analyzed using Nikon Elements (Nikon, Melville, NY). Each individual neuron was analyzed separately using a region of interest (ROI) that encompassed the entire intracellular region. If required, ROIs were tracked over time to account for any cellular movement. For each imaging method (Fura-2AM, MitoSOX, and JC-1), ROIs with an unstable baseline, noisy baseline or insufficient loading were eliminated from the analysis. Neurons that possessed an initial JC-1

red/green (525nm/610nm) ratio under 0.5 were eliminated as this indicated mitochondrial depolarization prior to the start of the experiment. For statistical analyses, we analyzed the maximal Fura-2AM, JC-1 and MitoSOX responses during the three-minute drug treatment (see below for calculations). For specifics regarding FURA-2AM imaging analysis and quantification of response, see common methods.

Mitochondrial superoxide production was analyzed using MitoSOX fluorescence (F, excitation at 535nm). Given that the reaction of superoxide with MitoSOX red is irreversible and that baseline physiologic ROS production by mitochondria will vary between individual neurons, we have chosen to correct for the slope in the time series studies using $F_{1(adjusted)} = F_1 - (S_0 * t)$, where F_1 is the raw fluorescence at a given timepoint (in arbitrary fluorescent units), S0 is the slope of the baseline (arbitrary fluorescent units/s) and t is time of the F_1 measurement (in seconds). As MitoSOX loading varies between individual neurons, we have normalized the slope corrected data: $F_{1(adjusted)}/F_{0(adjusted)}$, where $F_{1(adjusted)}$ is the slope corrected fluorescence at a given timepoint and $F_{0(adjusted)}$ is the average of the slope corrected baseline. In order to determine the percentage of neurons that exhibited meaningful mitochondrial superoxide production compared to vehicle, we calculated the percentage of neurons whose individual maximal $F_{1(adjusted)}/F_{0(adjusted)}$ was greater than the average maximal $F_{1(adjusted)}/F_{0(adjusted)}$ for vehicle treatment + 3 * standard deviation of the maximal $F_{1(adjusted)}/F_{0(adjusted)}$ for vehicle treatment.

Mitochondrial polarization was determined using JC-1 fluorescence at both the green (525nm, which measures the monomeric form of JC-1) and red (610nm, which measures the aggregated form of JC-1) emission wavelengths. JC-1 accumulates in negatively charged mitochondria and forms ‘red’ aggregates. Upon mitochondrial depolarization, JC-1 disperses into the cytosol as the ‘green’ monomeric form. As mentioned above, the 525nm/610nm ratio was used to identify neurons with depolarized mitochondria at baseline. However, we chose to determine the effect of mitochondrial modulation on mitochondrial polarization using only the

'green' monomeric form (F, 525nm fluorescence), as JC-1 fluorescence of 'red' aggregates is susceptible to quenching, prone to oxidation and requires ~90 minutes to reach equilibrium (versus ~15 minutes for monomers)(Perry et al., 2011). Data were normalized (F_1/F_0) where F_1 is the emission fluorescence at 610nm at a given time point and F0 is the baseline emission fluorescence at 610nm. This normalization process allowed for the calculation of the relative change of mitochondrial membrane potential independent of baseline polarization and JC-1 loading. In order to determine the percentage of neurons that exhibited meaningful mitochondrial depolarization compared to vehicle, we calculated the percentage of neurons whose individual maximal F_1/F_0 was greater than the average maximal F_1/F_0 for vehicle treatment + 3 * standard deviation of the maximal F_1/F_0 for vehicle treatment.

CHAPTER 4

Contribution of ROS to antimycin A evoked activation of TRPA1 and TRPV1

INTRODUCTION

Mitochondrial dysfunction and oxidative stress are associated with inflammatory pulmonary diseases such as asthma, COPD, and chronic cough(Kirkham and Rahman, 2006). Events which cause inflammation such as viral infection and allergen exposure can induce oxidative stress through events such as leucocyte activation, mitochondrial dysfunction and hypoxia. Inflammatory signaling pathways including TNFα and IL-1β directly inhibit complexes of the mETC, inducing a state mitochondrial dysfunction wherein ROS production is increased as a result of slippage of electrons from the mETC and the incomplete reduction of O_2(Zell et al., 1997; Moe et al., 2004; Mariappan et al., 2009). While ROS are involved in cellular signaling, excessive ROS can oxidize lipids and proteins to cause cellular damage(Stowe and Camara, 2009). To prevent this damage, cells express many antioxidant proteins and contain GSH to reduce ROS to H_2O_2(Stowe and Camara, 2009). Although ROS activates bronchopulmonary C-fibers and inhalation of ROS evokes defensive reflexes in animal models(Ruan et al., 2003; Lin et al., 2010), the influence of mitochondrially derived ROS on sensory nerve activation is largely unknown. In addition to ROS, many oxidized lipids including 4-hydroxynonenol, and 4-oxononenal present in states of oxidative stress also activate bronchopulmonary C-fibers(Trevisani et al., 2007; Andersson et al., 2008; Taylor-Clark et al., 2008a).

As TRPA1 is directly activated both ROS and oxidized lipids(Andersson et al., 2008; Takahashi et al., 2008), it may be responsible for the activation of these fibers by product of

oxidative stress. Previously, we demonstrated that antimycin A activates bronchopulmonary C-fibers through the activation of TRPA1 and TRPV1 and that there is a correlation between mitochondrial O_2^- production and Ca^{2+} fluxes in wild type (express TRPA1 and TRPV1) and TRPV1$^{-/-}$ (only express TRPA1) neurons but not TRPA1$^{-/-}$ (only express TRPV1) neurons(Stanford and Taylor-Clark, 2018). This provides evidence for the activation of TRPA1 but not TRPV1 by mitochondrial ROS. TRPA1 contains highly reactive cysteines in its cytosolic domain which form reversible covalent bonds with electrophiles (ex: ROS) producing channel activation(Macpherson et al., 2007; Bahia et al., 2016). As little evidence suggests that TRPV1 is directly activated by ROS(Taylor-Clark and Undem, 2011) it is likely activated via another mechanism.

Here, we evaluate the impact of ROS on the activation of TRPA1 and TRPV1 downstream of mitochondrial modulation with antimycin A. To evaluate the impact of ROS, we used ROS scavengers to neutralize ROS and the ROS-insensitive TRPA1 K620A mutant(Bahia et al., 2016). In neurons we scavenged ROS with MnTMPyP (SOD/catalase mimetic) + Tempol (SOD mimetic) and isolated the effect of ROS on TRPA1 and TRPV1 by using KO neurons. In transfected HEK293 cells we scavenged ROS with the reducing agent dithiothreitol (DTT) and evaluated responses in the TRPA1 K620A mutant. We observed a diminished Ca^{2+} flux with TRPA1 but not TRPV1 in both HEK293 cells and vagal neurons with the use of ROS scavengers. Although diminished, the responses of TRPA1 were not abolished. Due to the high reactivity of TRPA1, we evaluated responses in the ROS unresponsive TRPA1 K620A mutant. Confirming our hypothesis, the TRPA1 K620A mutant was not activated during Antimycin A treatment.

RESULTS

Contribution of ROS to activation

The contribution of ROS to the activation of TRPA1 and TRPV1 was evaluated by treating cells with MnTMPyP and Tempol to scavenge ROS. This resulted in a decreased Ca^{2+} flux with

TRPA1 (TRPV1$^{-/-}$, Fig. 4.1 A, B) but not TRPV1 (TRPA1$^{-/-}$, Fig. 4.1 C, D) expression only conditions. This is consistent with present knowledge regarding the activation of TRPA1 but not TRPV1 by ROS. Although the percentage of responding neurons was also decreased, this was not significant ($p > .05$). This could be explained by the high sensitivity of TRPA1 to electrophiles such as ROS and products of lipid peroxidation. Therefore, even with large concentrations of ROS scavenging agents, small amounts of remaining ROS may be capable of activating TRPA1. We further investigated the impact of ROS in TRPA1 and TRPV1 transfected HEK293 cells and scavenged ROS with dithiothreitol (DTT). In both TRPA1 and TRPV1 transfected cells, antimycin A produced a large Ca^{2+} flux (Fig. 4.2 A-C). As observed in vagal neurons, only a portion of HEK293 cells responded to mitochondrial modulation (Fig. 4.2 D-F). Again, scavenging ROS diminished but did not abolish Ca^{2+} fluxes in TRPA1 ($p < .05$) transfected cells while having no effect on TRPV1 ($p > .05$) responses. Due to the exceptional reactivity of TRPA1 to ROS, evaluated the responses in the ROS unresponsive TRPA1 K620A mutant. Indeed, with this ROS unresponsive mutant the Ca^{2+} flux ($p > .05$ vs non-transfected) observed during antimycin A treatment was abolished (Fig 4.3 A-B).

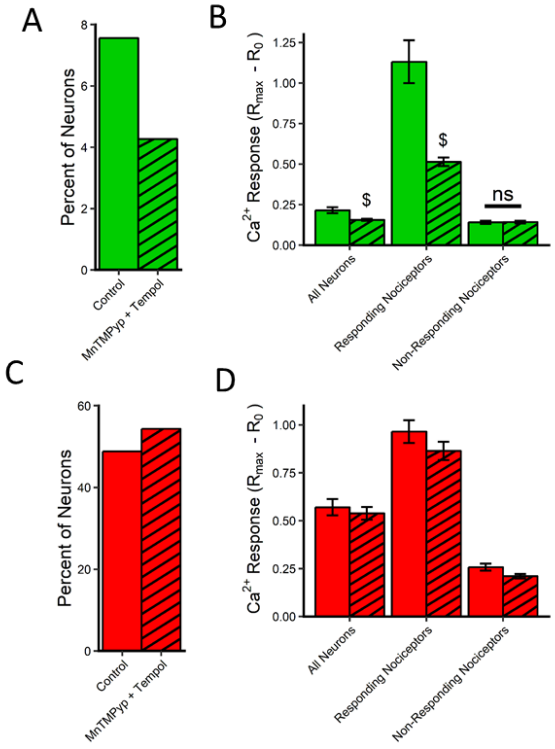

Figure 4.1: Scavenging ROS decreases TRPA1 but not TRPV1 responses. The (A and C) percentage of neurons responding to antimycin A treatment and (B and D) magnitude of Ca^{2+} fluxes in TRPV1$^{-/-}$ (green, A and B) and TRPA1$^{-/-}$ (red, C and D) vagal neurons. Ca^{2+} flux magnitude, but not the percentage of neurons responding was decreased in TRPV1$^{-/-}$ but not TRPA1$^{-/-}$ neurons. $ denotes significant difference between MnTMPyP + Tempol and control ($p < .05$).

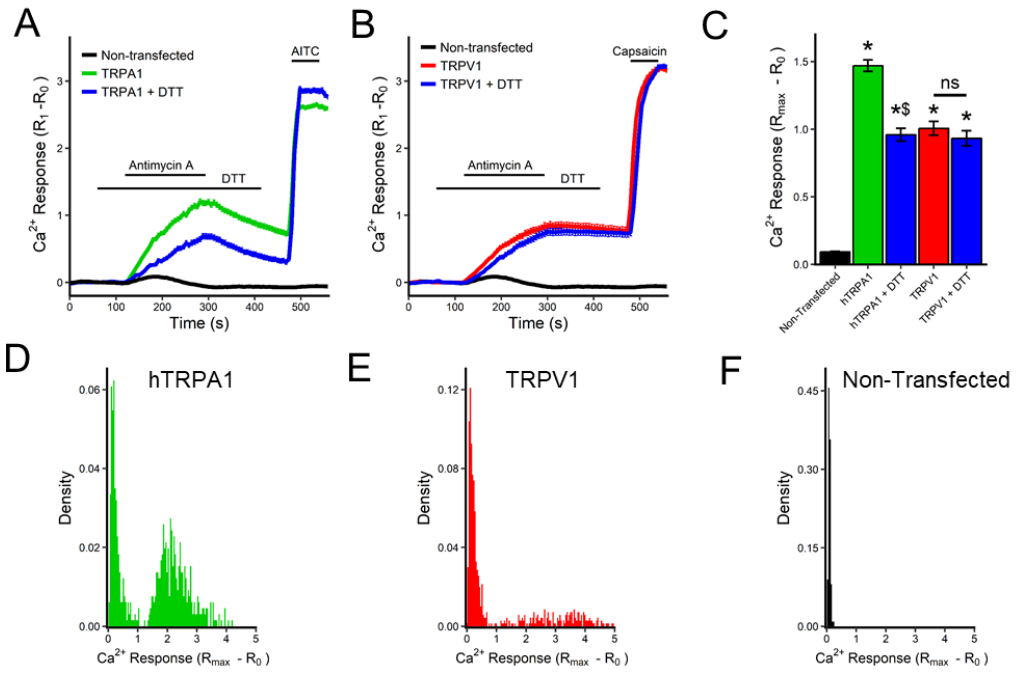

Figure 4.2 Scavenging ROS with DTT decreases TRPA1 but not TRPV1 responses in HEK293 cells. Antimycin A evoked cytosolic Ca^{2+} fluxes in (A) TRPA1 and (B) TRPV1 transfected HEK293 cells were decreased in TRPA1 but not TRPV1 expressing cells with DTT treatment. With (C) bar graph of mean +/- SEM Ca^{2+} flux and Ca^{2+} flux density histograms for (D) TRPA1, (E) TRPV1 and (F) non-transfected cells. * denotes significant difference from non-transfected cells ($p < .05$); $ denotes significant difference between + DTT and control ($p < .05$).

DISCUSSION

ROS are produced at increased levels in individuals with pulmonary disease. Additionally, it has been shown that H_2O_2 activates bronchopulmonary C-fiber fibers(Ruan et al., 2003; Lin et al., 2010). However, the direct influence of mitochondrially derived ROS on sensory nerve activity has not been previously studied. We observed decreased Ca^{2+} fluxes in the presence of ROS scavengers with TRPA1 but not TRPV1 in both vagal neurons and HEK293 cells. This suggests that TRPA1 activation is ROS dependent while TRPV1 is activated through a ROS-independent mechanism. Although some studies suggest that ROS can activate TRPV1, these studies have relied on whole cell techniques and there are no reports of direct ROS-induced TRPV1 activation of using excised patch clamp techniques. These studies also used H_2O_2 at concentrations (1mM and 10mM) which exceed physiologic ROS levels(Taylor-Clark and Undem, 2011). As ROS

activates cellular signaling pathways through the activation of serine/threonine kinases (such as PKC), and NF-kB(Stowe and Camara, 2009), this excess amount of ROS could activate signaling pathways in a manner which is not present under physiologic conditions. As several isoforms of PKC are activated by ROS(Cosentino-Gomes et al., 2012), this provides a possible mechanism for the activation of TRPV1 by H_2O_2 in whole cell studies. In our experiments using antimycin A, ROS scavenging did not affect Ca^{2+} fluxes in TRPV1 expressing vagal neurons or HEK293 cells, its activation downstream of mitochondrial modulation is likely ROS independent.

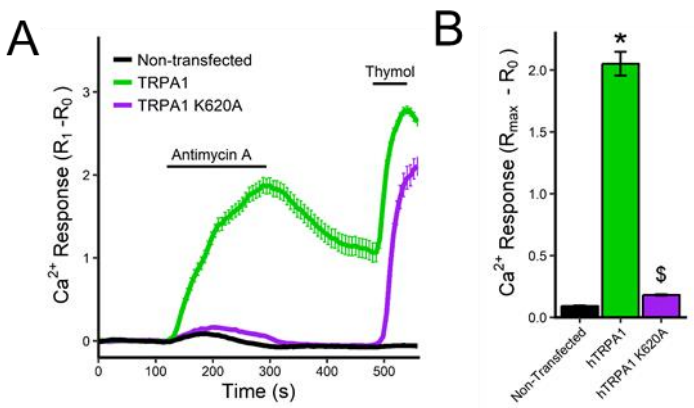

Figure 4.3: The ROS unresponsive TRPA1 K620A mutant did not respond to antimycin A treatment. Cytosolic Ca^{2+} fluxes expressed as (A) a time course and (B) as mean +/- SEM maximal Ca^{2+} response. $ denotes significant difference from TRPA1 transfected control ($p > .05$).

In the case of TRPA1, ROS scavengers reduced Ca^{2+} fluxes, suggesting a role for ROS. Interestingly, the Ca^{2+} fluxes in vagal neurons and HEK293 cells expressing TRPA1 were not abolished. For these experiments, we used the maximal concentrations of ROS scavengers which were previously used in the literature. In the case of DTT, we were unable to increase the concentration of DTT as higher concentrations activate TRPV1(Susankova et al., 2006). The lack of complete abolishment of the TRPA1 response with DTT could be due to its participation in redox cycling. Interestingly, DTT reduced TRPA1 responses in HEK293 cells but not in vagal neurons (vagal neuron data not shown). The underlying reason the diminished Ca^{2+} fluxes in HEK293 cells but not TRPA1 only expressing vagal neurons is unknown. It is possible that cellar components present in vagal neurons but not HEK293 cells drive redox cycling and prevent our ability to scavenge ROS and electrophilic compounds. There may also be differences between

vagal neurons and HEK293 cells in regard to baseline cellular conditions as cell culture alters both mitochondrial function and cellular signaling. These unknown differences between vagal neurons and transfected HEK293 cells may result in differential effects of antimycin A and ROS scavengers in these systems which may account to the diminished Ca^{2+} fluxes with DTT in HEK293 cells but not vagal neurons. Another possibility for these differences is that HEK293 cells were transfected with human TRPA1 and vagal neurons were from mice. However, both human and mouse TRPA1 are highly sensitive to ROS-mediated activation(Macpherson et al., 2007; Taylor-Clark et al., 2007). Therefore, the differences between mouse and human TRPA1 likely do not affect the mechanism underlying TRPA1 activation by antimycin A.

In addition to DTT and MnTMPyP + Tempol, we evaluated Ca^{2+} fluxes in TRPA1 neurons with 10μM lipoic acid and 2000U/mL pegylated SOD + pegylated catalase 2000U/mL (data now shown). For ROS scavengers tested, we used the largest concentrations observed in prior literature, all of which reduced ROS-mediated responses(Beckman et al., 1988; Foo et al., 2011; Lu et al., 2017). However, these failed to diminish Ca^{2+} fluxes. It has been previously shown that SOD and catalase can reduce antimycin A-evoked apoptosis but not substantially reduce ROS production or decrease GSH depletion(Park et al., 2007). This demonstrates that Antimycin A-evoked ROS is difficult to scavenge. Thus, in the case of TRPA1, effectively scavenging ROS to abolish activation may not be possible with current methods. This indicates that our ability to diminish but not abolish TRPA1 mediated responses is likely not due to the presence of two mechanisms (a ROS-dependent and ROS-independent mechanism), or the inhibition of TRPA1 by ROS scavenging agents. Work in our lab has demonstrated that TRPA1 exhibits exceptionally high reactivity to electrophilic activation occurring at a rate of 500–900 $M^{-1}s^{-1}$, over 6,000-fold faster than that of antioxidant enzymes and GSH (33 $M^{-1}s^{-1}$)(Bednar, 1990; Bahia et al., 2016). Therefore, the possibility remains that even with high concentrations of ROS scavengers and reducing agents, the small amounts of ROS remaining may activate TRPA1. Additionally, ROS

oxidizes cellular lipids which also activate TRPA1. Therefore, it is possible that these compounds be generated before ROS can be adequately scavenged and activate TRPA1.

Due to the difficulties involved with assessing the ROS induced activation of TRPA1, we evaluated responses in a ROS and electrophile unresponsive human TRPA1 K620A mutant(Bahia et al., 2016). In these experiments, the antimycin A evoked Ca^{2+} flux was abolished. This seems to indicate that the diminished but not abolished responses were due to our inability to effectively scavenge ROS. However, the lack of reduced Ca^{2+} flux with TRPV1 is likely not due to high reactivity. As previously discussed, there is little evidence to suggesting that TRPV1 is activated by ROS and its ROS-induced activation has only been demonstrated in intact cells using concentrations which far exceed physiologic ROS(Taylor-Clark and Undem, 2011). This is in direct contrast to TRPA1 where there is a large body of evidence for its direct activation by ROS and electrophilic compounds present in oxidative states. Therefore, our inability to abolish TRPV1 activation evoked Ca^{2+} fluxes is not due to our inability to scavenge ROS. This suggests an alternate mechanism for the activation of TRPV1, likely involving activation of cellular signaling. As TRPV1 is sensitized by PKC and ROS can activate several isoforms of PKC(Knapp and Klann, 2000; Wang et al., 2015), this may result in TRPV1 activation. However, the expression of PKC isoforms is heterogenous and as isoforms differ based on the factors required for activation and site of action(Parker, 2004). As PKC inhibitors have varying specificities for these isoforms and often have off-target effects, more studies on the activation of PKC by antimycin A in vagal neurons are required before studying the effects on TRPV1 activation.

Interestingly, only a portion TRPV1 and TRPA1 HEK293 cells and vagal neurons responded during antimycin A treatment. The reason underlying this is unknown. Although these differential responses could be a result of differential protein expression in vagal neurons, this is unlikely given that this phenomenon was also observed in HEK293 cells. In the previous chapter, we found that many of TRPA1 only expressing neurons which failed to exhibit a Ca^{2+} flux exhibited

increased mitochondrial ROS production. This is particularly interesting given the exceptionally high sensitivity of TRPA1 to ROS and our difficulties with adequately scavenging ROS. As we specifically measured mitochondrial ROS, it is possible that ROS were scavenged by cellular antioxidants prior to their reaching the plasma membrane. Furthermore, antimycin A evokes O_2^- production on the matrix and the intermembrane space faces of the inner mitochondrial membrane(Muller et al., 2004). Therefore, both mitochondrial ROS scavenging and the ability of ROS to diffuse to the plasma membrane may have an effect on TRPA1 activation. Another possible influence is cytosolic Ca^{2+} which can both potentiate and inhibit TRPA1. Therefore, mitochondrial Ca^{2+} release may affect the sensitivity of TRPA1 to activation by ROS. It is also possible that cellular signaling pathways may alter the sensitivity of TRPA1. Unfortunately, given the complexities regarding the *in situ* study of mitochondrial function and activation of ion channels studies of the mechanisms behind these differential responses are exceptionally difficult. Another complication is that mitochondrial inhibition has varying effects based on not only the site of inhibition, but also the tissue or origin and baseline metabolic status(Tahara et al., 2009). Therefore, the reasons underlying these differential effects remain unknown and require much further research.

UNIQUE METHODS

Scavenging ROS

To scavenge ROS, neurons were pre-treated with 1mM tempol for 45 minutes at 37^{o}C, then transferred to the microscope and perfused with 50μM MnTMPyp + 100μM tempol for 15 minutes prior to the start of imaging and washed off 1 minute after the completion of antimycin A treatment. In HEK293 cells, ROS was scavenged with 100μM DTT with treatment commencing 1 minute prior to antimycin A exposure and ending 2 minutes after the completion of antimycin A treatment.

CHAPTER 5

Improving roGFP1 sensitivity by incorporation of selenocysteine at position 147

INTRODUCTION

The study of reactive oxygen species (ROS) signaling has received increased attention in the pathogenesis of a wide variety of pathophysiologies such as neurodegeneration, cancer, and inflammation(Lin and Beal, 2006; Zhang et al., 2015; Garaude et al., 2016). However, investigations into ROS signaling has been hindered by a lack of available methods to accurately measure small and localized ROS fluctuations. Current methods to measure ROS include redox-sensitive dyes and genetically-encoded reporter proteins such as redox-sensitive green fluorescent protein (roGFP)(Dooley et al., 2004; Chen et al., 2011; Guo et al., 2014). Unfortunately, redox-sensitive dyes often lack the ability to localize in sub-cellular compartments and are generally incompatible with *in vivo* use. Genetically-encoded reporter proteins such as roGFP have been used *in vivo* and targeted to many organelles, but they lack the sensitivity of dyes(Breckwoldt et al., 2014; Wagener et al., 2016). Although roGFP2, a variant of roGFP, is sensitive to hypoxia-mediated ROS production, its responses are slow(Dooley et al., 2004; Waypa et al., 2011), suggesting significant limitations for the detection of local, small-scale, and transient fluctuations involved in physiologic ROS signaling. This highlights the need to develop reporter proteins with increased redox-sensitivity.

roGFP1 is a commonly used variant of roGFP that is largely unaffected by pH and produces a strong fluorescent signal(Roma et al., 2012). Additionally, roGFP1 has been targeted and optimized for use in cellular compartments such as the mitochondria and endoplasmic

reticulum(Hanson et al., 2004; Delic et al., 2010). roGFP1 contains two redox-sensitive cysteines at amino acids 147 and 204 which serve as a biological switch. Oxidation and reduction of these cysteines shifts fluoresce between two excitation maxima (approximately 405 and 470nm)(Dooley et al., 2004; Hanson et al., 2004). As such, the cellular redox state is expressed as a ratio of these excitation maxima (405/470). Upon exposure to ROS, the redox-sensitive cysteines are oxidized, resulting in intramolecular disulfide bond formation, increased fluorescence at 405nm and decreased fluorescence at 470nm (increased 405/470 ratio)(Hanson et al., 2004). Cellular glutathione reductase reduces the disulfide bond, restoring fluorophore structure and fluorescent properties to the pre-oxidized state.

These ratiometric and reversible properties of roGFP1 make it well-suited to measure cellular ROS. However, its lack of sensitivity renders it unsuitable for detecting ROS fluctuations involved in physiologic signaling(Dooley et al., 2004). One factor contributing to the relative insensitivity of roGFP1 is the protonation of its redox-sensitive cysteines under physiologic cellular conditions: only deprotonated cysteines are able to react with ROS(Roberts et al., 1986). To overcome this barrier, several attempts have been made to decrease the pKa (from ~8.2) of the roGFP1 cysteines by mutating surrounding amino acids(Cannon and Remington, 2006). Unfortunately, the resulting proteins also lacked the sensitivity to detect small ROS fluctuations. An alternative approach to increase the sensitivity of roGFP1 is to replace the fluorophore cysteines with selenocysteine, a more reactive nucleophile with a lower pKa (5.5 vs 8.2)(Byun and Kang, 2011). Selenocysteine is capable of forming bridges upon oxidation with either selenocysteine or cysteine(Müller et al., 1994). These properties indicate that incorporation of selenocysteine has the potential to increase the sensitivity of roGFP1.

Selenocysteine incorporation into proteins is more complex and inefficient compared to insertion of canonical amino acids. Selenocysteine incorporation occurs at UGA codons, which typically serve to stop protein translation(Chambers et al., 1986). Thus, incorporation requires

additional elements including a selenocysteine insertion sequence (SECIS) in the 3' untranslated region of the mRNA and a selenocysteine specific elongation factor(Zinoni et al., 1990; Tujebajeva et al., 2000). Even in the presence of all required elements, insertion remains inefficient with translation stalling at the UGA codon, resulting in protein truncation. To increase incorporation, selenoproteins can be co-expressed with selenocysteine binding protein 2 (SBP2), which helps coordinate the proximity of the required insertional elements. This results in increased insertion efficiency and decreased truncation(Copeland et al., 2000; Copeland et al., 2001).

Here we attempted to increase the sensitivity of roGFP1 by mutating the functional cysteine (at position 147) to selenocysteine (roGFP1-Se147). To allow for selenocysteine insertion, we incorporated a 3' SECIS element and supplemented media with sodium selenite. To maximize expression of roGFP1-Se147, we developed two expression systems (selenovectors), both of which co-expressed SBP2 and roGFP1-Se147. We successfully expressed roGFP1-Se147 which exhibited similar excitation and emission spectra to roGFP1. Though roGFP1-Se147 demonstrated increased sensitivity, it exhibited a poor dynamic range and photoinstability.

RESULTS

Western Blot

HEK293T cells were transfected with roGFP1-N1 (control vector), roGFP1-pLuc01, roGFP1-Se147pLuc01, roGFP1-pSel, or roGFP1-Se147pSel (Fig. 5.1). roGFP1 was highly expressed in the control vector (roGFP1-N1). Interestingly, roGFP expression was reduced with use of both the selenovectors (roGFP1-pSel, and roGFP1-pLuc01). Expression of roGFP1-Se147 was limited but detectable for both selenovectors, although expression was consistently higher with the roGFP1-Se147pSel vector. Previous studies have demonstrated protein truncation at selenocysteine insertion sites(Tujebajeva et al., 2000; Mehta et al., 2004;

Novoselov et al., 2007). However, no evidence of protein truncation was observed for the selenoproteins.

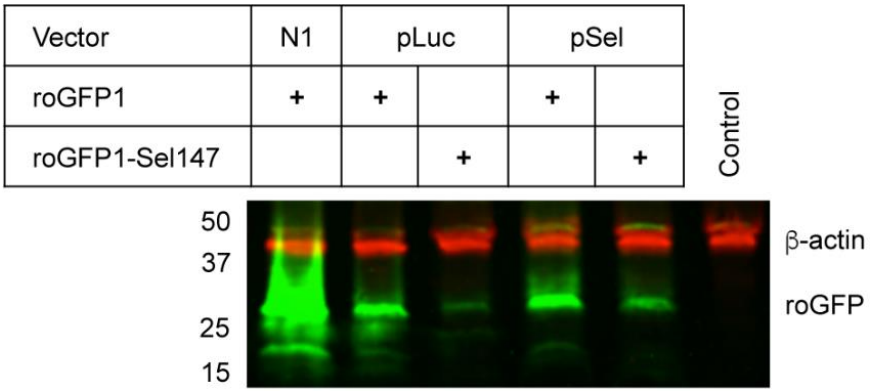

Figure 5.1: Expression of roGFP1 constructs. Western blot of lysates from HEK293 cells following expression of roGFP1-N1, roGFP1-pLuc, roGFP1-Se147pLuc01, roGFP1-pSel, roGFP1-Se147pSel and a non-transfected control. B-actin (red) used as a loading control.

Spectral analysis

Using transfected HEK293T cells suspended in PBS, we evaluated the excitation (detected at 530nm, Fig. 5.2 A) and emission spectra (excited at 405nm, Fig. 5.2 B) of GFP, roGFP1-pSel and roGFP1-Se147pSel. Redox-insensitive GFP exhibited a large excitation peak at ~480nm and roGFP1-pSel exhibited two excitation peaks with the largest peak at ~405nm and a smaller peak at ~475nm, consistent with previous studies(Dooley et al., 2004). The excitation spectrum for roGFP1-Se147pSel was similar to roGFP1-pSel with its maximum at ~405nm. All proteins exhibited similar emission spectra with a single maximum at ~530nm.

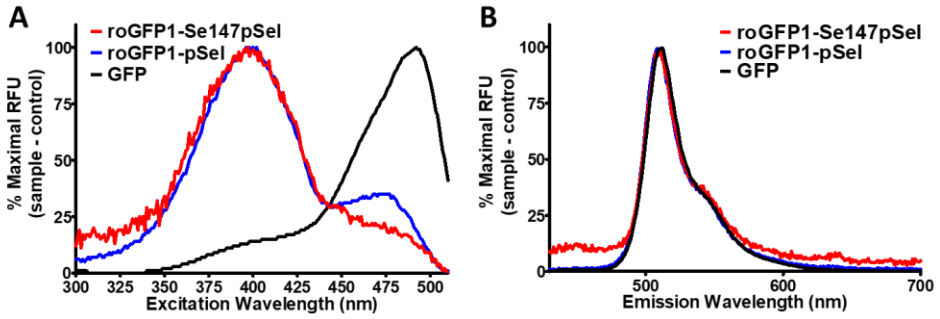

Figure 5.2: Spectra of GFP, roGFP1, and roGFP1-Se147. Constructs expressed in HEK293T. (A) Excitation spectra, measured at 530nm. (B) Emission spectra, excited by 405nm.

Functional analysis

Though expression of roGFP1-Se147pSel was limited according to our western blot data, sufficient fluorescent signals were observed in living HEK293 cells to evaluate the responsiveness of roGFP1-Se147pSel to oxidation and reduction (Fig. 5.3). Omission of sodium selenite from the culture prevented roGFP1-Se147pSel expression (data not shown). roGFP1-pSel was insensitive to oxidation with 3µM H_2O_2, but oxidation with 30, and 300µM H_2O_2 evoked substantial increases in the 405/470 ratio, which was reversed by the reducing agent dithiothreitol (DTT) (3mM). The selenoprotein, roGFP1-Se147pSel, exhibited minor responses to oxidation with 3, 30, and 300µM hydrogen peroxide as well as to reduction with 3mM DTT, indicating a lack of dynamic range of the fluorophore. In comparison to roGFP1-pSel, roGFP1-Se147pSel exhibited an elevated baseline 405/470 ratio, which increased by ~5% under resting conditions until leveling off after 2 minutes, suggesting photoinstability of the selenoprotein.

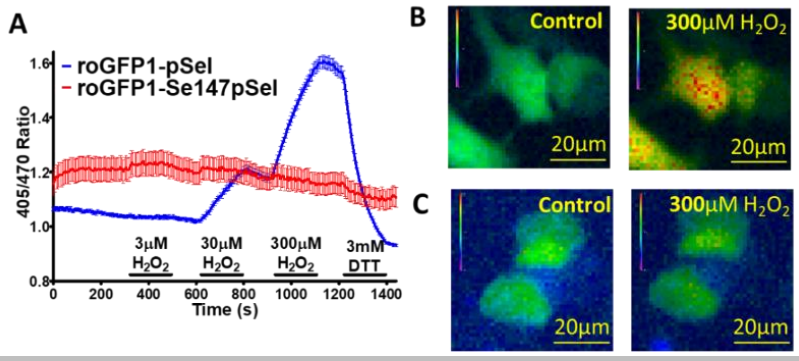

Figure 5.3: Response of roGFP1 selenoprotein to oxidation and reduction. (A) Mean +/- SEM of the 405/470 ratio of HEK293 cells transfected with roGFP1-Se147pSel (red, n=52) and roGFP1-pSel (blue, n=220) treated with 3, 30, and 300µM H_2O_2 followed by 3mM DTT. (B) and (C) Representative pseudocolor image of 405/470 ratio of HEK293 cells transfected with roGFP1-pSel (B) and roGFP1-Se147pSel (C) at baseline and after 300µM H_2O_2.

In order to determine the redox-sensitivity of roGFP1-Se147pSel while minimizing any excitation-associated photoinstability, we reduced the exposure time and frequency of the sequential excitation. As the baseline for roGFP1-Se147pSel was greater than roGFP1-pSel, we normalized results (fold change baseline) to facilitate comparison between the constructs. Again,

roGFP1-pSel exhibited a robust response to ≥30μM H_2O_2 ($p<0.01$), but again failed to respond to 3μM H_2O_2 ($p>0.05$) (Fig. 5.4 A). However, roGFP1-Se147pSel exhibited an increased normalized 405/470 ratio in response to ≥300nM H_2O_2 ($p<0.01$) (Fig. 5.4 B). Thus, the threshold for H_2O_2 detection for roGFP1-Se147pSel was approximately 100-fold lower than that of roGFP1-pSel. Curve fitting of the dose-response relationships showed that roGFP1-Se147pSel was approximately 20 times more sensitive to oxidation with H_2O_2 compared to roGFP1-pSel (EC50 of 9.8×10^{-7}M and 2.0×10^{-5}M, respectively)(Fig. 5.4 C). Consistent with our previous data, roGFP1-Se147pSel demonstrated a greatly diminished dynamic range compared to roGFP1-pSel (Fig. 5.4 A and B).

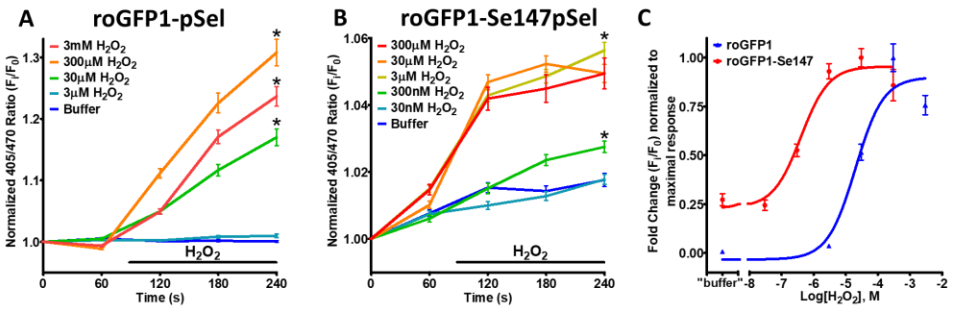

Figure 5.4: Response of roGFP1 selenoprotein to oxidation and reduction with reduced recording frequency. (A) HEK293 expressing roGFP1-pSel (n=62 to 263). (B) HEK293 expressing roGFP1-Se147pSel (103 to 346). Data are normalized mean +/- SEM 405/470 ratio in response to buffer, and 30nM to 3mM H_2O_2. * denotes difference at 240 seconds in normalized ratio between different treatment groups ($p<0.01$). (C) Concentration-response relationship of H_2O_2 treatment in roGFP1-pSel and roGFP1-Se124pSel expressing HEK293 cells fitted using a non-linear regression. EC_{50} for roGFP1-pSel and roGFP1-Se147pSel was 2.0×10^{-5} (R^2 of 0.94) and 9.8×10^{-7} (R^2 of 0.97), respectively.

Finally, we evaluated the sensitivity of the selenoprotein to endogenous ROS evoked by the mitochondrial complex III inhibitor antimycin A(Turrens et al., 1985b; Gyulkhandanyan and Pennefather, 2004). Antimycin A (10μM) failed to increase the 405/470 ratio of roGFP1-pSel ($p>0.05$, compared to untreated cells) (Fig. 5.5 A). Whereas antimycin A increased the 405/470 ratio of roGFP1-Se147pSel ($p<0.01$), compared to the 0.1% ethanol vehicle or untreated control) (Fig. 5.5 B). Unexpectedly, the 0.1% ethanol vehicle decreased the roGFP1-pSel 405/470 ratio

(p<0.01) but this did not occur with roGFP1-Se147pSel (p>0.05). Overall, the data suggest that roGFP1-Se147pSel is sufficiently sensitive to detect endogenous oxidative stress produced downstream of mitochondrial dysfunction.

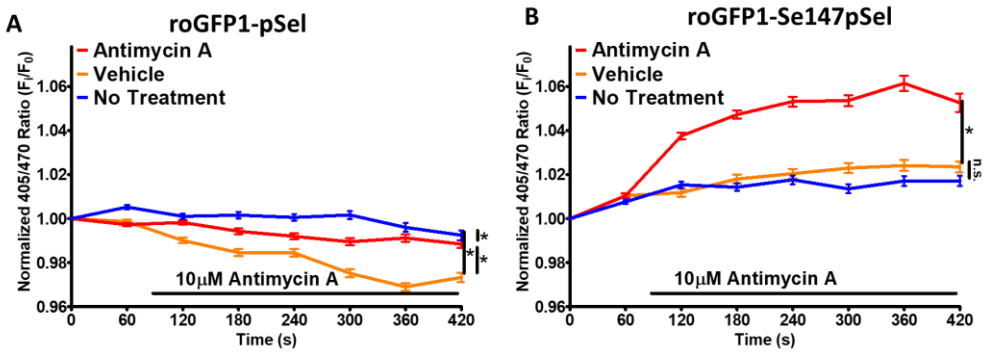

Figure 5.5: Response of roGFP1 selenoprotein to mitochondrial oxidation with antimycin A. (A) HEK293 expressing roGFP1-pSel (n=221 to 363). (B) HEK293 expressing roGFP1-Se147pSel (n=237 to 346). Data are normalized mean +/- SEM 405/470 ratios in response to buffer (blue lines), 0.1% ethanol vehicle (green lines), and 10uM antimycin A (red lines). * denotes significant difference in normalized ratio between different treatment groups (repeated measures ANOVA, p<0.01). n.s. denotes no significant difference between groups (p>0.05).

Redox titration

As roGFP-se147pSel exhibits decreased expression as compared to roGFP1-pSel and roGFP1-N1, we concentrated the protein to perform a redox titration. To protect the selenocysteines and cysteines, we used DTT in the cellular lysis buffer which was washed off prior to performing the titration during our buffer exchange step, this DTT was removed along with any cellular glutathione. The roGFP1-pSel protein was successfully concentrated (Fig. 5.6 A) and we performed a redox titration using a 10mM lipoate buffer with increasing ratios oxidized: reduced lipoate (from 0:10 to 10:0 in increments of 1mM). The 405/470 excitation ratios and fluorescent spectra obtained during these experiments are presented in Fig. 5.6 B and C. Using these data, we calculated the redox potential to be -290mV, similar to results obtained in other labs which calculated the redox potential to be -288mV (Hanson et al., 2004). Although our results are similar, we did not use a known concentration of protein and our measurement of redox potential

is inaccurate. Additionally, even with concentration, we were unable to obtain sufficient signal to evaluate the redox potential of roGFP1-Se147 (Fig. 5.7 A and B).

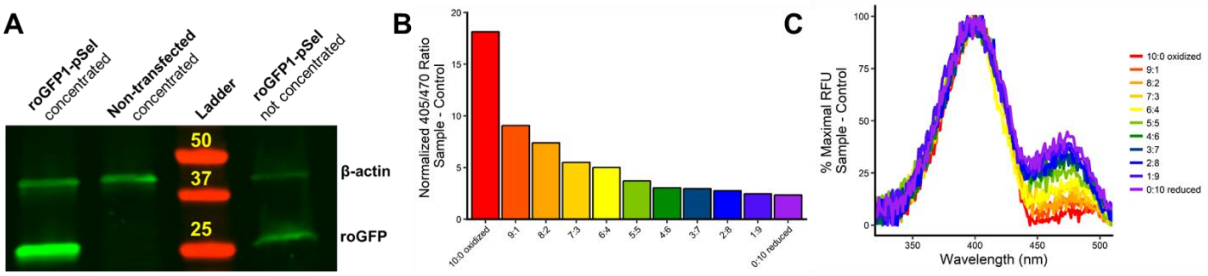

Figure 5.6: Concentration and redox titration of roGFP1-pSel. (A) 405/470 ratio and (B) excitation spectra at varying ratios of oxidized: reduced 10mM lipoate buffer.

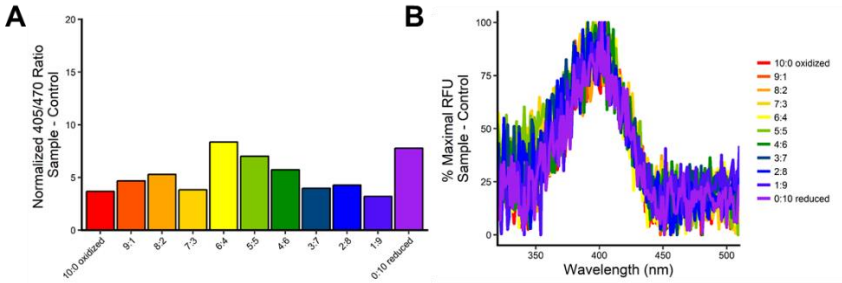

Figure 5.7: Redox titration of concentrated roGFP-Se147pSel. (A) 405/470 ratio and (B) excitation spectra at varying ratios of oxidized: reduced 10mM lipoate buffer. Due to the poor signal to noise ratio was obtained and we were unable to calculate the redox potential.

DISCUSSION

The mutation of cysteine to selenocysteine (UGA) at position 147 in both selenovectors yielded a full-length protein (~27kDa), indicating successful incorporation of the selenocysteine. We found that the pSelExpress1 vector (contains both the selenoprotein and SBP2) produced relatively more selenoprotein, consistent with its reported increased efficiency(Novoselov et al., 2007). Though there was no indication of truncation, this could be a result of polyclonal primary antibody insensitivity to this portion of roGFP1, or levels of truncated protein below the detection threshold. Spectral analysis revealed similar excitation and emission spectra for both roGFP1 and roGFP1-Se147, indicating that the 405/470 ratio was appropriate for determining redox-sensitivity of roGFP1-Se147. Despite the relatively low selenoprotein expression, sufficient roGFP1-Se147

was produced to perform fluorescent live cell imaging of transfected HEK293 cells. Consistent with previous reports roGFP1 responded robustly to substantial oxidation caused by concentrations of ≥30μM H_2O_2 but failed to respond to either 3μM H_2O_2 or 10μM antimycin A(Dooley et al., 2004). roGFP1-Se147 demonstrated a 100-fold lower H_2O_2 detection threshold than roGFP1. Additionally, roGFP10Se147 demonstrated sufficient sensitivity to detect mitochondrial ROS evoked by 10μM antimycin A. This indicates increased sensitivity of the selenoprotein to oxidation with both exogenous and endogenous ROS.

Unfortunately, roGFP1-Se147 exhibited a decreased dynamic range and photoinstability. By decreasing the excitation exposure to roGFP1-Se147, we were able to resolve stimuli-induced responses. However, these characteristics limit the usefulness of roGFP1-Se147 as an effective reporter. Both the diminished dynamic range and photoinstability can likely be attributed to unforeseen structural consequences resulting from the replacement of cysteine with selenocysteine. Other groups have shown that roGFP1 exhibits some photoswitching with prolonged exposure to 405nm light(Schwarzländer et al., 2008). This results in a shift toward the 470nm excitation maximum independent of disulfide bond formation. It is possible that selenocysteine altered the protein structure in such a way that it worsened the existing photoinstability of roGFP1.

We were unable to perform a successful redox titration of roGFP1-Se147. The main reason for this is our inability to concentrate roGFP1-Se147 and obtain a high signal to noise ratio. While we were able to concentrate our sample, this did not provide a sufficient signal to perform a redox titration. However, we were able to concentrate roGFP1-pSel and perform a redox titration. We calculated the redox potential of roGFP1 to be -289mV which is similar to results obtained in other labs indicating a redox potential of -288mV(Hanson et al., 2004) although we did not use a known protein concentration. Other than our use of an unknown protein concentration, another reason for the slight discrepancy in the calculated redox potential is that

other experiments regarding redox potential were performed in an oxygen free environment while ours were performed in room air. Unfortunately, performing a redox titration on roGFP1-Se147 was not possible due to a low signal to noise ratio. This suggests that roGFP1-Se147 may have degraded or lost fluorescence during the concentration and buffer exchange procedure which was used to remove cellular glutathione. This low signal meant that we were unable to determine whether the 405/470 excitation ratio was altered by reduction or oxidation in the lipoate buffer.

Selenocysteine incorporation occurs in approximately 25 native human proteins, the vast majority of which incorporate a single selenocysteine residue(Kryukov et al., 2003). Selenocysteine incorporation requires multiple elements including SECIS, a selenocysteine specific elongation factor and selenium. As such, the incorporation efficiency of selenocysteine is reduced compared to that of canonical amino acids(Leonard et al., 1996; Lesoon et al., 1997; Gonzalez-Flores et al., 2010). Here, we found that expression levels of roGFP1-Se147 were sufficient, yet the functionality (dynamic range, photostability) was disrupted. Previous studies have successfully inserted selenocysteine (in the place of cysteine) into proteins normally lacking selenocysteine. This has been performed in numerous proteins including luciferase, rat growth hormone receptor and the human thyroid hormone receptor without substantially reducing functional responses(Leonard et al., 1996; Latrèche et al., 2009). Furthermore, replacement of cysteine with selenocysteine has been shown to increase catalytic activity in mouse glutoredoxin and plant phospholipid hydroperoxide glutathione peroxidase(Hazebrouck et al., 2000; Ge et al., 2009). This is consistent with the greater redox reactivity of selenocysteine. These reports demonstrate that selenocysteine incorporation in non-selenoproteins is generally feasible and yields functional proteins. Thus, the decreased functionality of roGFP1-Se147 is likely a specific effect on roGFP1, rather than a general property of non-native selenocysteine incorporation.

In conclusion, we present a selenocysteine-containing mutant of roGFP1 that displays increased sensitivity to ROS but decreased dynamic range and photoinstability. The development

of probes with increased sensitivity is a pre-requisite for the understanding of the multiple roles of ROS and oxidative stress in physiological and pathophysiological processes.

UNIQUE METHODS

Creation of roGFP1 selenoprotein

All roGFP constructs were derived from roGFP1-N1 (generous gift from Dr. SJ Remington, University of Oregon). To maximize selenoprotein expression, we used two systems for expression of the roGFP1 selenoprotein (roGFP1-Se147): pLuc01 and pSel. Both selenoprotein expression vectors (selenovectors) contained a 3' SECIS element. To increase selenocysteine incorporation, roGFP1-Se147 was co-expressed with SBP2 by either co-transfection of a second plasmid (pLuc01 system) or co-expression on the same vector (pSel system). The pLuc01 system involved co-transfection of two plasmids: the LucC258U/wtP plasmid containing a 3' PHGPx SECIS element (generous gift from Dr. P Copeland, Rutgers)(Mehta et al., 2004), and the hSBP2/V5-HIS plasmid (generous gift from Dr. P Copeland, Rutgers), contained human SBP2. roGFP1 was subcloned from roGFP1-N1 into LucC258U/wtP (generous gift from Dr. P Copeland, Rutgers) plasmid using HindIII and PacI (inserted using primer) restriction sites (roGFP1-pLuc01)(Hanson et al., 2004; Mehta et al., 2004). Custom designed primers with a single point mutation were then used to mutate roGFP1 nucleic acid 441 from C to A, creating a UGA codon for selenocysteine insertion (roGFP1-Se147pLuc01). The pSel system utilized a dual expression in the pSelExpress1 plasmid (generous gift from Dr. V Gladyshev, Brigham and Women's Hospital, Harvard Medical School) which contains a modified Toxoplasma gondii SECIS element and the C terminal functional domain of rat SBP2(Novoselov et al., 2007). Both roGFP1 and roGFP1-Se147 were PCR amplified from the pLuc01 expression system and inserted into pSelExpress1 using XbaI and HindIII restriction sites (roGFP1-pSel and roGFP1-Se147pSel). The success of all insertions and mutations were confirmed by sequencing.

Cell Culture

HEK293 cells were used for functional analysis. HEK239T cells were used for all other studies to maximize protein expression. Cells transfected with roGFP1-Se147 constructs were supplemented with 10nM sodium selenite at the time of transfection to allow for selenocysteine insertion. For general HEK293 cell culture methods, see common methods.

Western Blot

Cells were transfected with roGFP1-pLuc01, roGFP1-Se147pLuc01, roGFP1-pSel, roGFP1-Se147pSel, and roGFP1-N1 (vector control). Transfected cells were lysed using lysis buffer (50mM TRIS, 150mM NaCl, 2% TritonX-100, and 0.05% SDS) and protein collected via centrifugation. The amount of total protein was calculated using a bicinchoninic acid assay (Thermo Scientific, Rockford, IL). Samples were diluted to 1ug/ul in Licor 4X protein sample loading buffer. The diluted protein (10µg) was loaded onto a Mini-Protean TGX 4-20% precast gel (Bio-Rad, Hercules, CA). Following electrophoresis, proteins were transferred onto a nitrocellulose membrane using a Trans-Blot Turbo transfer pack (Bio-Rad, Hercules, CA) on a Trans-Blot Turbo (Bio-Rad, Hercules, CA). Membranes were blocked in Odyssey blocking buffer (LI-COR, Lincoln, NE) for 60 minutes then incubated in 1:500 chicken anti GFP (Aves cat# GFP-1020) and 1:500 mouse anti β–actin (Novus, Minneapolis, MN, Cat# NB600-501) diluted in Odyssey blocking buffer + 0.15% Tween-20 overnight at 4°C. Gels were washed 6x10 minutes with PBS + 0.1% Tween-20 then incubated the secondary antibodies: 1:20,000 donkey anti mouse 680 (LI-COR, Lincoln, NE, Cat# 926-68022) and 1:20,000 donkey anti chicken 800 (LI-COR, Lincoln, NE, Cat# 926-32218) diluted in in Odyssey blocking buffer + 0.15% tween +0.02% SDS. After six washes with PBS + 0.1% Tween-20, membranes were imaged using a Licor Odyssey (LI-COR, Lincoln, NE) to evaluate expression of the roGFP1 and roGFP1-Se147 constructs.

Spectral analysis

Cells were transfected with pEGFP-N1 (Clonetech, Mountain View, CA), roGFP1-pSel, or roGFP1-Se147pSel. To obtain a cell suspension for analysis, cells were lifted with Accutase, spun down then resuspended in 600µl PBS (250,000 cells for GFP control, and 750,000 roGFP1-pSel and roGFP1-Se147pSel transfected cells). 100µl of each cell suspension was loaded into a well on an optical 96 well plate. Scans were performed using a Synergy Mx Microplate Reader (BioTek, Winooski, VT). Excitation scans between 350-520nm were detected at 530nm, emission scans were detected between 430 and 700nm following excitation at 405nm. For analysis, background fluorescence (non-transfected cells) was subtracted from the sample fluorescence. To normalize the data we calculated the percent maximal relative fluorescence units (RFU) of the background subtracted data.

Functional Analysis

Transfected cells on Poly-D Lysine and laminin coverslips were placed in a chamber and perfused with 10mM HEPES buffer (154mM NaCl, 1mMKCl, 0.5M MgCl2, 2.5mM CaCl2, 5.6mM D-glucose) at 33-34˚C and evaluated for changes in cellular redox state. Drugs were diluted in HEPES (DTT, 3mM, 2mM; H_2O_2, 30nM to 3mM; Antimycin A, 10µM). Cells were monitored using sequential excitation at 405 and 470nm every 6 or 60 seconds with emissions recorded at 510nm using microscopy (CoolSnapHQ2; Photometrics Surrey, BC, Canada), and analyzed using NIS elements software (Nikon, Melville, NY).

Redox Titration

Cells were transfected with roGFP1-pSel, and roGFP1-Se147pSel (see cell culture). After 24 hours, cells were lifted with Accutase, then transferred to a conical tube then spun at 700 x g for 2 minutes. Each pellet was resuspended in chilled PBS + 100ug/ul Saponin + 0.5mg/ml Roche

Complete Mini protease inhibitor + 1mM DTT and incubated on ice for 3 minutes. The use of saponin permitted extraction of roGFP1 from cells while leaving larger proteins inside the cell. The DTT was used to protect the cysteines and selenocysteines of roGFP1-Se147pSel and roGFP-pSel from oxidation during extraction. The saponin-permeabilized cells were centrifuged at 700 x g for two minutes. The supernatant was removed and placed in a microcentrifuge tube and spun at 1400g for 10 minutes at 4^{o}C to remove any remaining debris. Again, the supernatant was removed, then placed in a pierce spin column (10,000 MW cutoff), volume adjusted to 6mL and centrifuged at 4^{o}C at 4000 x g until the volume was reduced 90-95%. To exchange the buffer and remove DTT, remaining liquid was diluted to 2mL with 75mM HEPES + 125mM KCl + 1mM EDTA and centrifuged again at 4^{o}C at 4000 x g until the volume was reduced by 90-95%. The remaining liquid was removed and volume adjusted to account for variations in cellular growth. For each condition, 180µl of sample was pipetted into each of 11 wells on a 96 well optical plate with 20µl of the appropriate lipoic acid buffer (10mM final) and incubated at room temperature for one hour.

An excitation scan (350-520nm excitation; 530nm emission) was performed using a Synergy Mx Microplate Reader (BioTek, Winooski, VT) using the same procedure as for the spectral analysis. For analysis, background fluorescence (non-transfected cells) was subtracted from the sample fluorescence. To calculate the 405/470 ratio, we used the average of 403-407 excitation and 468-472 of the normalized data (see spectral analysis) to minimize the impact of the low signal to noise ratio caused by low protein expression. For each titration increment (from 0:10 to 10:0) we calculated: $Y = (R_n-R_{min})/(R_{max}-R_n)$.

R_n	405/470 ratio at a specific oxidized: reduced buffer ratio
R_{min}	minimum 405/470 ratio (0:10 reduced)
R_{max}	is the maximal 405/470 ratio (10:0 oxidized)

A plot of Y versus log([oxidized] / [reduced]) was generated. The buffer ratio required to achieve 50% protein oxidation (A) was determined by calculating the Y intercept of the trendline. K_{eq} was calculated form the following equation: $\log K_{eq}=\log(F470_{red})/(F470_{ox})- \log A$.

$F470_{red}$	fully reduced protein at 470nm excitation
$F470_{ox}$	fully oxidized protein 470nm excitation
A	buffer ratio where the protein is 50% oxidized

The equilibrium potential was calculated using the Nernst equation: $E'= E'_0 - (RT/nF) \ln K_{eq}$.

E'	equilibrium potential
E'_0	redox potential of the buffer (lipoate = -290 mV)
R	gas constant (8.313 J/mol/K)
T	temperature (K)
n	number of electrons exchanged (2)
F	Faraday's constant (96490 J/mol/V)

Data Analysis

Using SPSS (IBM, Armonk, New York), a repeated measures ANOVA was used to evaluate effects of hydrogen peroxide and Antimycin A treatments. To evaluate the effects of treatment for each time point a one way ANOVA was performed (SPSS). A p value less than 0.05 was taken as significant. Using Prism (GraphPad, La Jolla, CA), a non-linear regression was used to generate a concentration response-curve and calculate the EC50 of H_2O_2.

CHAPTER 6

Discussion

The impact of ROS and mitochondrial dysfunction is gaining increased attention in many disease states involving the aberrant activity of sensory nerves. Here, we evaluated the impact of mitochondrial modulation on the activation of TRPA1 and TRPV1 using CCCP, Rotenone, and Antimycin A. Interestingly, all three inhibitors activated only a portion of nociceptive vagal neurons which express TRPA1 and/or TRPV1. As vagal neurons are heterogenous, the lack/presence of a response mitochondrial modulation could be due to the presence of more than one neuronal subtype. However, this is unlikely given that this same phenomenon was present in genetically identical transfected HEK293 cells. Therefore, this lack of response in a portion of cells is likely due to mitochondrial metabolic status, or baseline cellular redox state. Our co-imaging studies which simultaneously monitored mitochondrial function and ion channel activation demonstrated that many neurons that did not display evidence of channel activation exhibited substantial mitochondrial ROS production and mitochondrial depolarization. This seems to indicate that numerous factors are involved in these responses. Although activation of TRPA1 is ROS-dependent, many neurons with substantial ROS production failed to exhibit a Ca^{2+} flux. This seems to indicate that some preexisting cellular factor is responsible for sensitizing responses to mitochondrial modulation. As TRPA1 is potentiated by Ca^{2+}(Wang et al., 2008), mitochondrial Ca^{2+} release observed during mitochondrial depolarization may act to sensitize TRPA1 to ROS-evoked activation. Unfortunately, we are unable to study the combined impacts of mitochondrial

polarization, and ROS production on ion channel activation as co-imaging using three probes is not possible due to the overlap of excitation and emission fluorescence spectra.

Although the mechanism underlying TRPV1 activation by mitochondrial modulation remains unknown, its activation is likely also affected by numerous factors as not all TRPV1 expressing cells responded to mitochondrial modulation. The regulation of TRPV1 is complex and involves many factors. Therefore, several mechanisms may serve to activate TRPV1 downstream of mitochondrial modulation. The most likely being the PLC/PKC pathway which acts to sensitize TRPV1 through several mechanisms. The PLC/PKC pathway is activated by inflammatory signaling, downstream of Receptor Tyrosine Kinases (RTK), and by antimycin A(Joseph and Levine, 2010; Wu et al., 2010b; Zhang et al., 2012). Many inflammatory mediators result in the activation of PLC. This results in the cleavage of PIP_2 into DAG and IP_3. Not only does this release the constitutive inhibition of PIP_2 on TRPV1, but it generates DAG, a TRPV1 agonist(Woo et al., 2008; Cao et al., 2013). Furthermore, mitochondrial depolarization can result in the activation of PLC. The combined effects of PLC activation including the production of DAG and increased cytosolic Ca^{2+} can activate PKC, which has been shown to activate TRPV1(Lee et al., 2012; Wang et al., 2015). Furthermore, antimycin A results in PKC activation and translocation to the cellular membrane(Wu et al., 2010b; Hadley et al., 2014). Although this may occur through the activation of PLC, this may also occur through the production of ROS which activates non-canonical isoforms of PKC. This mechanism explains the great variation in responses to mitochondrial modulation. Many isoforms of PLC an PKC are present in vagal neurons. As their expression is heterogeneous and they have differing substrate affinities, PLC and PKC expression in sensory nerve subsets may have an impact on TRPV1 activation.

We gained many insights into the effects of mitochondrial function on the activation of TRPA1 and TRPV1. However, much remains unknown and our studies are complicated by the issues regarding obtaining measurements of mitochondrial function. One such issue is that the

use of mitochondrially targeted indicators such as MitoSOX and JC-1 can themselves induce mitochondrial dysfunction. To minimize this, we used low dye concentrations, short loading times, and minimized the length of individual experiments. Another potential problem is that the exact mechanisms by which ROS indicator dyes undergo oxidation is still under debate. Although ROS sensitive probes exhibit specificities for individual ROS, the specificity of these probes is still under debate. One reason for this being that these probes are oxidized in a different manner *in situ* than *in vitro*. Another caveat of measurements in intact cells is that exact measurements of ROS production and mitochondrial depolarization can only be made in isolated mitochondria, not intact cells. Therefore, measurements in intact cells are not exact and can only determine the extent of mitochondrial polarization and ROS production relative to baseline.

Another complication regarding our studies is the identification of nociceptive neurons. The main reason for this is the heterogenous nature of vagal neurons. As most nociceptors express TRPV1, TRPV1 is typically used to identify nociceptive neurons. However, a small portion of nociceptors do not express TRPA1 or TRPV1. In general, nociceptors are defined as being a population of sensory neurons which are activated by noxious stimuli(Sherrington, 1906). As such, they are inactive in healthy tissues and active in the presence of cellular damage and potential threats. The specific set of activating stimuli for a single nociceptor is dependent on the expression of ion channels at the nerve terminal. As the expression of these channels varies greatly, and identifications are somewhat ambiguous this complicates the identification of nociceptive neurons. However, for our experiments devising a method for the identification was necessary as mitochondrial modulation evoked neuronal activation a subset of nociceptive neurons. To aid in the identification of nociceptors which may not express TRPA1 or TRPV1, we used the VR1 CreRosa mouse model which expresses td Tomato in all cells which have ever expressed TRPV1 (TRPV1 lineage neurons). Here, we identified nociceptors as neurons which exhibited a functional response to TRPA1 or TRPV1 agonists and/or express td Tomato (TRPV1

lineage neurons). The VR1 CreRosa neurons allow for the identification of nociceptors in experiments using the TRPV1 inhibitor I-RTX which not wash off, preventing the functional responses to capsaicin typically used to identify TRPV1 expresion. Unfortunately, VR1 CreRosa method for nociceptor identification is not available in KO mouse models. In co-imaging experiments, we also used functional classifications of TRPA1 and TRPV1 expression as td Tomato fluorescence interferes with the visualization of JC-1 and MitoSOX. Therefore, we only used the functional responses to TRPV1 and TRPA1 agonists to identify nociceptors in co-imaging and KO experiments. Due to these complications regarding nociceptor classification, we did not perform statistics on the percentage of nociceptors which responded and only used these classifications in data visualization.

A complication of these studies are the methods available to study ROS, which often have many caveats. Therefore, we created a roGFP1 selenoprotein to increase the sensitivity of roGFP1 to ROS. This roGFP1 selenoprotein which exhibited increased sensitivity to ROS as compared to roGFP1 as its 405/470 ratio was increased by lower concentrations of H_2O_2 (30nM) whereas the fluorescence of roGFP1 was unaltered. Most importantly, the roGFP1 selenoprotein, but not roGFP1, responded during antimycin A treatment. Unfortunately, this protein exhibited a poor dynamic range and low expression due to the inefficiencies in selenocysteine incorporation. While we were able to measure the excitation and emission profile of the roGFP1 selenoprotein, we failed to generate sufficient material to perform a redox titration which may be in part due to protein degradation. Unfortunately, the low expression of the roGFP1 selenoprotein coupled by its low dynamic range makes its practical use limited. Therefore, other strategies must be used to develop improved genetically encoded ROS sensors and dyes to permit studies of ROS in disease states and cellular signaling. If an increased understanding of the high reactivity of TRPA1 is gained, this mechanism may be exploited to increase the reactivity of the reactive cystines of roGFP1 and other genetically encoded redox sensing proteins.

CHAPTER 7

Common Methods

MOUSE MODELS

Female TRPV1$^{-/-}$ mice were mated with male TRPV1$^{-/-}$ mice. Female TRPA1$^{-/-}$ mice were mated with male TRPA1$^{+/-}$ mice. Genotype of the offspring was confirmed using polymerase chain reaction. Wild type C57BL/6J mice were purchased from The Jackson Laboratory. For the VR1 CreRosa mouse model, TRPV1-Cre mice(Cavanaugh et al., 2011) were crossed with Rosa-tdTomato mice(Madisen et al., 2010). All experiments were performed with approval from the University of South Florida Institutional Animal Care and Use Committee (AAALAC #000434).

NEURONAL DISSOCIATION

To obtain individual neurons on coverslips for live cell imaging experiments, we performed a neuronal dissociation. Male 5-10 week old mice were euthanized via CO_2 asphyxiation followed by exsanguination. Heads (skin removed) were placed in chilled HBSS then transferred to a dissecting microscope. Vagal ganglia (nodose and jugular) were dissected out and a nick placed in the outer layer to allow for penetration of the enzymes and placed in 2mL chilled, sterile-filtered HBSS with 2mg/mL collagenase and 2mg/mL Dispase I. The ganglia were placed in a 37^{o}C water bath for 30 minutes then triturated with a large bore and medium bore pipette and returned to the water bath for another 20 minutes. After incubation, neurons were triturated with a small bore pipette then placed in the centrifuge and spun for 2 minutes at 700g. Supernatant was removed, and neurons were resuspended in 10mL L-15 media centrifuged for 2 minutes at 700g. This wash

was repeated once more using L-15 media with 5ul/mL pen/strep. Neurons were then resuspended in 100ul L-15 + pen/strep and 20ul drops placed on the center of each of 5 PDL laminin coverslips inside of a 6 well plate. Neurons were placed in an incubator and allowed to adhere for 1-2 hours before flooding with 2mL L-15 + 10% FBS. Neurons were returned to the incubator and used within 24 hours.

HEK293 CELL CULTURE

HEK293 cells were used for functional analysis. HEK239T cells were used for all other studies to maximize protein expression. Cells were lifted using Acutase and seeded onto poly-D lysine/laminin coverslips (live cell imaging), six well plates (roGFP western) or culture flasks (roGFP spectral analysis) and cultured in Dubecco's modified Eagle's medium containing 4.5g/L glucose, L-glutamine, and sodium pyruvate (Corning, Manassas, VA, REF: 10-013-CV). The media was supplemented with 0.5% penicillin/streptomycin and 10% fetal bovine serum. Cells were transfected at 80% confluency cells using lipofectamine 2000 (Thermo Fisher Scientific, Waltham, MA). Cells were allowed to incubate at 37^{o}C with 5% CO_2 and used within 36 hours.

LIVE CELL IMAGING

For live cell Ca^{2+} imaging experiments, cells were incubated with 4μM FURA-2AM for 30-60 minutes at 37^{o}C. For co-imaging experiments, cells were incubated with 4μM FURA-2AM for 30-60minutes before with 2μM 5,5′,6,6′-Tetrachloro-1,1′,3,3′-tetraethyl-imidacarbocyanine iodide (JC-1), or 5μM MitoSOX Red was added for the last 15 minutes of incubation. Coverslips were loaded into a chamber on an inverted microscope and perfused with heated (33-34^{o}C) HEPES buffer (154mM NaCl, 1.2mM KCl, 1.2mM MgCl2, 2.5mM $CaCl_2$, 5.6mM D-Glucose). Slides equilibrated for 10 minutes prior to the start of the experiment and if using the VR1 CreRosa neurons, an image was taken to visualize td Tomato fluorescence 535nm (excitation, emission at

610nm). Changes in cytosolic Ca^{2+} was monitored using sequential excitation at 340nm and 380nm (510nm emissions) with images taken every 6 seconds using a CoolSnap HQ2 camera (Photometerics, Surry, BC) and evaluated ratiometrically using the 340nm/380nm FURA-2 fluorescence. In co-imaging experiments, Fura-2AM imaging was followed by either MitoSOX Red imaging (mitochondrial O_2^- production) with excitation 535nm (emission at 610nm) or JC-1 imaging (mitochondrial polarization) with 470nm (emission at 525nm and 610nm).

All drugs were diluted in in HEPES buffer. Following 10μM antimycin A, 10μM CCCP, or 5μM rotenone treatment, TRPA1 and TRPV1 expression was evaluated using the average cytosolic Ca^{2+} flux during 100μM AITC (TRPA1 agonist), and 1μM capsaicin (TRPV1 agonist) treatments (details regarding classification of neurons below). In co-imaging experiments with FURA-2AM and JC-1 or MitoSOX, capsaicin and AITC were combined. In live-cell co-imaging experiments of vagal neurons, capsaicin and AITC were combined to decrease experiment duration. This was followed by 75mM KCl (neuronal experiments only) to identify neurons and 5μM ionomycin to evaluate the maximal Ca^{2+} response.

IMAGE ANALYSIS

Image analysis was performed by using Nikon Elements (Nikon, Melville, NY) by drawing individual regions of interest (ROI) that around the intracellular region for each neuron and tracked over time. ROI's with an unstable, high, or noisy baseline were eliminated from analysis. Neurons which failed to exhibit an increase in $[Ca^{2+}]_i$ either AITC, capsaicin or KCl challenges (> 30% the ionomycin maximal response) were eliminated. HEK293 cells failing to exhibit an increased $[Ca^{2+}]_i$ in response to AITC (TRPA1 transfected) or capsaicin (TRPV1 transfected) were omitted. Relative changes in $[Ca^{2+}]_i$ were determined ratiometrically (R) using Fura-2 fluorescence: 340nm/380nm as to negate the impact of cell to cell variations in FURA-2AM loading. In the time series analyses, changes in the 340/380 ratio ($\Delta R = R_1—R_0$) are presented. Antimycin A

responses were calculated using the maximal change in the 340/380 ratio (see Calculation of responses to mitochondrial modulation).

CLASSIFICATION OF VAGAL NEURONS

Methods are adapted from Stanford and Taylor-Clark 2018(Stanford and Taylor-Clark, 2018). The average Ca^{2+} flux during AITC and capsaicin (chapters 1 and 3) or combined AITC/capsaicin (chapter 2) treatments were used to classify neuronal expression of TRPA1 and TRPV1. Responses were classified as follows:

	$R_{AITC/Caps}$	average 340/380 ratio during AITC/capsaicin treatment
$R_{AITC/Caps} > (R_{bl} + 2*SD_{bl})$	R_{bl}	baseline 340/380 ratio prior to treatment
	SD_{bl}	standard deviation of R_{bl}

The functional responses (Ca^{2+} fluxes) to capsaicin and AITC were used to classify TRPA1 and TRPV1 expression. This method allows for the classification of most, but not all, nociceptors as nociceptors. The reason for this is the heterogenous nature of vagal neurons and the expression of TRPA1 and TRPV1 on most but not all nociceptors. Unfortunately, this lack of TRPA1 and TRPV1 expression complicates the identification of nociceptors. Therefore, when available we used the VR1 CreRosa mouse model which expresses td Tomato in all neurons which have ever expressed TRPV1. This allows for the identification of TRPV1 lineage neurons by visualizing td Tomato fluorescence. Furthermore, this model is also useful in experiments using the TRPV1 inhibitor I-RTX as it does not wash off, preventing the identification of TRPV1 expression using functional classifications. In chapter 1, we characterized this mouse model and found that 61% of neurons (n = 68) expressed td Tomato expressed TRPV1 and/or TRPA1, 17% of neurons (n = 21) were td Tomato positive and did not express TRPV1 and/or TRPA1 and 4%

of neurons were td Tomato negative and expressed TRPA1 and/or TRPV1. As we classified nociceptors as the population of neurons which expresses td Tomato, TRPA1 and/or TRPV1, this results in approximately 82% of neurons being classified as nociceptive.

In studies of mitochondrial inhibitors on the Ca^{2+} fluxes in vagal neurons, we found that mitochondrial modulation evoked plasma membrane ion channel activation in a portion of nociceptive, but not non-nociceptive neurons. This underscores the importance of the proper identification of nociceptive neurons. Unfortunately, this the VR1 CreRosa mouse model was not available for all experiments as td Tomato fluoresce interferes with visualization of MitoSOX Red and JC-1 and it is not available in KO models. Therefore, in these experiments we relied on functional classifications of TRPV1 and TRPA1 expression. In experiments where the VR1 CreRosa mouse model was available, we used the above method to classify nociceptors (nociceptive versus non-nociceptive) whereas when this model was not available, we did not identify neurons as nociceptive and relied on evaluating TRPA1 and TRPV1 expression using functional responses to agonists (A1/V1+ versus A1/V1-).

CALCULATION OF RESPONSES TO MITOCHONDRIAL MODULATION

In the bar graphs, scatterplots and statistical analyses we used maximal responses to mitochondrial modulation expressed as the maximal change in the 340/340 ratio during three-minute treatment with mitochondrial modulators (ΔR_{max}). In our experiments, only a portion of neurons responded. These responses were isolated to nociceptive neurons, many of which express TRPA1 and/or TRPV1. Unfortunately, nociceptor classification is complicated by the heterogenous nature of vagal neurons. While most express TRPA1 and/or TRPV1, many do not. Due to the individual requirements of each experiment and our ability to use the VR1 CreRosa mouse model, we classified neurons using two methods (see nociceptor classifications) one which classified neurons as nociceptive or nonnociceptive and the other which classified neurons

based on TRPA1/TRPV1 expression. Therefore, we defined responses to mitochondrial modulation based on either the nonnociceptive population or the A1/V1- population as follows:

$\Delta R_{max(noci)} > \Delta R_{max(noci)} + 3*SD_{(nonnoci)}$

$\Delta R_{max(noci)}$ maximal response in a single nociceptor

$\Delta Rmax_{(nonnoci)}$ average maximal response in non-nociceptors

$SD_{(nonnoci)}$ standard deviation of $\Delta R_{max(nononoci)}$

NOTE: *For experiments using expressional classification of TRPA1/TRPV1, A1/V1+ was used in place of nociceptive neurons and A1/V1- was used in the place of nonnociceptive neurons.*

Using the above calculations, we were able to classify neurons based on their response vs. nonresponse to mitochondrial modulation. This allowed for the evaluation of the percentage of responding neurons and magnitude of the Ca^{2+} flux in responding neurons. In HEK293 cells the response vs. non-response classifications were not used. Therefore, in experiments using HEK293 cells, only the maximal responses to mitochondrial modulation across all cells were evaluated.

REFERENCES

Adrian, E.D. 1933. Afferent impulses in the vagus and their effect on respiration. *J Physiol*. 79:332-358.

Agostoni, E., J.E. Chinnock, M.B. De Daly, and J.G. Murray. 1957. Functional and histological studies of the vagus nerve and its branches to the heart, lungs and abdominal viscera in the cat. *J Physiol*. 135:182-205.

Aguilera-Aguirre, L., A. Bacsi, A. Saavedra-Molina, A. Kurosky, S. Sur, and I. Boldogh. 2009. Mitochondrial dysfunction increases allergic airway inflammation. *J Immunol*. 183:5379-5387.

Andersson, D.A., C. Gentry, S. Moss, and S. Bevan. 2008. Transient receptor potential A1 is a sensory receptor for multiple products of oxidative stress. *J Neurosci*. 28:2485-2494.

Andre, E., B. Campi, S. Materazzi, M. Trevisani, S. Amadesi, D. Massi, C. Creminon, N. Vaksman, R. Nassini, M. Civelli, P.G. Baraldi, D.P. Poole, N.W. Bunnett, P. Geppetti, and R. Patacchini. 2008. Cigarette smoke-induced neurogenic inflammation is mediated by alpha,beta-unsaturated aldehydes and the TRPA1 receptor in rodents. *J Clin Invest*. 118:2574-2582.

Bahia, P.K., T.A. Parks, K.R. Stanford, D.A. Mitchell, S. Varma, S.M. Stevens, Jr., and T.E. Taylor-Clark. 2016. The exceptionally high reactivity of Cys 621 is critical for electrophilic activation of the sensory nerve ion channel TRPA1. *J Gen Physiol*. 147:451-465.

Bandell, M., G.M. Story, S.W. Hwang, V. Viswanath, S.R. Eid, M.J. Petrus, T.J. Earley, and A. Patapoutian. 2004. Noxious cold ion channel TRPA1 is activated by pungent compounds and bradykinin. *Neuron*. 41:849-857.

Barnes, P.J. 2012. Severe asthma: Advances in current management and future therapy. *J Allergy Clin Immunol*. 129:48-59.

Bautista, D.M., S.E. Jordt, T. Nikai, P.R. Tsuruda, A.J. Read, J. Poblete, E.N. Yamoah, A.I. Basbaum, and D. Julius. 2006. TRPA1 Mediates the Inflammatory Actions of Environmental Irritants and Proalgesic Agents. *Cell*. 124:1269-1282.

Bautista, D.M., P. Movahed, A. Hinman, H.E. Axelsson, O. Sterner, E.D. Hogestatt, D. Julius, S.E. Jordt, and P.M. Zygmunt. 2005. Pungent products from garlic activate the sensory ion channel TRPA1. *Proc Natl Acad Sci U S A*. 102:12248-12252.

Beckman, J.S., R.L. Minor, Jr., C.W. White, J.E. Repine, G.M. Rosen, and B.A. Freeman. 1988. Superoxide dismutase and catalase conjugated to polyethylene glycol increases endothelial enzyme activity and oxidant resistance. *J Biol Chem*. 263:6884-6892.

Bednar, R.A. 1990. Reactivity and pH dependence of thiol conjugation to N-ethylmaleimide: detection of a conformational change in chalcone isomerase. *Biochemistry*. 29:3684-3690.

Berthound, H., and W. Neuhuber. 2000. Functional and chemical anatomy of the afferent vagal system. *Auton Neurosci*. 85:1-17.

Bessac, B.F., and S.E. Jordt. 2008. Breathtaking TRP channels: TRPA1 and TRPV1 in airway chemosensation and reflex control. *Physiology (Bethesda)*. 23:360-370.

Biringerova, Z., S. Gavliakova, M. Brozmanova, M. Tatar, E. Hanuskova, I. Poliacek, and J. Plevkova. 2013. The effects of nasal irritant induced responses on breathing and cough in anaesthetized and conscious animal models. *Respir Physiol Neurobiol*. 189:588-593.

Birrell, M.A., M.G. Belvisi, M. Grace, L. Sadofsky, S. Faruqi, D.J. Hele, S.A. Maher, V. Freund-Michel, and A.H. Morice. 2009. TRPA1 Agonists Evoke Coughing in Guinea-pig and Human Volunteers. *Am J Respir Crit Care Med*. 180:1042-1047.

Bobkov, Y.V., E.A. Corey, and B.W. Ache. 2011. The pore properties of human nociceptor channel TRPA1 evaluated in single channel recordings. *Biochim Biophys Acta*. 1808:1120-1128.

Boillat, A., O. Alijevic, and S. Kellenberger. 2014. Calcium entry via TRPV1 but not ASICs induces neuropeptide release from sensory neurons. *Mol Cell Neurosci*. 61:13-22.

Bonham, A.C., C.Y. Chen, S. Sekizawa, and J.P. Joad. 2006. Plasticity in the nucleus tractus solitarius and its influence on lung and airway reflexes. *J Appl Physiol (1985)*. 101:322-327.

Braunstahl, G.J., W.J. Fokkens, S.E. Overbeek, A. KleinJan, H.C. Hoogsteden, and J.B. Prins. 2003. Mucosal and systemic inflammatory changes in allergic rhinitis and asthma: a comparison between upper and lower airways. *Clin Exp Allergy*. 33:579-587.

Breckwoldt, M.O., F.M.J. Pfister, P.M. Bradley, P. Marinković, P.R. Williams, M.S. Brill, B. Plomer, A. Schmalz, D.K. St Clair, R. Naumann, O. Griesbeck, M. Schwarzländer, L. Godinho, F.M. Bareyre, T.P. Dick, M. Kerschensteiner, and T. Misgeld. 2014. Multiparametric optical analysis of mitochondrial redox signals during neuronal physiology and pathology in vivo. *Nat Med*. 20:555-560.

Brozmanova, M., V. Bartos, L. Plank, and M. Tatar. 2007. Experimental allergic rhinitis-related cough and airway eosinophilia in sensitized guinea pigs. *J Physiol Pharmacol*. 58 Suppl 5:57-65.

Brozmanova, M., L. Mazurova, F. Ru, M. Tatar, and M. Kollarik. 2012. Comparison of TRPA1-versus TRPV1-mediated cough in guinea pigs. *Eur J Pharmacol*. 689:211-218.

Buckley, T.L., and F.P. Nijkamp. 1994. Airways hyperreactivity and cellular accumulation in a delayed-type hypersensitivity reaction in the mouse. Modulation by capsaicin-sensitive nerves. *Am J Respir Crit Care Med*. 149:400-407.

Byun, B.J., and Y.K. Kang. 2011. Conformational preferences and pKa value of selenocysteine residue. *Biopolymers*. 95:345-353.

Caceres, A.I., M. Brackmann, M.D. Elia, B.F. Bessac, D. del Camino, M. D'Amours, J.S. Witek, C.M. Fanger, J.A. Chong, N.J. Hayward, R.J. Homer, L. Cohn, X. Huang, M.M. Moran, and S.E. Jordt. 2009. A sensory neuronal ion channel essential for airway inflammation and hyperreactivity in asthma. *Proc Natl Acad Sci U S A*. 106:9099-9104.

Canning, B.J. 2007. Encoding of the cough reflex. *Pulm Pharmacol Ther*. 20:396-401.

Canning, B.J., and A. Fischer. 2001. Neural regulation of airway smooth muscle tone. *Respir Physiol*. 125:113-127.

Canning, B.J., S.B. Mazzone, S.N. Meeker, N. Mori, S.M. Reynolds, and B.J. Undem. 2004. Identification of the tracheal and laryngeal afferent neurones mediating cough in anaesthetized guinea-pigs. *J Physiol*. 557:543-558.

Canning, B.J., N. Mori, and S.B. Mazzone. 2006. Vagal afferent nerves regulating the cough reflex. *Respir Physiol Neurobiol*. 152:223-242.

Cannon, M.B., and S.J. Remington. 2006. Re-engineering redox-sensitive green fluorescent protein for improved response rate. *Protein Sci.* 15:45-57.

Cao, E., J.F. Cordero-morales, B. Liu, F. Qin, and D. Julius. 2013. TRPV1 Channels Are Intrinsically Heat Sensitive and Negatively Regulated by Phosphoinositide Lipids. *Neuron*. 77:667-679.

Carr, M.J., M. Kollarik, S.N. Meeker, and B.J. Undem. 2003. A role for TRPV1 in bradykinin-induced excitation of vagal airway afferent nerve terminals. *J Pharmacol Exp Ther*. 304:1275-1279.

Carr, M.J., and B.J. Undem. 2003. Bronchopulmonary afferent nerves. *Respirology*. 8:291-301.

Caterina, M.J., M.A. Schumacher, M. Tominaga, T.A. Rosen, J.D. Levine, and D. Julius. 1997. The capsaicin receptor: a heat-activated ion channel in the pain pathway. *Nature*. 389:816-824.

Cavanaugh, D.J., A.T. Chesler, A.C. Jackson, Y.M. Sigal, H. Yamanaka, R. Grant, D. O'Donnell, R.A. Nicoll, N.M. Shah, D. Julius, and A.I. Basbaum. 2011. Trpv1 reporter mice reveal highly restricted brain distribution and functional expression in arteriolar smooth muscle cells. *J Neurosci*. 31:5067-5077.

Celik, M., A. Tuncer, O.U. Soyer, C. Sackesen, H. Tanju Besler, and O. Kalayci. 2012. Oxidative stress in the airways of children with asthma and allergic rhinitis. *Pediatr Allergy Immunol*. 23:556-561.

Chambers, I., J. Frampton, P. Goldfarb, N. Affara, W. McBain, and P.R. Harrison. 1986. The structure of the mouse glutathione peroxidase gene: the selenocysteine in the active site is encoded by the 'termination' codon, TGA. *The EMBO journal*. 5:1221-1227.

Chandel, N.S. 2014. Mitochondria as signaling organelles. *BMC biology*. 12:34.

Chen, Q., E.J. Vazquez, S. Moghaddas, C.L. Hoppel, and E.J. Lesnefsky. 2003. Production of reactive oxygen species by mitochondria: central role of complex III. *J Biol Chem*. 278:36027-36031.

Chen, X., X. Tian, I. Shin, and J. Yoon. 2011. Fluorescent and luminescent probes for detection of reactive oxygen and nitrogen species. *Chem. Soc. rev.* 40:4783-4804.

Chinopoulos, C., L. Tretter, and V. Adam-Vizi. 1999. Depolarization of in situ mitochondria due to hydrogen peroxide-induced oxidative stress in nerve terminals : inhibition of α-ketoglutarate dehydrogenase. *J Neurochem*. 73:220-228.

Chou, Y.L., M.D. Scarupa, N. Mori, and B.J. Canning. 2008. Differential effects of airway afferent nerve subtypes on cough and respiration in anesthetized guinea pigs. *Am J Physiol Regul Integr Comp Physiol*. 295:R1572-1584.

Chuang, H.H., and S. Lin. 2009. Oxidative challenges sensitize the capsaicin receptor by covalent cysteine modification. *Proc Natl Acad Sci U S A*. 106:20097-20102.

Chubanov, V., Y. Mederos, M. Schnitzler, M. Meißner, S. Schäfer, K. Abstiens, T. Hofmann, and T. Gudermann. 2012. Natural and synthetic modulators of SK (K(ca)2) potassium channels inhibit magnesium-dependent activity of the kinase-coupled cation channel TRPM7. *Br J Pharmacol*. 166:1357-1376.

Colell, A., A. Morales, C. Ferna, C. García-Ruiz, A. Colell, M. Marí, A. Morales, and J.C. Fernández-Checa. 1997. Direct effect of ceramide on the mitochondrial electron transport chain leads to generation of reactive oxygen species. *J Biol Chem*. 272:11369-11377.

Copeland, P.R., J.E. Fletcher, B.A. Carlson, D.L. Hatfield, and D.M. Driscoll. 2000. A novel RNA binding protein, SBP2, is required for the translation of mammalian selenoprotein mRNAs. *EMBO J*. 19:306-314.

Copeland, P.R., V.A. Stepanik, and D.M. Driscoll. 2001. Insight into mammalian selenocysteine insertion: Domain structure and ribosome binding properties of Sec insertion sequence binding protein 2. *Mol Cell Biol*. 21:1491-1498.

Cosentino-Gomes, D., N. Rocco-Machado, and J.R. Meyer-Fernandes. 2012. Cell Signaling through Protein Kinase C Oxidation and Activation. *Int J Mol Sci*. 13:10697-10721.

Costello, R.W., C.M. Evans, B.L. Yost, K.E. Belmonte, G.J. Gleich, D.B. Jacoby, and A.D. Fryer. 1999. Antigen-induced hyperreactivity to histamine: role of the vagus nerves and eosinophils. *Am J Physiol*. 276:L709-714.

Cuchillo-Ibáñez, I., T. Lejen, A. Albillos, S. Rosé, R. Olivares, M. Villarroya, A. García, and J. Trifaró. 2004. Mitochondrial calcium sequestration and protein kinase C cooperate in the regulation of cortical F-actin disassembly and secretion in bovine chromaffin cells. *J Physiol*. 560:63-76.

D'Agostino, B., C. Advenier, R. de Palma, L. Gallelli, G. Marrocco, G.F. Abbate, and F. Rossi. 2002. The involvement of sensory neuropeptides in airway hyper-responsiveness in rabbits sensitized and challenged to Parietaria judaica. *Clin Exp Allergy*. 32:472-479.

D'Autréaux, B., and M.B. Toledano. 2007. ROS as signalling molecules: mechanisms that generate specificity in ROS homeostasis. *Nat Rev Mol Cell Biol*. 8:813-824.

Davis, J.B., J. Gray, M.J. Gunthorpe, J.P. Hatcher, P.T. Davey, P. Overend, M.H. Harries, J. Latcham, C. Clapham, K. Atkinson, S.A. Hughes, K. Rance, E. Grau, A.J. Harper, P.L. Pugh, D.C. Rogers, S. Bingham, A. Randall, and S.A. Sheardown. 2000. Vanilloid receptor-1 is essential for inflammatory thermal hyperalgesia. *Nature*. 405:183-187.

Delic, M., D. Mattanovich, and B. Gasser. 2010. Monitoring intracellular redox conditions in the endoplasmic reticulum of living yeasts. *FEMS Microbiol Lett*. 306:61-66.

Dickinson, B.C., D. Srikun, and C.J. Chang. 2010. Mitochondrial-targeted fluorescent probes for reactive oxygen species. *Curr Opin Chem Biol*. 14:50-56.

Dinh, Q.T., D.A. Groneberg, E. Mingomataj, C. Peiser, W. Heppt, S. Dinh, P.C. Arck, B.F. Klapp, and A. Fischer. 2003. Expression of substance P and vanilloid receptor (VR1) in trigeminal sensory neurons projecting to the mouse nasal mucosa. *Neuropeptides*. 37:245-250.

Diogenes, A., A.N. Akopian, and K.M. Hargreaves. 2007. NGF up-regulates TRPA1: implications for orofacial pain. *J Dent Res*. 86:550-555.

Doherty, M.J., R. Mister, M.G. Pearson, and P.M. Calverley. 2000. Capsaicin responsiveness and cough in asthma and chronic obstructive pulmonary disease. *Thorax*. 55:643-649.

Dooley, C.T. 2006. Green fluorescent protein based indicators of dynamic redox changes and reactive oxygen species. Dissertation, UC San Diego, UC San Diego Electronic Theses and Dissertations.

Dooley, C.T., T.M. Dore, G.T. Hanson, W.C. Jackson, S.J. Remington, and R.Y. Tsien. 2004. Imaging dynamic redox changes in mammalian cells with green fluorescent protein indicators. *J Biol Chem*. 279:22284-22293.

Eid, S.R., E.D. Crown, E.L. Moore, H.A. Liang, K.C. Choong, S. Dima, D.A. Henze, S.A. Kane, and M.O. Urban. 2008. HC-030031, a TRPA1 selective antagonist, attenuates inflammatory- and neuropathy-induced mechanical hypersensitivity. *Mol Pain*. 4:48.

Ellis, J.L., J.S. Sham, and B.J. Undem. 1997. Tachykinin-independent effects of capsaicin on smooth muscle in human isolated bronchi. *Am J Respir Crit Care Med*. 155:751-755.

Emelyanov, A., G. Fedoseev, A. Abulimity, K. Rudinski, A. Fedoulov, A. Karabanov, and P.J. Barnes. 2001. Elevated concentrations of exhaled hydrogen peroxide in asthmatic patients. *Chest*. 120:1136-1139.

Fernandes, E.S., F.A. Russell, D. Spina, J.J. McDougall, R. Graepel, C. Gentry, A.A. Staniland, D.M. Mountford, J.E. Keeble, M. Malcangio, S. Bevan, and S.D. Brain. 2010. A distinct role for TRPA1, in addition to TRPV1, in TNFalpha-induced inflammatory hyperalgesia and CFA-induced mono-arthritis. *Arthritis Rheum*.

Ferreira, J., K.M. Trichês, R. Medeiros, and J.B. Calixto. 2005. Mechanisms involved in the nociception produced by peripheral protein kinase c activation in mice. *Pain*. 117:171-181.

Fischer, M.J., D. Balasuriya, P. Jeggle, T.A. Goetze, P.A. McNaughton, P.W. Reeh, and J.M. Edwardson. 2014. Direct evidence for functional TRPV1/TRPA1 heteromers. *Pflugers Arch*. 466:2229-2241.

Fitzpatrick, A.M., W.G. Teague, F. Holguin, M. Yeh, and L.A. Brown. 2009. Airway glutathione homeostasis is altered in children with severe asthma: evidence for oxidant stress. *J Allergy Clin Immunol*. 123:146-152 e148.

Foo, N.P., S.H. Lin, Y.H. Lee, M.J. Wu, and Y.J. Wang. 2011. alpha-Lipoic acid inhibits liver fibrosis through the attenuation of ROS-triggered signaling in hepatic stellate cells activated by PDGF and TGF-beta. *Toxicology*. 282:39-46.

Forrester, S.J., D.S. Kikuchi, M.S. Hernandes, Q. Xu, and K.K. Griendling. 2018. Reactive oxygen species in metabolic and inflammatory signaling. *Circ Res*. 122:877-902.

Garami, A., Y.P. Shimansky, E. Pakai, D.L. Oliveira, N.R. Gavva, and A.A. Romanovsky. 2010. Contributions of different modes of TRPV1 activation to TRPV1 antagonist-induced hyperthermia. *J Neurosci.* 30:1435-1440.

Garaude, J., R. Acín-Pérez, S. Martínez-Cano, M. Enamorado, M. Ugolini, E. Nistal-Villán, S. Hervás-Stubbs, P. Pelegrín, L.E. Sander, J.A. Enríquez, and D. Sancho. 2016. Mitochondrial respiratory-chain adaptations in macrophages contribute to antibacterial host defense. *Nat Immunol.* 17:1037-1048.

Ge, Y., Z. Qi, Y. Wang, X. Liu, J. Li, J. Xu, J. Liu, and J. Shen. 2009. Engineered selenium-containing glutaredoxin displays strong glutathione peroxidase activity rivaling natural enzyme. *Int J Biochem Cell Biol*. 41:900-906.

Gold, M.S., and G.F. Gebhart. 2010. Nociceptor sensitization in pain pathogenesis. *Nat Med*. 16:1248-1257.

Gonzalez-Flores, J., S.P. Shetty, A. Dubey, and P.R. Copeland. 2010. The molecular biology of selenocysteine. *Biomol Concepts*. 48:1-6.

Gouin, O., K. L'Herondelle, N. Lebonvallet, C. Le Gall-Ianotto, M. Sakka, V. Buhe, E. Plee-Gautier, J.L. Carre, L. Lefeuvre, L. Misery, and R. Le Garrec. 2017. TRPV1 and TRPA1 in cutaneous neurogenic and chronic inflammation: pro-inflammatory response induced by their activation and their sensitization. *Protein Cell*. 8:644-661.

Gover, T.D., T.H. Moreira, J.P. Kao, and D. Weinreich. 2007. Calcium regulation in individual peripheral sensory nerve terminals of the rat. *J Physiol*. 578:481-490.

Grace, M., M.A. Birrell, E. Dubuis, S.A. Maher, and M.G. Belvisi. 2012. Transient receptor potential channels mediate the tussive response to prostaglandin E2 and bradykinin. *Thorax*. 67:891-900.

Guerra, F., N. Guaragnella, A.A. Arbini, C. Bucci, S. Giannattasio, and L. Moro. 2017. Mitochondrial dysfunction: a novel potential driver of epithelial-to-mesenchymal transition in cancer. *Front Oncol*. 7:295.

Guo, H., H. Aleyasin, B.C. Dickinson, R.E. Haskew-Layton, and R.R. Ratan. 2014. Recent advances in hydrogen peroxide imaging for biological applications. *Cell Biosci*. 4:64.

Gvozdjáková, A., J. Kucharská, M. Bartkovjaková, K. Gazdíková, and F.E. Gazdík. 2005. Coenzyme Q10 supplementation reduces corticosteroids dosage in patients with bronchial asthma. *Biofactors*. 25:235-240.

Gyulkhandanyan, A.V., and P.S. Pennefather. 2004. Shift in the localization of sites of hydrogen peroxide production in brain mitochondria by mitochondrial stress. *J Neurochem*. 90:405-421.

Hadley, S.H., P.K. Bahia, and T.E. Taylor-Clark. 2014. Sensory nerve terminal mitochondrial dysfunction induces hyperexcitability in airway nociceptors via protein kinase C. *Mol Pharmacol*. 85:839-848.

Han, D., E. Williams, and E. Cadenas. 2001. Mitochondrial respiratory chain-dependent generation of superoxide and its release into the intermembrane space. *Biochem J*. 353:411-416.

Hanson, G.T., R. Aggeler, D. Oglesbee, M. Cannon, R.A. Capaldi, R.Y. Tsien, and S.J. Remington. 2004. Investigating mitochondrial redox potential with redox-sensitive green fluorescent protein indicators. *J Biol Chem*. 279:13044-13053.

Hathaway, T.J., T.W. Higenbottam, J.F. Morrison, C.A. Clelland, and J. Wallwork. 1993. Effects of inhaled capsaicin in heart-lung transplant patients and asthmatic subjects. *Am Rev Respir Dis*. 148:1233-1237.

Hazebrouck, S., L. Camoin, Z. Faltin, A.D. Strosberg, and Y. Eshdat. 2000. Substituting selenocysteine for catalytic cysteine 41 enhances enzymatic activity of plant phospholipid hydroperoxide glutathione peroxidase expressed in Escherichia coli. *J Biol Chem*. 275:28715-28721.

Hinman, A., H.H. Chuang, D.M. Bautista, and D. Julius. 2006. TRP channel activation by reversible covalent modification. *Proc Natl Acad Sci U S A*. 103:19564-19568.

Ho, C.Y., Q. Gu, J.L. Hong, and L.Y. Lee. 2000. Prostaglandin E(2) enhances chemical and mechanical sensitivities of pulmonary C fibers in the rat. *Am J Respir Crit Care Med*. 162:528-533.

Ho, C.Y., and L.Y. Lee. 1998. Ozone enhances excitabilities of pulmonary C fibers to chemical and mechanical stimuli in anesthetized rats. *J Appl Physiol*. 85:1509-1515.

Hoffman, D.L., and P.S. Brookes. 2009. Oxygen sensitivity of mitochondrial reactive oxygen species generation depends on metabolic conditions. *J Biol Chem*. 284:16236-16245.

Hsu, C.C., and L.Y. Lee. 2015. Role of calcium ions in the positive interaction between TRPA1 and TRPV1 channels in bronchopulmonary sensory neurons. *J Appl Physiol*. 118:1533-1543.

Hughes, P.A., A.M. Harrington, J. Castro, T. Liebregts, B. Adam, D.J. Grasby, N.J. Isaacs, L. Maldeniya, C.M. Martin, J. Persson, J.M. Andrews, G. Holtmann, L.A. Blackshaw, and S.M. Brierley. 2013. Sensory neuro-immune interactions differ between Irritable Bowel Syndrome subtypes. *Gut*. 62:1456-1465.

Hung, K.S., M.S. Hertweck, J.D. Hardy, and C.G. Loosli. 1973. Ultrastructure of nerves and associated cells in bronchiolar epithelium of the mouse lung. *J Ultrastruct Res*. 43:426-437.

Hwang, S.W., H. Cho, J. Kwak, S.Y. Lee, C.J. Kang, J. Jung, S. Cho, K.H. Min, Y.G. Suh, D. Kim, and U. Oh. 2000. Direct activation of capsaicin receptors by products of lipoxygenases: endogenous capsaicin-like substances. *Proc Natl Acad Sci U S A*. 97:6155-6160.

Jatakanon, A., S. Lim, S.A. Kharitonov, K.F. Chung, and P.J. Barnes. 1998. Correlation between exhaled nitric oxide, sputum eosinophils, and methacholine responsiveness in patients with mild asthma. *Thorax*. 53:91-95.

Joseph, E.K., and J.D. Levine. 2010. Multiple PKCepsilon-dependent mechanisms mediating mechanical hyperalgesia. *Pain*. 150:17-21.

Kesler, B.S., and B.J. Canning. 1999. Regulation of baseline cholinergic tone in guinea-pig airway smooth muscle. *J Physiol*. 518 (Pt 3):843-855.

Kharitonov, S.A., and P.J. Barnes. 2001. Exhaled markers of pulmonary disease. *Am J Respir Crit Care Med*. 163:1693-1722.

Kim, B.M., S.H. Lee, W.S. Shim, and U. Oh. 2004. Histamine-induced Ca(2+) influx via the PLA(2)/lipoxygenase/TRPV1 pathway in rat sensory neurons. *Neurosci Lett*. 361:159-162.

Kirkham, P., and I. Rahman. 2006. Oxidative stress in asthma and COPD: antioxidants as a therapeutic strategy. *Pharmacol Ther*. 111:476-494.

Knapp, L.T., and E. Klann. 2000. Superoxide-induced stimulation of protein kinase C via thiol modification and modulation of zinc content. *J Biol Chem*. 275:24136-24145.

Kobayashi, K., T. Fukuoka, K. Obata, H. Yamanaka, Y. Dai, A. Tokunaga, and K. Noguchi. 2005. Distinct expression of TRPM8, TRPA1, and TRPV1 mRNAs in rat primary afferent neurons with Aδ/C-fibers and colocalization with Trk receptors. *Journal of Comparative Neurology*. 493:596-606.

Kollarik, M., and B.J. Undem. 2002. Mechanisms of acid-induced activation of airway afferent nerve fibres in guinea-pig. *J Physiol*. 543:591-600.

Kryukov, G.V., S. Castellano, S.V. Novoselov, A.V. Lobanov, O. Zehtab, R. Guigó, and V.N. Gladyshev. 2003. Characterization of mammalian selenoproteomes. *Science*. 300:1439-1443.

Kubin, L., G.F. Alheid, E.J. Zuperku, and D.R. McCrimmon. 2006. Central pathways of pulmonary and lower airway vagal afferents. *J Appl Physiol*. 101:618-627.

Lai, B., L. Zhang, L.Y. Dong, Y.H. Zhu, F.Y. Sun, and P. Zheng. 2005. Inhibition of Qi site of mitochondrial complex III with antimycin A decreases persistent and transient sodium currents via reactive oxygen species and protein kinase C in rat hippocampal CA1 cells. *Exp Neurol*. 194:484-494.

Latrèche, L., O. Jean-Jean, D.M. Driscoll, and L. Chavatte. 2009. Novel structural determinants in human SECIS elements modulate the translational recoding of UGA as selenocysteine. *Nucleic Acids Res*. 37:5868-5880.

Lee, J., M.K. Chung, and J.Y. Ro. 2012. Activation of NMDA receptors leads to phosphorylation of TRPV1 S800 by protein kinase C and A-Kinase anchoring protein 150 in rat trigeminal ganglia. *Biochem Biophys Res Commun*. 424:358-363.

Lee, L.Y., and J.G. Widdicombe. 2001. Modulation of airway sensitivity to inhaled irritants: Role of inflammatory mediators. *Environ Health Perspect*. 109:585-589.

Lee, L.Y., and J. Yu. 2014. Sensory nerves in lung and airways. *Comprehensive Physiology*. 4:287-324.

Leonard, J.L., D.M. Leonard, Q. Shen, A.P. Farwell, and P.E. Newburger. 1996. Selenium-regulated translation control of heterologous gene expression: Normal function of selenocysteine-substituted gene products. *J Cell Biochem*. 61:410-419.

Lesoon, A., A. Mehta, R. Singh, G.M. Chisolm, and D.M. Driscoll. 1997. An RNA-binding protein recognizes a mammalian selenocysteine insertion sequence element required for cotranslational incorporation of selenocysteine. *Mol Cell Biol*. 17:1977-1985.

Lewis, C., and K. Broadley. 1995. Airway hyper- or hyporeactivity to inhaled spasmogens 24 h after ovalbumin challenge of sensitized guinea-pigs. *Br J Pharmacol*. 116:2351-2358.

Lewis, M., A. Shorta, and K. Lewis. 2006. Autonomic nervous system control of the cardiovascular and respiratory systems in asthma. *Respir Med*. 100:1688-1705.

Lin, M.T., and M.F. Beal. 2006. Mitochondrial dysfunction and oxidative stress in neurodegenerative diseases. *Nature*. 443:787-795.

Lin, Y.J., R.L. Lin, T. Ruan, M. Khosravi, and L.Y. Lee. 2015. A synergistic effect of simultaneous TRPA1 and TRPV1 activations on vagal pulmonary C-fiber afferents. *J Appl Physiol (1985)*. 118:273-281.

Lin, Y.S., C.C. Hsu, M.Y. Bien, H.C. Hsu, H.T. Weng, and Y.R. Kou. 2010. Activations of TRPA1 and P2X receptors are important in ROS-mediated stimulation of capsaicin-sensitive lung vagal afferents by cigarette smoke in rats. *J Appl Physiol*. 108:1293-1303.

Lopez-Armada, M., B. Carame, M. Martı, M. Lires-dean, I. Fuentes-boquete, J. Arenas, and F. Blanco. 2006. Mitochondrial activity is modulated by TNFalpha and IL-1beta in normal human chondrocyte cells. *Osteoarthritis and Cartilage*. 14:1011-1022.

López-Armada, M.J., R.R. Riveiro-Naveira, C. Vaamonde-García, and M.N. Valcárcel-Ares. 2013. Mitochondrial dysfunction and the inflammatory response. *Mitochondrion*. 13:106-118.

Lou, Y.P. 1993. Regulation of neuropeptide release from pulmonary capsaicin-sensitive afferents in relation to bronchoconstriction. *Acta Physiol Scand Suppl*. 612:1-88.

Lu, J., P. Risbood, C.T. Kane, Jr., M.T. Hossain, L. Anderson, K. Hill, A. Monks, Y. Wu, S. Antony, A. Juhasz, H. Liu, G. Jiang, E. Harris, K. Roy, J.L. Meitzler, M. Konate, and J.H. Doroshow. 2017. Characterization of potent and selective iodonium-class inhibitors of NADPH oxidases. *Biochem Pharmacol*. 143:25-38.

Lundberg, J.M., E. Brodin, X. Hua, and A. Saria. 1984a. Vascular permeability changes and smooth muscle contraction in relation to capsaicin-sensitive substance P afferents in the guinea-pig. *Acta Physiol Scand*. 120:217-227.

Lundberg, J.M., T. Hokfelt, C.R. Martling, A. Saria, and C. Cuello. 1984b. Substance P-immunoreactive sensory nerves in the lower respiratory tract of various mammals including man. *Cell Tissue Res*. 235:251-261.

Mabalirajan, U., A.K. Dinda, S. Kumar, R. Roshan, P. Gupta, S.K. Sharma, and B. Ghosh. 2008. Mitochondrial structural changes and dysfunction are associated with experimental allergic asthma. *J Immunol*. 181:3540-3548.

Mabalirajan, U., A.K. Dinda, S.K. Sharma, and B. Ghosh. 2009. Esculetin restores mitochondrial dysfunction and reduces allergic asthma features in experimental murine model. *J Immunol.* 183:2059-2067.

Macpherson, L.J., A.E. Dubin, M.J. Evans, F. Marr, P.G. Schultz, B.F. Cravatt, and A. Patapoutian. 2007. Noxious compounds activate TRPA1 ion channels through covalent modification of cysteines. *Nature*. 445:541-545.

Madisen, L., T. Zwingman, S. Sunkin, S. Oh, H. Zariwala, H. Gu, L. Ng, R. Palmiter, M. Hawrylycz, A. Jones, E. Lein, and Z. H. 2010. A robust and high-throughput Cre reporting and characterization system for the whole mouse brain. *Nat Neurosci*. 13:133-140.

Mandadi, S., M. Numazaki, M. Tominaga, M.B. Bhat, P.J. Armati, and B.D. Roufogalis. 2006a. Activation of protein kinase C reverses capsaicin-induced calcium-dependent desensitization of TRPV1 ion channels. *Cell Calcium*. 35:471-478.

Mandadi, S., T. Tominaga, M. Numazaki, N. Murayama, N. Saito, P.J. Armati, B.D. Roufogalis, and M. Tominaga. 2006b. Increased sensitivity of desensitized TRPV1 by PMA occurs through PKCε-mediated phosphorylation at S800. *Pain*. 123:106-116.

Marchand, F., M. Perretti, and S.B. McMahon. 2005. Role of the immune system in chronic pain. *Nat Rev Neurosci*. 6:521-532.

Mariappan, N., C.M. Elks, B. Fink, and J. Francis. 2009. TNF-induced mitochondrial damage: a link between mitochondrial complex I activity and left ventricular dysfunction. *Free Radic Biol Med*. 46:462-470.

Mazzone, S.B., and B.J. Undem. 2016. Vagal Afferent Innervation of the Airways in Health and Disease. *Physiol Rev*. 96:975-1024.

McAlexander, M.A., S.H. Gavett, M. Kollarik, and B.J. Undem. 2015. Vagotomy reverses established allergen-induced airway hyperreactivity to methacholine in the mouse. *Respir Physiol Neurobiol*. 212-214:20-24.

McBride, D.E., J.Q. Koenig, D.L. Luchtel, P.V. Williams, and W.R. Henderson, Jr. 1994. Inflammatory effects of ozone in the upper airways of subjects with asthma. *Am J Respir Crit Care Med*. 149:1192-1197.

McMahon, S.B., F. La Russa, and D.L.H. Bennett. 2015. Crosstalk between the nociceptive and immune systems in host defence and disease. *Nat Rev Neurosci*. 16:389-402.

Meents, J.E., M.J.M. Fischer, and P.A. McNaughton. 2017. Sensitization of TRPA1 by Protein Kinase A. *PLoS ONE*. 12:1-15.

Mehta, A., C.M. Rebsch, S.A. Kinzyi, J.E. Fletcher, and P.R. Copeland. 2004. Efficiency of mammalian selenocysteine incorporation. *J Biol Chem*. 279:37852-37859.

Michael, G.J., and J.V. Priestley. 1999. Differential expression of the mRNA for the vanilloid receptor subtype 1 in cells of the adult rat dorsal root and nodose ganglia and its downregulation by axotomy. *J Neurosci*. 19:1844-1854.

Miyazaki, K., and W.N. Ross. 2015. Simultaneous sodium and calcium imaging from dendrites and axons. *eNeuro*. 2.

Moe, G.W., J. Marin-Garcia, A. Konig, M. Goldenthal, X. Lu, and Q. Feng. 2004. In vivo TNF-alpha inhibition ameliorates cardiac mitochondrial dysfunction, oxidative stress, and apoptosis in experimental heart failure. *Am J Physiol Heart Circ Physiol*. 287:H1813-1820.

Mohapatra, D.P., and C. Nau. 2005. Regulation of Ca2+-dependent desensitization in the vanilloid receptor TRPV1 by calcineurin and cAMP-dependent protein kinase. *J Biol Chem*. 280:13424-13432.

Morales-Lázaro, S.L., S.A. Simon, and T. Rosenbaum. 2013. The role of endogenous molecules in modulating pain through transient receptor potential vanilloid 1 (TRPV1). *J Physiol*. 591:3109-3121.

Morris, J.B., P.T. Symanowicz, J.E. Olsen, R.S. Thrall, M.M. Cloutier, and A.K. Hubbard. 2003. Immediate sensory nerve-mediated respiratory responses to irritants in healthy and allergic airway-diseased mice. *J Appl Physiol*. 94:1563-1571.

Muller, F.L., Y. Liu, and H. Van Remmen. 2004. Complex III releases superoxide to both sides of the inner mitochondrial membrane. *Journal of Biolog*. 279:49064-49073.

Müller, S., H. Senn, B. Gsell, W. Vetter, C. Baron, and A. Böck. 1994. The formation of diselenide bridges in proteins by incorporation of selenocysteine residues: biosynthesis and characterization of (Se)2-thioredoxin. *Biochemistry*. 33:3404-3412.

Nakajima, T., Y. Nishimura, T. Nishiuma, Y. Kotani, H. Nakata, and M. Yokoyama. 2006. Cough sensitivity in pure cough variant asthma elicited using continuous capsaicin inhalation. *Allergol Int.* 55:149-155.

Nassenstein, C., K. Kwong, T. Taylor-Clark, M. Kollarik, D.M. Macglashan, A. Braun, and B.J. Undem. 2008. Expression and function of the ion channel TRPA1 in vagal afferent nerves innervating mouse lungs. *J Physiol*. 586:1595-1604.

Nassenstein, C., T.E. Taylor-Clark, A.C. Myers, F. Ru, R. Nandigama, W. Bettner, and B.J. Undem. 2010. Phenotypic distinctions between neural crest and placodal derived vagal C-fibres in mouse lungs. *J Physiol*. 588:4769-4783.

Nesuashvili, L., S.H. Hadley, P.K. Bahia, and T.E. Taylor-Clark. 2013. Sensory nerve terminal mitochondrial dysfunction activates airway sensory nerves via transient receptor potential (TRP) channels. *Mol Pharmacol*. 83:1007-1019.

Novoselov, S.V., A.V. Lobanov, D. Hua, M.V. Kasaikina, D.L. Hatfield, and V.N. Gladyshev. 2007. A highly efficient form of the selenocysteine insertion sequence element in protozoan parasites and its use in mammalian cells. *Proc Natl Acad Sci U S A*. 104:7857-7862.

Numata, T., T. Shimizu, and Y. Okada. 2007. TRPM7 is a stretch- and swelling-activated cation channel involved in volume regulation in human epithelial cells. *Am J Physiol Cell Physiol*. 292:C460–C467.

Ogawa, N., T. Kurokawa, and Y. Mori. 2016. Sensing of redox status by TRP channels. *Cell Calcium*. 60:115-122.

Ortega-Villasante, C., S. Buren, A. Baron-Sola, F. Martinez, and L.E. Hernandez. 2016. In vivo ROS and redox potential fluorescent detection in plants: Present approaches and future perspectives. *Methods*. 109:92-104.

Paintal, A.S. 1973. Vagal sensory receptors and their reflex effects. *Physiol Rev*. 53:159-227.

Park, W.H., Y.W. Han, S.H. Kim, and S.Z. Kim. 2007. An ROS generator, antimycin A, inhibits the growth of HeLa cells via apoptosis. *J Cell Biochem*. 102:98-109.

Parker, P.J. 2004. PKC at a glance. *J Cell Sci*. 117:131-132.

Perry, S.W., J.P. Norman, J. Barbieri, E.B. Brown, and A. Harris. 2011. Mitochondirial membrane potential probes and the proton Gradient: a Practical Usage Guide. *Biotechniques*. 50:98-115.

Petrus, M., A.M. Peier, M. Bandell, S.W. Hwang, T. Huynh, N. Olney, T. Jegla, and A. Patapoutian. 2007. A role of TRPA1 in mechanical hyperalgesia is revealed by pharmacological inhibition. *Mol Pain*. 3:40.

Potter, V.R., and A.E. Reif. 1952. Inhibition of an electron transport component by antimycin A. *J Biol Chem*. 194:287-297.

Prescott, E.D., and D. Julius. 2003. A modular PIP2 binding site as a determinant of capsaicin receptor sensitivity. *Science*. 300:1284-1288.

Quarcoo, D., O. Schulte-Herbruggen, M. Lommatzsch, K. Schierhorn, G.W. Hoyle, H. Renz, and A. Braun. 2004. Nerve growth factor induces increased airway inflammation via a neuropeptide-dependent mechanism in a transgenic animal model of allergic airway inflammation. *Clin Exp Allergy*. 34:1146-1151.

Raby, B.A., B. Klanderman, A. Murphy, S. Mazza, C.A. Camargo, E.K. Silverman, and S.T. Weiss. 2007. A common mitochondrial haplogroup is associated with elevated total serum IgE levels. *J Allergy Clin Immunol*. 120:351-358.

Radak, Z., Z. Zhao, S. Goto, and E. Koltai. 2011. Age-associated neurodegeneration and oxidative damage to lipids, proteins and DNA. *Mol Aspects Med*. 32:305-315.

Rahman, I., A.A. van Schadewijk, A.J. Crowther, P.S. Hiemstra, J. Stolk, W. MacNee, and W.I. De Boer. 2002. 4-Hydroxy-2-nonenal, a specific lipid peroxidation product, is elevated in lungs of patients with chronic obstructive pulmonary disease. *Am J Respir Crit Care Med*. 166:490-495.

Reddy, P. 2011. Mitochondrial dysfunction and oxidative stress in asthma: Implications for mitochondria-targeted antioxidant therapeutics. *Pharmaceuticals (Basel)*. 4:429-456.

Reers, M., T.W. Smith, and L.B. Chen. 1991. J-aggregate formation of a carbocyanine as a quantitative fluorescent indicator of membrane potential. *Biochemistry*. 30:4480-4486.

Rizzuto, R., D.D. Stefani, A. Raffaello, and C. Mammucari. 2012. Mitochondria as sensors and regulators of calcium signalling. *Nat Rev Mol Cell Biol*. 13:566-578.

Roberts, D.D., S.D. Lewis, D.P. Ballou, S.T. Olson, and J.a. Shafer. 1986. Reactivity of small thiolate anions and cysteine-25 in papain toward methyl methanethiosulfonate. *Biochemistry*. 25:5595-5601.

Rogers, D.F. 2001. Motor control of airway goblet cells and glands. *Respir Physiol*. 125:129-144.

Rohacs, T. 2015. Phosphoinositide regulation of TRPV1 revisited. *Pflugers Arch*. 467:1851-1869.

Rohacs, T., B. Thyagarajan, and V. Lukacs. 2008. Phospholipase C mediated modulation of TRPV1 channels. *Mol Neurobiol*. 37:153-163.

Roma, L.P., J. Duprez, H.K. Takahashi, P. Gilon, A. Wiederkehr, and J.-C.C. Jonas. 2012. Dynamic measurements of mitochondrial hydrogen peroxide concentration and glutathione redox state in rat pancreatic β-cells using ratiometric fluorescent proteins: confounding effects of pH with HyPer but not roGFP1. *Biochem J*. 441:971-978.

Ruan, T., C.Y. Ho, and Y.R. Kou. 2003. Afferent vagal pathways mediating respiratory reflexes evoked by ROS in the lungs of anesthetized rats. *J Appl Physiol*. 94:1987-1998.

Ruan, T., Y.S. Lin, K.S. Lin, and Y.R. Kou. 2005. Sensory transduction of pulmonary reactive oxygen species by capsaicin-sensitive vagal lung afferent fibres in rats. *J Physiol*. 565:563-578.

Ruan, T., Y.S. Lin, K.S. Lin, and Y.R. Kou. 2006. Mediator mechanisms involved in TRPV1 and P2X receptor-mediated, ROS-evoked bradypneic reflex in anesthetized rats. *J Appl Physiol*. 101:644-654.

Ruparel, N.B., A.M. Patwardhan, A.N. Akopian, and K.M. Hargreaves. 2008. Homologous and heterologous desensitization of capsaicin and mustard oil responses utilize different cellular pathways in nociceptors. *Pain*. 135:271-279.

Salas, M., K. Hargreaves, and A. Akopian. 2009. TRPA1-mediated responses in trigeminal sensory neurons: interaction between TRPA1 and TRPV1. *Eur J Neurosci*. 29:1568-1578.

Sawada, Y., H. Hosokawa, K. Matsumura, and S. Kobayashi. 2008. Activation of transient receptor potential ankyrin 1 by hydrogen peroxide. *Eur J Neurosci*. 27:1131-1142.

Schwarzländer, M., M.D. Fricker, C. Müller, L. Marty, T. Brach, J. Novak, L.J. Sweetlove, R. Hell, and A.J. Meyer. 2008. Confocal imaging of glutathione redox potential in living plant cells. *J Microsc*. 231:299-316.

Sherrington, C. 1906. The integrative action of the nervous system. Yale University Press, New Haven.

Shishkin, V., E. Potapenko, E. Kostyuk, O. Girnyk, N. Voitenko, and P. Kostyuk. 2002. Role of mitochondria in intracellular calcium signaling in primary and secondary sensory neurones of rats. *Cell Calcium*. 32:121-130.

Sipos, I., L. Tretter, and V. Adam-Vizi. 2003. The production of reactive oxygen species in intact isolated nerve terminals is independent of the mitochondrial membrane potential. *Neurochem Res*. 28:1575-1581.

Slater, E.C. 1973. The mechanism of action of the respiratory inhibitor, antimycin. *Biochim Biophys Acta*. 301:129-154.

Spahn, V., C. Stein, and C. Zollner. 2014. Modulation of transient receptor vanilloid 1 activity by transient receptor potential ankyrin 1. *Mol Pharmacol*. 85:335-344.

St-Pierre, J., J.A. Buckingham, S.J. Roebuck, and M.D. Brand. 2002. Topology of superoxide production from different sites in the mitochondrial electron transport chain. *J Biol Chem*. 277:44784-44790.

Stadler, J., B.G. Bentz, B.G. Harbrecht, M. Di Silvio, R.D. Curran, T.R. Billiar, R.A. Hoffman, and R.L. Simmons. 1992. Tumor necrosis factor alpha inhibits hepatocyte mitochondrial respiration. *Ann Surg*. 216:539-546.

Stanford, K.R., and T.E. Taylor-Clark. 2018. Mitochondrial modulation-induced activation of vagal sensory neuronal subsets by antimycin A, but not CCCP or rotenone, correlates with mitochondrial superoxide production. *PLoS One*. 13:e0197106.

Starkov, A.A., and G. Fiskum. 2001. Myxothiazol induces H2O2 production from mitochondrial respiratory chain. *Biochem Biophys Res Commun*. 281:645-650.

Staruschenko, A., N.A. Jeske, and A.N. Akopian. 2010. Contribution of TRPV1-TRPA1 interaction to the single channel properties of the TRPA1 channel. *J Biol Chem*. 285:15167-15177.

Story, G.M., A.M. Peier, A.J. Reeve, S.R. Eid, J. Mosbacher, T.R. Hricik, T.J. Earley, A.C. Hergarden, D.A. Andersson, S.W. Hwang, P. McIntyre, T. Jegla, S. Bevan, and A. Patapoutian. 2003. ANKTM1, a TRP-like channel expressed in nociceptive neurons, is activated by cold temperatures. *Cell*. 112:819-829.

Stowe, D.F., and A.K. Camara. 2009. Mitochondrial reactive oxygen species production in excitable cells: modulators of mitochondrial and cell function. *Antioxid Redox Signal*. 11:1373-1414.

Strzelak, A., A. Ratajczak, A. Adamiec, and W. Feleszko. 2018. Tobacco smoke induces and alters immune responses in the lung triggering inflammation, allergy, asthma and other lung diseases: A mechanistic teview. *Int J Environ Res Public Health*. 15.

Sugiura, K., T. Nagai, M. Nakano, H. Ichinose, T. Nakabayashi, N. Ohta, and T. Hisabori. 2015. Redox sensor proteins for highly sensitive direct imaging of intracellular redox state. *Biochem Biophys Res Commun*. 457:242-248.

Susankova, K., K. Tousova, L. Vyklicky, J. Teisinger, and V. Vlachova. 2006. Reducing and oxidizing agents sensitize heat-activated vanilloid receptor (TRPV1) current. *Mol Pharmacol*. 70:383-394.

Suski, J.M., M. Lebiedzinska, M. Bonora, P. Pinton, J. Duszynski, and M.R. Wieckowski. 2012. Relation between mitochondrial membrane potential and ROS formation. *Methods Mol Biol*. 1782:357-381.

Szolcsanyi, J., F. Anton, P.W. Reeh, and H.O. Handwerker. 1988. Selective excitation by capsaicin of mechano-heat sensitive nociceptors in rat skin. *Brain Res*. 446:262-268.

Tahara, E.B., F.D. Navarete, and A.J. Kowaltowski. 2009. Tissue-, substrate-, and site-specific characteristics of mitochondrial reactive oxygen species generation. *Free Radic Biol Med*. 46:1283-1297.

Takahashi, N., Y. Mizuno, D. Kozai, S. Yamamoto, S. Kiyonaka, T. Shibata, K. Uchida, and Y. Mori. 2008. Molecular characterization of TRPA1 channel activation by cysteine-reactive inflammatory mediators. *Channels (Austin)*. 2:287-298.

Tatar, M., S.E. Webber, and J.G. Widdicombe. 1988. Lung C-fibre receptor activation and defensive reflexes in anaesthetized cats. *J Physiol*. 402:411-420.

Taylor-Clark, T.E., S. Ghatta, W. Bettner, and B.J. Undem. 2009a. Nitrooleic acid, an endogenous product of nitrative stress, activates nociceptive sensory nerves via the direct activation of TRPA1. *Mol Pharmacol*. 75:820-829.

Taylor-Clark, T.E., F. Kiros, M.J. Carr, and M.A. McAlexander. 2009b. Transient receptor potential ankyrin 1 mediates toluene diisocyanate-evoked respiratory irritation. *Am J Respir Cell Mol Biol*. 40:756-762.

Taylor-Clark, T.E., M.A. McAlexander, C. Nassenstein, S.A. Sheardown, S. Wilson, J. Thornton, M.J. Carr, and B.J. Undem. 2008a. Relative contributions of TRPA1 and TRPV1 channels in the activation of vagal bronchopulmonary C-fibres by the endogenous autacoid 4-oxononenal. *J Physiol*. 586:3447-3459.

Taylor-Clark, T.E., and B.J. Undem. 2010. Ozone activates airway nerves via the selective stimulation of TRPA1 ion channels. *J Physiol*. 588:423-433.

Taylor-Clark, T.E., and B.J. Undem. 2011. Sensing pulmonary oxidative stress by lung vagal afferents. *Respir Physiol Neurobiol*. 178:406-413.

Taylor-Clark, T.E., B.J. Undem, S. Ghatta, and M.A. McAlexander. 2007. 4-Hydroxynonenal: a potential endogenous activator of transient receptor potential A1 (TRPA1) channels. *J Physiol*. 586:3447-3459.

Taylor-Clark, T.E., B.J. Undem, D.W. Macglashan, Jr., S. Ghatta, M.J. Carr, and M.A. McAlexander. 2008b. Prostaglandin-induced activation of nociceptive neurons via direct interaction with transient receptor potential A1 (TRPA1). *Mol Pharmacol*. 73:274-281.

Taylor-Clark, T.E., K.Y. Wu, J.A. Thompson, K. Yang, P.K. Bahia, and J.M. Ajmo. 2015. Thy1.2 YFP-16 transgenic mouse labels a subset of large-diameter sensory neurons that lack TRPV1 expression. *PLoS One*. 10:e0119538.

Tominaga, M., M.J. Caterina, A.B. Malmberg, T.A. Rosen, H. Gilbert, K. Skinner, B.E. Raumann, A.I. Basbaum, and D. Julius. 1998. The cloned capsaicin receptor integrates multiple pain-producing stimuli. *Neuron*. 21:531-543.

Trankner, D., N. Hahne, K. Sugino, M.A. Hoon, and C. Zuker. 2014. Population of sensory neurons essential for asthmatic hyperreactivity of inflamed airways. *Proc Natl Acad Sci U S A*. 111:11515-11520.

Trevisani, M., J. Siemens, S. Materazzi, D.M. Bautista, R. Nassini, B. Campi, N. Imamachi, E. Andre, R. Patacchini, G.S. Cottrell, R. Gatti, A.I. Basbaum, N.W. Bunnett, D. Julius, and P. Geppetti. 2007. 4-Hydroxynonenal, an endogenous aldehyde, causes pain and neurogenic inflammation through activation of the irritant receptor TRPA1. *Proc Natl Acad Sci U S A*. 104:13519-13524.

Tujebajeva, R.M., P.R. Copeland, X.M. Xu, B.a. Carlson, J.W. Harney, D.M. Driscoll, D.L. Hatfield, and M.J. Berry. 2000. Decoding apparatus for eukaryotic selenocysteine insertion. *EMBO reports*. 1:158-163.

Turrens, J., A. Alexandre, and A. Lehninger. 1985a. Ubisemiquinone is the electron donor for superoxide formation by complex III of heart mitochondria. *Arch Biochem Biophys.* 237:408-414.

Turrens, J.F. 2003. Mitochondrial formation of reactive oxygen species. *J Physiol*. 552:335-344.

Turrens, J.F., A. Alexandre, and A.L. Lehninger. 1985b. Ubisemiquinone is the electron donor for superoxide formation by complex III of heart mitochondria. *Arch Biochem Biophys*. 237:408-414.

Undem, B.J., D.D. Hunter, M. Liu, M. Haak-Frendscho, A. Oakragly, and A. Fischer. 1999. Allergen-induced sensory neuroplasticity in airways. *Int Arch Allergy Immunol*. 118:150-153.

Van Tilburg, M.A.L., E.A. Zaki, T. Venkatesan, and R.G. Boles. 2014. Irritable Bowel Syndrome may be associated with maternal inheritance and mitochondrial DNA control region sequence variants. *Dig Dis Sci*. 59:1392-1397.

Veatch, J.R., M.A. McMurray, Z.W. Nelson, and D.E. Gottschling. 2009. Mitochondrial dysfunction leads to nuclear genome instability via an iron-sulfur cluster defect. *Cell*. 137:1247-1258.

Vellani, V., S. Mapplebeck, A. Moriondo, J.B. Davis, and P.A. Mcnaughton. 2001. Protein kinase C activation potentiates gating of the vanilloid receptor VR1 by capsaicin, protons, heat and anandamide. *J Physiol*. 534:813-825.

von During, M., and K.H. Andres. 1988. Structure and functional anatomy of visceroreceptors in the mammalian respiratory system. *Prog Brain Res*. 74:139-154.

Votyakova, T.V., and I.J. Reynolds. 2001. ΔΨm -Dependent and -independent production of reactive oxygen species by rat brain mitochondria. *J Neurochem*. 79:266-277.

Wagener, K.C., B. Kolbrink, K. Dietrich, K.M. Kizina, L.S. Terwitte, B. Kempkes, G. Bao, and M. Müller. 2016. Redox indicator mice stably expressing genetically encoded neuronal roGFP: Versatile tools to decipher subcellular redox dynamics in neuropathophysiology. *Antioxid Redox Signal*. 25:41-58.

Wang, C.H., and Y.H. Wei. 2017. Role of mitochondrial dysfunction and dysregulation of Ca(2+) homeostasis in the pathophysiology of insulin resistance and type 2 diabetes. *J Biomed Sci*. 24:70.

Wang, S., J. Joseph, J. Ro, and M. Chung. 2015. Modality-specific mechanisms of PKC-induced hypersensitivity of TRPV1: S800 is a polymodal sensitization site. *Pain*. 156:931-941.

Wang, Y.Y., R.B. Chang, H.N. Waters, D.D. McKemy, and E.R. Liman. 2008. The nociceptor ion channel TRPA1 is potentiated and inactivated by permeating calcium ions. *J Biol Chem*. 283:32691-32703.

Watanabe, H., J. Vriens, J. Prenen, G. Groogmans, T. Voets, and B. Nilius. 2003. Anandamide and arachidonic acid use epoxyeicosatrienoic acids to activate TRPV4 channels. *Nature*. 424:434-438.

Waypa, G.B., J.D. Marks, R. Guzy, P.T. Mungai, J. Schriewer, D. Dokic, and P.T. Schumacker. 2011. Hypoxia triggers subcellular compartmental redox signaling in vascular smooth muscle cells. *Circ Res*. 106:526-535.

Weigand, L.A., A.P. Ford, and B.J. Undem. 2012. A role for ATP in bronchoconstriction-induced activation of guinea pig vagal intrapulmonary C-fibres. *J Physiol*. 590:4109-4120.

Wen, H., J. Östman, K.J. Bubb, C. Panayiotou, J.V. Priestley, M.D. Baker, and A. Ahluwalia. 2012. 20-hydroxyeicosatetraenoic acid (20-HETE) is a novel activator of transient receptor potential vanilloid 1 (TRPV1). *J Biol Chem*. 287:13868-13876.

Weng, H.J., K.N. Patel, N.A. Jeske, S.M. Bierbower, W. Zou, V. Tiwari, Q. Zheng, Z. Tang, G.C. Mo, Y. Wang, Y. Geng, J. Zhang, Y. Guan, A.N. Akopian, and X. Dong. 2015. Tmem100 is a regulator of TRPA1-TRPV1 complex and contributes to persistent pain. *Neuron*. 85:833-846.

Widdicombe, J. 2003. Functional morphology and physiology of pulmonary rapidly adapting receptors (RARs). *Anat Rec A Discov Mol Cell Evol Biol*. 270:2-10.

Widdicombe, J.G. 1954. Respiratory reflexes excited by inflation of the lungs. *J Physiol*. 123:105-115.

Woo, D.H., S.J. Jung, M.H. Zhu, C.K. Park, Y.H. Kim, S.B. Oh, and C.J. Lee. 2008. Direct activation of transient receptor potential vanilloid 1(TRPV1) by diacylglycerol (DAG). *Mol Pain*. 4:42.

Wu, L., T. Sweet, and D. Clapham. 2010a. International Union of Basic and Clinical Pharmacology. LXXVI. Current progress in the mammalian TRP ion channel family. *Pharmacol Rev*. 62:381-404.

Wu, P.Y., B. Lai, Y. Dong, Z.M. Wang, Z.C. Li, and P. Zheng. 2010b. Different oxidants and PKC isozymes mediate the opposite effect of inhibition of Qi and Qo site of mitochondrial complex III on calcium currents in rat cortical neurons. *Biochim Biophys Acta*. 1803:1072-1082.

Xue, Q., B. Jong, T. Chen, and M.A. Schumacher. 2007. Transcription of rat TRPV1 utilizes a dual promoter system that is positively regulated by nerve growth factor. *J Neurochem*. 101:212-222.

Yoshida, T., R. Inoue, T. Morii, N. Takahashi, S. Yamamoto, Y. Hara, M. Tominaga, S. Shimizu, Y. Sato, and Y. Mori. 2006. Nitric oxide activates TRP channels by cysteine S-nitrosylation. *Nat Chem Biol*. 2:596-607.

Yu, J. 2005. Airway mechanosensors. *Respir Physiol Neurobiol*. 148:217-243.

Yu, S., B.J. Undem, and M. Kollarik. 2005. Vagal afferent nerves with nociceptive properties in guinea-pig oesophagus. *J Physiol*. 563:831-842.

Zaccone, E.J., and B.J. Undem. 2016. Airway vagal neuroplasticity associated with respiratory viral infections. *Lung*. 194:25-29.

Zell, R., P. Geck, K. Werdan, and P. Boekstegers. 1997. TNF-α and IL-1α inhibit both pyruvate dehydrogenase activity and mitochondrial function in cardiomyocytes: Evidence for primary impairment of mitochondrial function. *Mol Cell Biochem*. 177:61-67.

Zhang, L., K. Wang, Y. Lei, Q. Li, E.C. Nice, and C. Huang. 2015. Redox signaling: Potential arbitrator of autophagy and apoptosis in therapeutic response. *Free Radic Biol Med*. 89:452-465.

Zhang, X., and F. Gao. 2015. Imaging mitochondrial reactive oxygen species with fluorescent probes: current applications and challenges. *Free Radic Res*. 49:374-382.

Zhang, Y.H., J. Kays, K.E. Hodgdon, T.C. Sacktor, and G.D. Nicol. 2012. Nerve growth factor enhances the excitability of rat sensory neurons through activation of the atypical protein kinase C isoform, PKMzeta. *J Neurophysiol*. 107:315-335.

Zifa, E., Z. Daniil, E. Skoumi, M. Stavrou, K. Papadimitriou, M. Terzenidou, K. Kostikas, V. Bagiatis, K.I. Gourgoulianis, and Z. Mamuris. 2012. Mitochondrial genetic background plays a role in increasing risk to asthma. *Mol Biol Rep*. 39:4697-4708.

Zinoni, F., J. Heider, and A. Bock. 1990. Features of the formate dehydrogenase mRNA necessary for decoding of the UGA codon as selenocysteine. *Proc Natl Acad Sci U S A.* 87:4660-4664.